ON THE COMPRESSION BEHAVIOUR OF HYBRID AND STRONG FLANGE STAINLESS STEEL I-SECTIONS

Thesis Manuscript by Gregory Langone
Supervised by Associate Professor Barbara Rossi
Master of Science by Research

Viva voce examination on June 24th, 2025, evaluated by
Emilio Martinez-Pañeda, Associate Professor of Engineering Science, University of Oxford
Katherine Cashell, Professor of Structural Engineering, University College London

University of Oxford. Department of Engineering Science.

Acknowledgements

To Associate Professor Barbara Rossi, my supervisor.
Thank you for your prudent advice, inspiring intellect, and interest in my development.

To Usman Ali, PhD candidate at KU Leuven and my co-worker on this project.
For two years he has been a diligent worker and a kind-hearted friend.

To friends and faculty at New College, University of Oxford.
They gave me an education, in far more than engineering.

Table of Contents

ABSTRACT 5
1. INTRODUCTION 6
1.1. Description of the Project in Phases 8
1.2. Description of the Thesis Manuscript Chapters 11
2. BACKGROUND & LITERATURE SURVEY 12
2.1. The History of Hybrid Steel Structures 12
2.2. Hybrid Steel Girders 16
2.3. Literature Survey of Fabricated I-Section Stub Column Tests 17
2.4. Theoretical Explanations of Compression Behaviour 19
2.4.1. Buckling Coefficient for End Conditions 20
2.4.2. Effective Strength of Plate Elements 22
2.5. Initial Observations of the Strong Flange Behaviour 24
2.6. Initial Design Method Developments from Langone et al., 2024 [11] 26
2.7. Detailed Description of Reliability Assessment Methods 29
2.7.1. American Standards for Reliability Assessment 29
2.7.2. Eurocode Standards for Reliability Assessment 31
3. TESTS OF HYBRID STRONG FLANGE I-SECTIONS UNDER COMPRESSION 34
Abstract 34
3.1. Introduction 35
3.2. Design Methods 39
3.2.1. Effective Width Method 39
3.2.2. Direct Strength Method 40
3.2.3. Continuous Strength Method 42
3.2.4. Strong Flange Behaviour 43
3.3. Design and Fabrication 45
3.4. Material Properties 48
3.5. Initial Geometric Imperfections 50
3.6. Stub Column Test Procedure 53
3.7. Tests and Numerical Validation 54
3.7.1. Test Results 55
3.7.2. Buckling Mechanisms 57
3.7.3. Numerical Modelling and Validation 61
3.8. Evaluation of Design Methods 64
3.8.1. Codified Design Methods 64

3.8.2. Alternative Design Methods 67
3.9. Conclusions 68
3.10. Acknowledgements 69
4. NUMERICAL MODELLING AND DESIGN OF STAINLESS STEEL I-SECTIONS WITH STRONG FLANGES 71
Abstract 71
4.1. Introduction 71
4.1.1. Tests and Design of Fabricated I-sections 73
4.2. Numerical Modelling 76
4.2.1. Validation Model 77
4.3. Parametric Study 81
4.3.1. Numerical Model Results 81
4.3.2. Development of the Strong Flange Parameters 87
4.3.3. Development of the Modified DSM 89
4.4. Design Method Assessments 92
4.4.1. Effective Width Method 92
4.4.2. Direct Strength Method 94
4.4.3. Continuous Strength Method 95
4.4.4. Modified DSM Proposal 97
4.5. Reliability Assessment 99
4.6. Conclusions 103
4.7. Acknowledgements 105
5. DISCUSSION & CONCLUSION 106
5.1. Treatment of Stainless Steel Families in Reliability Assessment 106
5.2. Conceptual Contextualization for Design Methods 108
5.3. Research Impact and Efficiency Gains 111
5.4. Limitations and Future Work 113
5.5. Conclusion 115
6. REFERENCES 118
7. APPPENDIX 125
Table A.1. Stub Column Test Data from Literature 125

ABSTRACT

Hybrid I-sections, designed with the stronger material in the flanges, are frequently used in construction applications to more efficiently withstand the non-uniform stress distributions induced by flexural loading. Substantially less is understood, however, about the performance of hybrid I-sections in the fundamental load case of pure compression. Numerical and experimental evidence from the past twenty years has suggested the existence of a distinct strong flange behaviour, where I-sections with flanges substantially stronger than the web can develop compressive strengths much greater than existing design predictions. This project develops design equations that accurately represent the behaviour of hybrid and strong flange I-sections. Representing the beneficial characteristics of these sections prevents over-conservative design, leading to reduced cost, reduced waste, and improved performance.

Experimental and numerical investigations are undertaken in this project to improve understanding of hybrid and strong flange I-sections. Thirteen stub column compression tests are completed on I-sections, including ten hybrid sections and a range of strong flange designs. The material properties and geometric imperfections of each plate in the stub columns are measured prior to testing. A finite element model of each stub column test is developed based on the measured properties, and the numerical models are validated against the experimental results. The validated model is used to conduct a parametric assessment, comparing the influence of individual material and geometric parameters among over 1325 simulated stub column tests. Based on the tests and FE model results, the shortcomings of existing design methods are demonstrated, and an alternative design method is developed which provides much more accurate ultimate strength predictions. The proposed method achieves a level of reliability consistent with the targets given in current design codes.

1. INTRODUCTION

Over the past twenty years, multiple studies reported numerical and experimental observations of high slenderness I-sections with compressive strengths much greater than predictions from the Direct Strength Method (DSM). These high strength sections generally featured flanges that were substantial relative to the web elements. Thus, the phenomenon was termed "strong flange" behaviour [1]. Despite these observations, most published literature did not address these high strength capacities as a singular related phenomenon and no explanation was accepted for why these sections exceeded the strength predictions.

Overconservative DSM predictions have been addressed in multiple previous instances. In 2012, Rossi and Rassmussen proposed a modification which increases the DSM prediction for stainless steel sections that develop loads greater than their fully plastic strength [2]. Lalthazuala and Singh proposed a modification in [3] to calculate higher strengths achievable by hybrid sections. These modifications, however, focus on sections in the low slenderness range. They provide no basis to explain why, for example, a section with high cross-section slenderness (e.g. $\lambda_l = 2$) and thick flanges may develop a strength 60% greater than the DSM prediction.

Uncertainty about the design of strong flange sections is compounded in the case of hybrid sections as they are frequently designed with the higher strength material in the flange. Experiments conducted by Chen et al. in [4] showed that hybrid sections under pure compression also exhibit characteristics of strong flange behaviour. Chan et al. extensively studied the local buckling in hybrid sections with strong flanges [5] and found that while the critical web plate did control local buckling, hybrid I-sections had greater normalized strengths than DSM predictions. They did not, however, explain why compressive strength is

underestimated by the DSM or to what extent the different material strengths in hybrid flanges influence the strong flange behaviour.

Stainless steel hybrid compression members have not been previously tested, leaving open questions about how the material's unique properties will affect behaviour. The primary motivation to investigate stainless steel structures is for increased durability relative to carbon steel alternatives, particularly in environments susceptible to corrosion, leading to reduced lifecycle cost [6]. Additional advantages include improved fire resistance [7], aesthetic desirability, and potential lifecycle CO_2 emissions reduction [8]. The non-linear stress-strain behaviour of stainless steel and extensive strain hardening can cause low-slenderness elements to develop stresses far greater than the yield stress. This characteristic of stainless steel can cause plates to develop widely different capacities in the case of strong flange sections where plates in the same section can have large differences in slenderness. The incorporation of stainless steel into hybrid sections also presents new challenges. For sections composed of multiple families of stainless steel or stainless steel connected to carbon or high strength steel [9, 10], the variable rates of thermal expansion and potential for bimetallic corrosion must be considered.

This thesis manuscript is the culmination of a 20-month project to investigate the strong flange behaviour of I-sections, with particular focus on the implications for design of hybrid sections. Independent of strong flange considerations, hybrid steel sections offer substantial structural advantages that are not fully realized, in part due to incomplete underlying research. Hybrid members are comprised of multiple steel grades in different elements of the cross section. This allows designers to select materials that are optimized for the demands placed on each element. Thus, structures can be designed more efficiently to meet service requirements, unlocking the potential to reduce cost, reduce emissions footprint, and improve performance.

Most hybrid research is focused on flexural loading applications for the simple fact that the load case leads to predictably non-uniform stress distributions that can be optimally accounted for by a hybrid design. In the case of compression for low-slenderness cross-sections, the uniformity of stresses gives minimal opportunity for efficiency increases with a hybrid design. When the slenderness is high enough that local buckling develops, however, the induced non-uniform stress distribution can be better managed by a well-designed hybrid section. In use cases where the limit state is controlled by ultimate strength – rather than serviceability limits that exclude local buckling – substantial structural efficiency gains can be achieved by hybrid members.

The design of both strong flange and hybrid sections is only possible with methods that contain information about the materials and dimensions of each individual member element. After all, the significant characteristic for these types of sections is that their constituent plates have different materials or slenderness. This is problematic for design methods like the DSM and CSM (Continuous Strength Method) which define a single slenderness and material strength to describe the whole cross section. To unlock the structural efficiency gains made possible in hybrid and strong flange sections, it is not sufficient to have only the theoretical characterization of their behaviour. It is also necessary to have sufficiently simple equations that enable a labour-efficient design process. Thus, it is a priority in this project to consider how methods like the DSM and CSM can be adapted to maintain design simplicity without overlooking the important advantages of hybrid and strong flange sections.

1.1. Description of the Project in Phases

Investigation into the strong flange behaviour was conducted in four phases: (1) literature review, (2) experiments, (3) numerical modelling, and (4) design method development.

The literature review phase included analysis of studies focused on four key areas: (1) the hypothesised strong flange behaviour and plate strength interactions in I-sections, (2) behaviour of fabricated I-sections under pure compression, (3) behaviour of hybrid sections, and (4) the development of design methods. For the first key area, a database was compiled of all I-section stub column compression tests available in the published literature. This database makes clear the gaps in existing experimental literature which needed to be filled to inform an understanding of the strong flange behaviour. Next, a survey of evidence for hybrid steel sections under compression was added. Because this field of the literature is more limited, studies on hybrid sections under flexure or combined loading were also reviewed. Finally, a detailed history and description of relevant design methods is compiled. The design methods primarily considered in this report are the Effective Width Method (EWM), Direct Strength Method (DSM), and Continuous Strength Method (CSM). Multiple non-codified methods and modifications proposed in published literature were also considered. At the conclusion of the literature review phase, Langone et al. published a paper in the 2024 Nordic Steel Conference proceedings which proposes a design methodology for hybrid I-sections based on the evidence compiled from existing literature [11].

In the second phase, stub column compression tests were conducted on welded stainless steel I-sections, including hybrid and homogeneous designs. Although there was no complete definition of what caused strong flange behaviour, the I-section specimens were designed based on the criteria proposed in [1] and [11] to ensure observation of a range of strong flange behaviours was likely. The stub columns were designed to ensure failure under local buckling modes, avoiding global buckling. Measurements were taken during the stub column tests for the applied load, end-shortening, and axial strains over time. A full three-dimensional strain field is measured on the web plate using digital image correlation. In addition to the stub columns, tensile coupons were tested to measure the material properties of the plates used in

the I-section specimens. The geometric imperfections of all stub column specimens were measured prior to the compression tests using an adapted CNC arm. Material properties and geometric imperfection measurements determined in the experimental phase were input parameters in the subsequent numerical investigations to develop a validated model of each stub column.

A numerical model of all stub column tests was created in the third phase using the finite element (FE) method in Abaqus Standard [12] to examine the effect of primary parameters on ultimate strength and buckling mechanisms. In this third phase, the geometric dimensions, material properties, and geometric imperfections measured in the experimental phase were reflected in the numerical model of each specimen. A residual stress model adapted from relevant literature was modelled as an initial stress field prior to the application of external loads. Imperfect initial contact between the column and loading platens in the experiments was accounted for in the numerical model by de-coupling the nodes of column and loading plate elements at locations initially out-of-contact. Extensive comparisons were made against the test results to validate that the numerical model properly approximates the physical reality. Finally, a parametric assessment was conducted modelling over 1,300 stub columns with nominal dimensions and material properties to test the effect of different geometries and materials on ultimate strength. The results of the numerical investigation provide further evidence of the strong flange behaviour and illuminate the specific parameters which contribute to it.

In the fourth phase, hypothesised descriptions of the strong flange behaviour were tested against the collected experimental and numerical evidence. A satisfying account is provided for what causes strong flange I-sections to reach greater ultimate strengths than DSM predictions, and a proposal was made for a modified design approach. The effect of hybridity on strong flange behaviour is considered based on the experimental evidence. The strong flange

I-section behaviour is described as a specific manifestation of two fundamental concepts in structural design: slenderness induced instability and interaction of connected elements. The case of strong flange behaviour brings attention to the differences between the three codified design methods considered in this paper: DSM, CSM, and EWM. The distinction between methods that address "whole section" slenderness and those which account for each element individually is emphasized. The new design approach proposed in this thesis aims to address the oversights of "whole section" design methods without entirely sacrificing their marked advantage of simplicity.

1.2. Description of the Thesis Manuscript Chapters

The past twenty months of investigations into strong flange and hybrid compression behaviour has produced two journal papers which will be submitted to the ASCE Journal of Structural Engineering. The first paper reports the procedure and results of stub column compression experiments. The second paper reports the results of the parametric assessment based on numerical modelling and design method developments. This thesis manuscript reproduces those two journal articles in their entirety, in Chapter 3 and Chapter 4, respectively. Each of these papers contains an introduction with the background information and literature summary relevant to its topic. The information covered in the journal articles was generally removed from the literature review in Chapter 2 to avoid redundance. Some instances of redundance were kept, such as reiterations of key equations that must be referred to in both journal articles. These cases are minimized, however, to make the thesis manuscript cohesive. Figures, tables, equations, and section labels are re-numbered according to their position within the thesis manuscript rather than the label assigned to them in the journal papers.

Literature review, background information, or analysis which is important to the development of this thesis but is not contained in the two journal papers is reported in

Chapter 2. This chapter provides additional background information including an expanded section on the buckling behaviour theory which informs the design methods analysed later in Chapters 3 and 4. A summary of all experimental evidence available in literature which is relevant to the behaviours studied in this thesis is also provided. These topics were necessary steps towards a wholistic understanding of hybrid and strong flange compression behaviour but did not fit within the length and scope constraints of journal articles. Chapter 2 also includes the conceptual insights first reported in the conference paper by Langone et al. [11]. While the conclusions in this paper were developed from limited available evidence, it advanced a design methodology which proved successful once tested against the experimental and numerical evidence produced later in this project.

Chapter 5 of this thesis provides a discussion of the implications for the findings in this project, as well as an opportunity to cover topics not immediately relevant to journal articles. For example, detailed recommendations are provided to improve the treatment of stainless steels in reliability assessments – findings which were inspired while completing the analysis for Chapter 4.5. The potential for wider adoption of hybrid and strong flange sections is discussed. In Chapter 5.5, the most important conclusions of the project are revisited.

2. BACKGROUND & LITERATURE SURVEY

2.1. The History of Hybrid Steel Structures

Since the popularization of structural steel in the 19th century, engineers have substantially broadened the shapes, sizes, and grades in which steel members are available. This allows designers to select members that are optimized for each application, making structures more efficient. I-profiles – particularly those with strong flanges – are geometrically best arranged to resist bending. Nonetheless, pure compression is the more fundamental loading form and the worst-case loading scenario for a member. Strong flange I-profiles are

characterised by flanges, usually in Class 1, that are significantly stronger and less slender than the web plate due to a combination of the plate dimensions and material strengths. Strong flange I-sections are of particular interest in this research as they have been shown to withstand loads much greater than multiple codified design predictions [1, 11].

Strong flange behaviour can be more common or more dramatic in hybrid designs due to the use of higher material strengths in the flanges. Hybrid steel members are fabricated, or built-up, and comprised of two or more types of steel in different plates. These hybrid members can, for example, include different grades of steel, combine stainless steel with carbon steel, or combine hot-rolled and cold-formed elements. Hybrid steel should not be confused with the very large adjacent literature on hybrid members which combine steel elements with other materials such as reinforced polymers of glass, carbon, other fibres, concrete, bamboo, etc. Hybrid steel members are fabricated by welding or bolting plates together. When the material properties of the plates are relatively similar, hybrid members can behave similarly to homogeneous steel members [13]. When properly designed, however, hybrid members optimize the placement of materials to efficiently withstand the stresses and strains specific to each plate. This optimization reduces the weight and environmental footprint of structures.

Most hybrid members are concerned with the optimized placement of material strengths. For example, hybrid I-profile girders are designed to have higher strength materials in the flanges than webs because the flange carries the greater portion of stresses under flexural loading. In addition, using a weaker material in the web reduces the webs vulnerability to local buckling – as will be shown in Chapter 3.8.1 with the determination of slenderness classes. By using a stronger material in the flange, the larger stresses are resisted using less material, while a cheaper and weaker material can be employed in the web. This common example is shown in Chapter 2.2. Hybrid member designs can also optimize for corrosion resistance of vulnerable elements. For example, in hybrid research from Yuan et. al. [10], connections are designed such

that elements exposed to weathering are made of stainless steel – for its corrosion resistant properties [6] – while less vulnerable elements are made of carbon steel to reduce cost.

The precise magnitude of the benefit of hybrid members varies greatly depending on what the hybrid design is compared to (e.g. an 'equivalent' homogenous design, or some other alternative). For context, in one design comparison the cost of a reference bridge was reduced by 6% by replacing S355 girders with S355/S690 hybrid girders. In another, the hybrid girders provided 15% savings [14]. Other benefits of hybridity are harder to quantify. For example, a hybrid column can be more expensive than a homogeneous alternative, but it may take up less space by relying on stronger material components to reduce the cross-sectional area. Hybrid members also pose several design and manufacturing challenges. The more optimized design of hybrid members corresponding to the anticipated applied stresses means that there are less strength reserves at full plasticity [13]. Additionally, welding different steel grades together adds manufacturing complexity, and different rates of thermal expansion in the joined materials can cause cracks and durability issues.

In the 1960s, American engineers developed the idea to further structural efficiency with a hybrid steel member to support bridges in a rapidly growing interstate highway system. Hybrid girders became common in both research and commercial applications for efficient flexure resistance. The earliest available literature on hybrid steel members dates to the 1960s and investigated design methods for I-profile girders [15, 16]. In 1968, the American Society of Civil Engineers (ASCE) and American Association of State Highway and Transportation Officials (AASHTO) released a joint study into the application of these hybrid girders for highway bridge design [17]. Hybrid steel compression behaviour was studied from 1969-1972 by researchers at Lehigh University [18, 19]. From this point, however, the study of hybrid members under pure compression was almost entirely neglected until 2020.

Table 1. Keyword searches in *Web of Science* digital archive.

	Keywords	Results
1	**Topic:** steel	640,059
2	**Topic:** "hybrid beam" OR "hybrid steel beam" OR "hybrid steel bridges" OR "hybrid plate girder" OR "hybrid steel columns" OR "hybrid I-profile" or "hybrid column" or "hybrid stub-column" OR "hybrid W-sections"	634
3	**Title:** concrete OR glass OR FRP OR GFRP OR "carbon fibre" OR timber OR aluminium OR CFRP	588,157
4	1 AND 2	184
5	(1 AND 2) NOT 3	72

A keyword search on Web of Science was completed to track the development of this research area over time. For searches by “topic”, all articles with the keyword in the title, abstract, or article/author keywords were returned. For searches by “title”, only results where the keyword is in the title were included. The Boolean operators of AND, OR, and NOT were used to combine and exclude searches for multiple keywords in different combinations. Table 1 shows the combination of keywords used to find the appropriately focused combination of papers. The focused search returned 72 sources relevant to hybrid steel beams and columns. Most of these 72 works have been produced since 2010. Also note that over 90% of the works in this field directly address hybrid girders, bending, or flexural loading – compared to less than 10% that directly address columns or compression.

Portions of hybrid behaviour in compression have been understood since the 1960s, when Nagarajarao et. al. found theoretical and experimental evidence that hybrid columns could be more cost efficient than their homogeneous counterparts within a certain column slenderness range [18]. Then, for nearly 50 years, no studies on compression behaviour in hybrid members were submitted into literature – with authors preferring to focus on flexural behaviour and the design of hybrid girders. In 2020, interest in compression re-emerged to fully understand the more fundamental loading pattern, and to support new commercial applications. In the

following literature review sections, the history of hybrid steel research will be tracked to highlight the findings from research on bending behaviour and explain the reemergence of compression research as a significant topic.

2.2. Hybrid Steel Girders

I-profile girders with strong flanges employed under flexural loading has long been the most simple and advantageous application for hybrid steel members. Girders are rigid members arranged horizontally which mostly support loads from smaller beams above them. Much of the available literature on hybrid structures pertains to girders, and the analysis completed to design hybrid girders provides some useful insights for analysing such members under compression. Hybrid girders are particularly useful because the distribution of stresses is predictable during flexural loading. The example of a simple bending problem in Figure 1 shows the maximum magnitude of pure bending stresses will always be in the flanges of the I-profile, where most material is adequately concentrated. This is why hybrid girders with strong flanges are by far the most common commercial application for hybrid members.

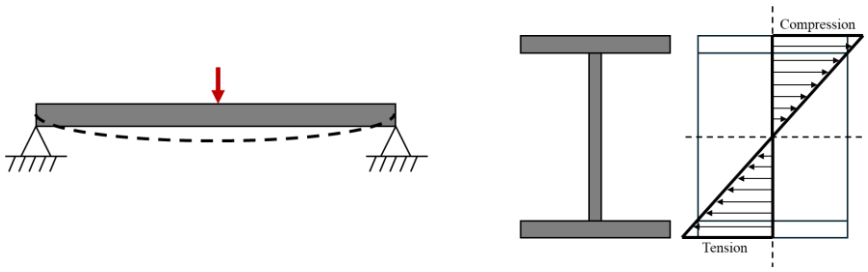


Figure 1. Bending stresses diagram for an I-profile beam under a simple loading condition.

All papers on hybrid steel members submitted into literature from 2000 to 2010 were concerned with girders and flexural loading. Early characterizations of hybrid I-profiles under bending estimated that hybrid girders would exhibit strengths somewhere between that of equivalent homogeneous profiles of the stronger and weaker material. Because bending stresses are mostly carried in the flange, the hybrid beam would more closely resemble the higher strength profile [13]. The vast literature focused on hybrid girders has also assessed the

appropriate requirements for web stiffeners [20, 21] and investigated specific loading types such as patch loading with a numerical study [22] and design recommendations [23].

The most cited paper from 2000 to 2010 on hybrid steel members made design recommendations for sections classification, bending, and fatigue resistance. Veljkovic & Johansson recommended that the class of the web be determined using the yield strength of the compression flange. They then noted that the difference in yield strength between web and flange and the initial partial yielding of the web will affect sections differently based on their classification [14]. Equations are provided to calculate bending resistance for each cross-section's classification. They also showed that local buckling in the web should not limit the fatigue resistance of hybrid girders. Their methodology of observing the distributions of stresses and strains in numerical simulations then developing equations to characterize the behaviour is a good blueprint for understanding hybrid members in compression.

From 2011 to the present, hybrid member research continued to focus on increasingly specialized conditions for hybrid girders. Experimental investigations also became more abundant in the literature [24] [25] [26]. Other studies were completed on the effects of elevated temperature and fire [27] [7], residual stresses were measured [26] [28], and the interaction of web shear buckling, local buckling, and lateral-torsional buckling modes was investigated [29].

2.3. Literature Survey of Fabricated I-Section Stub Column Tests

Prior to conducting new investigations, a literature survey of all previous research into fabricated I-sections under compression was completed to assess gaps in the published knowledge. A database of all welded I-profile stub-column compression tests in the literature was collected to investigate the applicability of different design methods. The database includes 92 I-profile stub-columns tests under pure compression gathered from 11 articles. I-sections that had bolted connections were omitted from the list [30]. Other papers excluded from the

list were those that did not provide a complete set of specified and measured dimensions and material strengths, including [31, 32, 33, 34, 35]. These values are required for analysing design predictions, and for completing a reliability assessment. A partial exception to this rule is made for Salem et al. because it includes some of the very few instances of strong flange behaviour in experimental literature. The experimental database includes mostly homogeneous carbon steel, high strength carbon steel, or stainless steel sections, and a minority of hybrid I-profiles. Table 2 lists the sources of experimental literature included in the database. The full compiled database is provided in Table A.1 in the Appendix.

Table 2. Sources of experimental literature on I-section stub columns.

Author, Year	Citation	Description	Author, Year	Citation	Description
Chen, 2023	[4]	Hybrid, HSS	Rasmussen, 1992	[36]	HSS
Davids, 1989	[37]	CS	Zhou, 2013	[38]	HSS
Su, 2021	[39]	HSS	Yuan, 2015	[40]	SS
Kuwamura, 2003	[41]	SS	Ran, 2022	[42]	SS
Saliba, 2013	[43]	SS	Gardner, 2016	[44]	SS
Salem, 2005	[45]	CS			

Carbon Steel (CS), High-strength Steel (HSS), Stainless Steel (SS), different grade in web and flange (Hybrid)

Figure 2 shows the experimental results from literature plotted alongside FE model results from Rossi & Li and the DSM nominal strength prediction curve. Rossi & Li's FE model was developed only for carbon steel using an elastic-perfectly-plastic material model. This explains why it did not predict column strengths greater than the fully plastic capacity in the low slenderness range, as was observed particularly in experiments of low-slenderness stainless steel columns. Rossi and Li's results are presented in greater detail in Chapter 2.5 on the strong flange behaviour. Chen, 2023, provides the only experiments that include hybrid steel members, with columns that combine high-strength steel with conventional carbon steel [4]. Additional evidence of hybrid steel behaviour under pure compression, observed in other section shapes, is provided in Chapter 3.1.

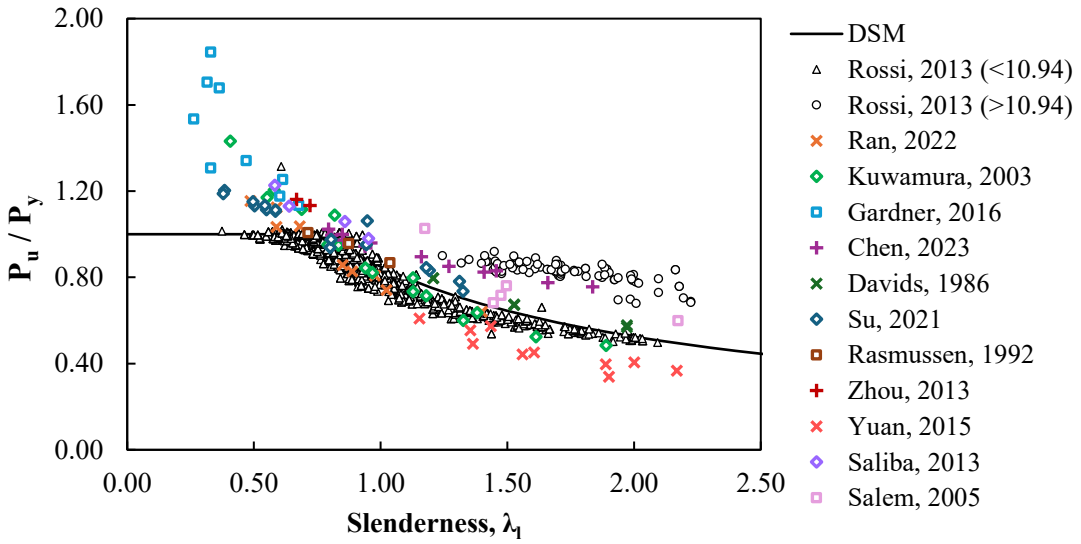


Figure 2. Normalized strength of I-section stub column compression tests by slenderness.

2.4. Theoretical Explanations of Compression Behaviour

Columns made from hot-rolled carbon steel, high-strength carbon steel, or stainless steel are susceptible to multiple strength limits. The controlling limit must be determined based on the material and geometric properties of the column. For members in pure compression, material failure, global buckling, local buckling, and the combination of them, must be considered. The case of failure under flexural and flexural-torsional buckling is not studied in this project due to the focus on stub columns where the effective lengths are too short, or adequately restrained in practice, to exhibit this failure. Global buckling of *perfect* hybrid sections, as well as homogeneous sections, is governed by Euler's theory including material elastic modulus, cross-section second moment of area, length of the column, and end conditions, as shown in *Eq. 1*. Geometrically imperfect elastic columns will exhibit Ayrton-Perry type buckling [46].

Hybrid sections are, however, much more susceptible to local buckling because of the higher material strengths included in the cross-section. It is particularly common in I-profiles for designs to include flanges that are much thicker and stronger than the web, which could lead to greater stresses and different relative end restraints on the webs. This extreme difference

in the strength of the walls causes some existing design methods to produce inaccurate design strength predictions – particularly in methods that do not provide a way to individually account for the material strength and slenderness of each element. Chapter 2.4.1 will discuss the interacting effects of plate elements within a member and Chapter 2.4.2 provides background on the quantification of strength reductions due to local buckling. These two characteristics are shown to substantially explain stub column buckling behaviour in hybrid and strong flange I-sections.

2.4.1. Buckling Coefficient for End Conditions

Because most practical I-profiles are designed with the web as the most slender element, much attention is paid to the buckling of the web plate. The foundational solution for the critical buckling stress of a plate comes from Bryan's formula of 1980 (*Eq. 2*) [47]. The plate buckling coefficient in Bryan's formula is assumed to be 4.0 for simply supported plates, and 7.0 for fixed-fixed end conditions. The simply supported assumption generally applies well to web plates in hot-rolled homogeneous I-profiles. In these formulas, E is the Young's modulus, I is the second moment of area, K is the end condition coefficient, L is column length, f_{cr} is elastic critical buckling stress, k is the plate buckling coefficient, μ is Poisson's ratio, t is the plate thickness, and b is the plate width.

$$P_{cr} = \frac{\pi^2 EI}{(KL)^2} \tag{1}$$

$$f_{cr} = k\frac{\pi^2 E}{12(1-\mu^2)}\left(\frac{t}{b}\right)^2 \tag{2}$$

While Bryan's formula with k = 4.0 works reasonably well for homogeneous profiles, hybrids are different because the stronger flange plates change the end conditions for the buckling problem in the web. To demonstrate this, consider an example I-profile with very substantial flanges modelled in CUFSM – an open-source finite strip analysis software. The critical buckling stress of the web plate was first calculated according to Bryan's Formula, then

through CUFSM when considering the plate with pin-pin ends, fixed-fixed ends, and with the flange providing the end conditions. The results in Table 3, show that the flange end conditions in this example section cause the web to buckle as if it has fixed ends. Table 3 also confirms that k = 4.0 is an accurate assumption for the simply supported condition.

Table 3. Web critical elastic local buckling stress calculated through four methods.

	Eq. 2 $\boldsymbol{k = 4}$	CUFSM Web (pin-pin)	CUFSM Web (fix-fix)	CUFSM w/ flange
$\boldsymbol{f_{cr}}$ $[\boldsymbol{MPa}]$	80.4	79.58	140.72	139.16

In 2010, Seif and Schafer addressed this topic and empirically developed equations to calculate the buckling coefficient k based on the section dimensions for multiple shapes [48]. A finite strip analysis was used to determine the true k value for sections in the AISC database. Then, predictive equations were developed by fitting a regression analysis that related k to the combination of geometric properties they determined. In the equation for I-profiles under axial compression, given in *Eq. 3*, note that height is defined as from the centre of top flange to centre of bottom flange.

$$\frac{1}{k_w} = \frac{1.5}{\left(\left(\frac{h}{t_w}\right)\left(\frac{2t_f}{b_f}\right)\right)^{2.5}} + 0.18 \tag{3}$$

$$1.80 \leq LD \leq 10.94 \qquad \text{with } LD = \left(\frac{h}{t_w}\right)\left(\frac{2t_f}{b_f}\right) \tag{4}$$

The reliability domain for *Eq. 3* is provided in *Eq. 4* in terms of the limiting normalized section dimension (LD). For sections where LD is greater than 10.94, the k expressions developed by Seif and Schafer should not be assumed applicable. This is particularly problematic for fabricated sections with slender webs and stocky flanges that exceed the geometrical range of studied hot-rolled catalogue sections.

The calculation of elastic local buckling stresses was further studied by Gardner et. al. in 2019 [49]. This research provided a method such that applicability was no longer limited to only hot-rolled sections or a narrow range of geometrical ratios while also adding consideration

of all elements into the cross section local buckling stress. Expressions were developed for the coefficient ϕ to represent the relative susceptibility of the web and flange plates to local buckling. When $\phi \geq 1$ the web is more susceptible to local buckling than the flange, as is expected for I-profiles. The coefficient ζ represents the amount of restraint provided to the critical plate by the surrounding plates, called element interaction. $\zeta = 0$ corresponds to simply supported end conditions, while $\zeta = 1$ corresponds to fixed-fixed. *Eq. 5-6* are the simplified forms of these equations applied specifically to I-profiles.

$$\phi = 0.108\left(\frac{2t_f}{b}\frac{h-t_f}{t_w}\right)^2 \quad (5)$$

$$\zeta = \frac{t_f}{t_w}\left(0.45 - \frac{0.3}{\phi^2}\right) \quad \text{if } \phi \geq 1 \text{ (web critical)} \quad (6)$$

$$\sigma_{cr,cs} = \sigma_{cr,p}^{SS} + \zeta\left(\sigma_{cr,p}^{F} - \sigma_{cr,p}^{SS}\right) \quad (7)$$

In *Eq. 5-7* above, the developed coefficients are combined to calculate the full cross-section local buckling stress. ϕ is calculated to determine which plate is critical. The lower bound ($\sigma_{cr,p}^{SS}$) and upper bounds ($\sigma_{cr,p}^{F}$) to the full cross-section local buckling stress value is determined by separately assuming simply supported and fixed end conditions. Finally, the element interaction coefficient determines where the correct solution lies relative to the upper and lower bound. $\sigma_{cr,cs}$ is the cross sections critical local buckling capacity. The research in this section from Bryan, Schafer, and Gardner has developed a strong foundation to understand the interaction between web and flange plates.

2.4.2. Effective Strength of Plate Elements

Members in pure compression can fail prior to developing their yield capacity or global buckling capacity due to local buckling instability. Strength reductions due to local buckling are generally represented as a function of slenderness, determined based on material properties and ratios of geometrical dimensions. One way to consider the problem of local buckling for an I-section under pure compression is to analyse the member as three distinct plate elements.

This assumption, neglecting interactions between the plates, is taken on in current forms of the effective width method codified worldwide, including America [50], Europe [51], China [52], Australia and New Zealand [53].

Seminal advancements in understanding the stability of plate elements took root in the early 20th century with the works of von Karman, Timoshenko, and Winter. The expansion of aeronautical industries (e.g. naval operations and air flight) in this period drove demand for thin metallic elements with high strength-to-weight ratios. The demand for increasingly thin plated structures supported efforts to understand the instabilities resulting from slenderness. With this historical backdrop, von Karman's study of thin-walled steel tubes in 1910 demonstrated that members can continue to develop greater strengths after local buckling. The concept of the effective width was developed based on the hypothesis that only portions of a buckled plate provide significant resistance. As contemporaries to von Karman, Timoshenko and Gere's *Theory of Elastic Stability* provided the mathematical basis to understand local buckling behaviour [54]. In 1932, von Karman showed that a variable stress distribution over a total width could be consistently approximated by a uniform stress over a smaller effective width b, as seen in *Eq. 8* [55]. That effective width is approximated as the function of plate thickness t, Young's Modulus E, and yield stress f_y, and Poisson's ratio ν. The term represented by B is the solution derived for simply supported ends on the thin plate, and solutions for other end conditions can be substituted in for this term.

$$b = Bt\sqrt{E/f_y} \qquad (8)$$
$$B = \frac{\pi}{\sqrt{3(1-\nu^2)}}$$

George Winter at Cornell University conducted local buckling experiments on thin plates and continued to develop the EWM for estimation of ultimate load capacity [56] through the 1940's. These developments lead to the Effective Width Method's inclusion in AISI standard in 1946 [57]. Winter's 1940 report to the National Advisory Committee for Aeronautics

specifically focused on the local buckling of wide flanges in beams [58]. Winter demonstrated that stresses in flange elements can become unevenly distributed when these elements are given considerable width and small thickness, as was already known for web elements. Winter argued that design methods for multi-element members "which treat the behaviour of the beam as a whole are concerned with special cases."

Winter's quoted insight that I-sections are a collection of plate elements – which must each have their own local buckling characteristics – is particularly helpful to keep in mind for the study of hybrid and strong flange I-sections. Approximated descriptions of a whole cross-section can fall short of explaining the behaviour of sections with unique geometric or material combinations.

In a review of the EWM published 25 years after its inclusion in AISI code, von Karman and Winter's theory was upheld based on evaluation using newly developed experimental evidence, computing technology, and reliability theory [59]. In modern codes, the relationship between the full plate width and the reduced effective width is defined by a reduction factor ρ, derived from greatly expanded experimental and numerical evidence. This approach has replaced the theoretical solution given in *Eq. 8* which represented the full width and effective width as independent. Nonetheless, the representation of a non-uniform stress distributions in locally buckled elements as a uniform distribution over a reduced width remains completely in place as the fundamental design insight.

2.5. Initial Observations of the Strong Flange Behaviour

In 2013, Rossi and Li studied the compression behaviour of hot-rolled I-sections [24]. They used a FE model to simulate stub column compression tests on over 1450 catalogued sections. The FE model was validated against experiments from the Semi Comp, 2007, project [38]. The numerical results identified a distinct group of sections exhibiting ultimate strengths

much higher than DSM predictions. The DSM of design is more completely introduced in Chapter 3.2.2. Rossi and Li made the connection that the high strength sections fell outside the applicability range of Seif and Schafer's 2010 analysis, given as $LD > 10.94$ in *Eq. 4*. This limiting dimension threshold is the ratio of I-profile dimensions that that the catalogued sections considered by Saif & Schafer did not exceed. The much larger sample of catalogued sections considered by Rossi & Li, however, did include sections beyond this threshold.

Figure 3 shows the two distinct behavioural groups discovered by Rossi and Li. The y-axis gives the column ultimate strength normalized by its nominal yield load. The x-axis is cross-sectional slenderness as defined for the DSM [50], given in *Eq. 36*. Based on the numerical results, Rossi and Li hypothesized that I-sections that exceed the *LD* threshold form a distinct behavioural category with increased ultimate strength performance. They predicted that for I-sections with $LD > 10.94$ the flanges approach their fully plastic capacity while the webs develop only the local buckling capacity. This design prediction is algebraically represented in *Eq. 42*, as discussed further in Chapter 3.2.4.

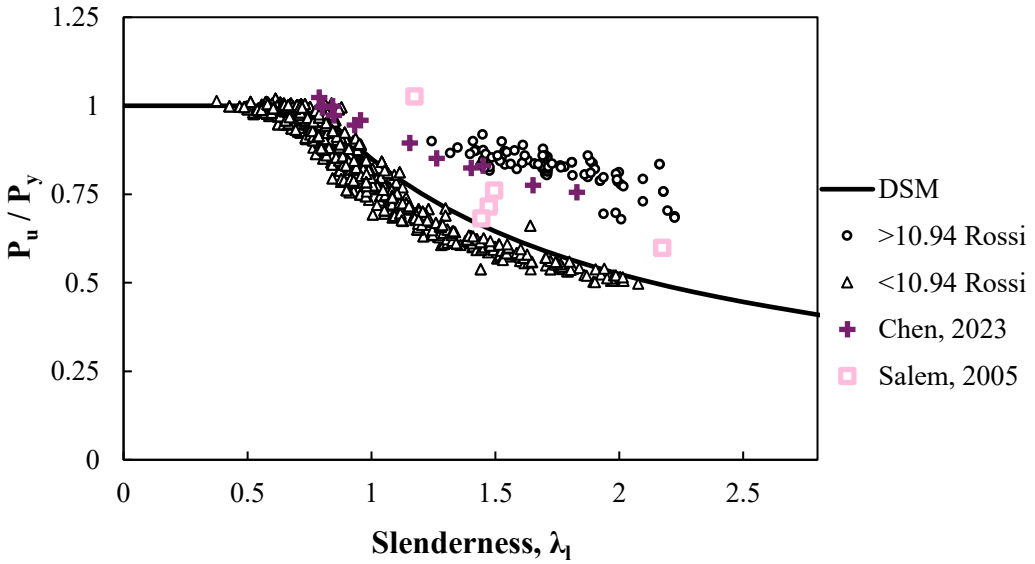


Figure 3: Evidence from literature of I-sections with *LD* > 10.94.

Tests conducted by Chen et al. [4] and Salem et. al. [45] are the only experiments available in literature which include I-sections with $LD > 10.94$. Chen and Salem did not

directly identify the results of their experiments as evidence of a distinct I-section behavioural category. However, their results are consistent with Rossi & Li's observation that sections with $LD > 10.94$ tend to exhibit ultimate strengths greater than the DSM prediction.

Rossi & Li's hypothesis of a distinct strong flange behaviour raises multiple questions. Why do sections with $LD > 10.94$ exhibit higher normalized ultimate strengths than those with $LD \leq 10.94$ at equal slenderness? Is the empirically set threshold of $LD = 10.94$ the best way to predict this behaviour? The experimental and numerical investigations in the following chapters aim to answer these questions.

For all subsequent uses in this thesis, strong flange behaviour is defined as the interaction between connected plates that occurs when the effective strength in the flanges is greater than the web effective strengths – resulting in larger ultimate strengths than would be predicted by "whole section" definitions of slenderness. The theoretical foundation established in Chapter 2.4 provides the basis to explain the strong flange behaviour in terms of element interactions, local buckling and material strain hardening.

2.6. Initial Design Method Developments from Langone et al., 2024 [11]

One principal disadvantage of the limiting dimensions used by Rossi and Li to distinguish strong flange behaviour is that it does not contain any material strength parameters. Thus, it has not opportunity to account for the unique characteristics of hybrid sections. In a 2024 conference paper, Langone et al. proposed an extension to the direct strength method which is more applicable to hybrid members [11].

The limiting dimension does not account for material strength because it was initially developed for hot-rolled sections that are homogeneous across the cross-section. The sections with the largest limiting dimensions tend to be Class 1 in the flange and Class 4 in the web. To

make a method applicable to hybrid sections, the yield strength in both the web and the flange must be independently incorporated to account for their separate effects on plate slenderness.

The slenderness ratio given in *Eq. 9* was developed to incorporate the different material strengths in hybrid sections, with $f_{y,w}$ and $f_{y,f}$ as the yield stresses in the web and flanges, respectively, in MPa. Both the limiting dimension and slenderness ratio produce similar results when compared against the ratio of predicted-to-observed strength. This is expected because the two produce identical results for non-hybrid sections, which is most of the available literature.

$$SlR = \left(\frac{h_w}{t_w}\sqrt{\frac{235}{f_{y,w}}}\right) / \left(\frac{(b_f - t_w)/2}{t_f}\sqrt{\frac{235}{f_{y,f}}}\right) \tag{9}$$

$$StR = \frac{2\, t_f\, b_f\, f_{y,f}}{t_w\, h_w\, f_{cr,w}} \tag{10}$$

For sections with very stocky flanges, it may not make sense to predict ultimate strength by comparing vulnerability to local buckling in the web and flange, as the limiting dimension and slenderness ratio do. Rather, Rossi and Li's equation (*Eq. 42*) for the ultimate strength of sections with *LD > 10.94* is designed based on effective strengths from the assumption that the web would locally buckle, and the flange would develop fully plastic capacity. The strength ratio, given in *Eq. 10*, was developed from this theory of the strength available in each plate. In *Eq. 10*, the critical elastic local buckling stress of the web, $f_{cr,w}$, can once again be calculated in multiple ways. A numerical method such as CUFSM is most desirable, and the most suitable analytical solutions are the methods from Schafer [48] or Gardner [49]. The two parameters, slenderness ratio and strength ratio, captured an approach to understanding and predicting the strength of fabricated sections with strong flanges.

It is already evident in Figure 3 that there is a clear change in section behaviour when the slenderness ratio exceeds 10.97. Sections with *SlR* above the limiting dimension tend to exceed DSM strength predictions by 20-60%. But once the critical threshold is exceeded, higher values

for the slenderness ratio are not strongly correlated with greater deviation from DSM predictions. It appears that the slenderness ratio is successful in identifying a critical threshold to classify section behaviour but is not well suited to make precise modifications for predicted strengths because of this weak correlation.

The ratio of web local buckling strength to flange fully plastic strength (i.e. the strength ratio) is substantially correlated with deviation from the DSM prediction. The ratio of DSM predicted strength-to-numerically determined strength from Rossi and Li's data formed a linear trend when plotted against the strength ratio. It was therefore hypothesized that a new prediction for section strength can be expressed as a function of the existing DSM prediction, strength ratio, and an empirically derived coefficient to represent their relationship. The slope of the linear trend was taken as the initial hypothesis for this coefficient. The intercept was forced through $y = 1.0$. Using the coefficients from the trendline, DSM equations are established, as discussed further in Chapter 3.2.4. The methodology used to represent the relationship for this trend is explained more completely in Chapter 3.8.2.

An initial assessment of design performance demonstrated that for the codified DSM, the average ratio of predicted-to-observed strength for strong flange sections was 0.72 with standard deviation 0.06. The modified DSM equation improved this performance to an average of 0.96 and standard deviation of 0.09. Additionally, no notable outliers were generated by the modified DSM equation.

There was some conflict in the data as the experimental results from Chen et al. [4] seemed to suggest a different trendline than the FE results from Rossi and Li [1]. The trend from Rossi and Li's data was followed as a preliminary hypothesis, but it was clear that further experimental and numerical evidence was needed to properly assess this method; this is why collecting these two types of evidence forms the majority of the work presented in this thesis. Chapters 3 and 4 of this thesis provide the experimental and numerical investigations

completed following the initial paper by Langone et. al [11]. The additional experimental and numerical evidence, combined with the conceptual insights achieved in [11], ultimately produce the modified DSM formulation endorsed in the conclusion of this thesis.

2.7. Detailed Description of Reliability Assessment Methods

Further explanation is provided here of the American code method used in Chapter 4.5 to assess reliability of the design method proposed in that chapter. A parallel description of the Eurocode method is also provided here. In Chapter 5.1, these methods are contrasted and two limitations for the treatment of stainless steels are discussed.

2.7.1. American Standards for Reliability Assessment

The American reliability assessment standard described here is provided in AISI S100-16 (2020) [50]. Analysis of structural performance reliability is based on the *rational engineering analysis* to determine a resistance factor or safety factor, which is done through the statistical assessment of variation among the test results of comparable structures. A slightly simplified equation to calculate ϕ is given in the commentary of AISC 370-21 [60] where the factors C_p and C_c are omitted. The only alternatives to these methods are (1) using safety factors established in the code within their applicability limits or (2) to produce three, or more, tests of structures/members *identical* to the one being designed. AISI S100-16 encourages the use of Load and Resistance Factor Design (LRFD), calculated by *Eq. 11* where γ_i is the load factor, Q_i is the load effect, R_n is the nominal strength, and ϕ is the resistance factor obtained through *Eq. 12*.

$$\sum \gamma_i Q_i \leq \phi R_n \tag{11}$$

$$\phi = C_\phi (M_m F_m P_m) e^{-\beta_0 \sqrt{V_M^2 + V_F^2 + C_P V_P^2 + V_Q^2}} \tag{12}$$

In *Eq. 12*, the quantifies the probability of failure targeted by the code. For compression members, the reliability index is β_0=*2.5*, corresponding to a target probability of failure of 0.62%. The general equation to determine the parameter β_0 is shown in *Eq. 13*. R_m is the mean nominal resistance, Q_m is the mean nominal load effect, and V_R and V_Q are the coefficient of variation (CoV) for resistances and load effects, respectively.

$$\beta = \frac{ln(R_m/Q_m)}{\sqrt{V_R^2+V_Q^2}} \tag{13}$$

From *Eq. 12*, the parameters with subscript "m" are the mean values of all tests in the dataset for the measured-to-specified ratio for yield stress (M_m), the actual-to-specified ratio for the relevant geometrical property (F_m), and the observed-to-predicted ratio for strength (P_m). The parameters V_m, V_F, and V_P are the CoV for each of these measurements. V_Q is a function of a comparison between dead and live loads which considers both their magnitude and variation. The value of V_Q for reliability assessment of a compression member with an unknown general use case for loading is given in the code as 0.21 for LRFD. C_p is a coefficient for the sample size of the reliability assessment database, calculated in accordance with *Eq. 14* where n is the number of tests and $m = n - 1$. The only remaining parameter of *Eq. 12* is an empirically derived calibration coefficient C_φ, given in the code as 1.52 for LRFD. In addition to *Eq. 12*, the correlation coefficient C_c, given in *Eq. 15,* is calculated to quantify the level of agreement between the resistance function and the experimental results. The C_c value must be greater than 0.8 for the rational engineering analysis method to apply. Additionally, the square of the correlation coefficient, C_c^2, is equal to the proportion of variance in experimentally observed strength which is predicted by the theoretical resistance equation. $R_{t,i}$ is the experimentally observed strength of sample i and $R_{n,i}$ is the nominal resistance prediction for sample i, and n is the number of samples.

$$C_p = \begin{cases} \frac{\left(1+\frac{1}{n}\right)m}{m-2} & for\ n \geq 4 \\ 5.7 & for\ n = 3 \end{cases} \quad (14)$$

$$C_c = \frac{n\sum R_{t,i}R_{n,i} - (\sum R_{t,i})(\sum R_{n,i})}{\sqrt{n(\sum R_{t,i}^2) - (\sum R_{t,i})^2}\sqrt{n(\sum R_{n,i}^2) - (\sum R_{n,i})^2}} \quad (15)$$

Codified resistance factors for the DSM and EWM are included in the AISI standard. However, some of the hybrid and strong flange I-profiles investigated in this research violate the material and geometric applicability limits provided in the code. Nonetheless, these values are still a useful benchmark for comparison. The AISI standard for cold-formed steel defines a resistance factor of $\phi_c = 0.85$ for LRFD with the DSM and EWM [50]. The AISC standard for stainless steel provides $\phi_c = 0.90$ for LRFD with the EWM [60].

2.7.2. Eurocode Standards for Reliability Assessment

Similar to the American code, the Eurocode calculates design resistance r_d by dividing the nominal resistance r_n by a safety factor γ (called a partial factor in the Eurocode due to the nature of the method employed), as seen in *Eq. 16*. Eurocode rules for reliability assessment come from EN1990 – Basis of Structural Design [61]. The probability of failure is tied to a probability function based on structural resistance and effects (or loads), as seen in *Eq. 17* where Φ is the cumulative distribution function (CDF) of the standardized normal distribution, R is the structural resistance, E is the load effects, and β is the reliability index. *Eq. 18* demonstrates that the equations provided in the code and the minimum Eurocode reliability index of β=*3.8* for a 50-year design life targets a probability of failure of 0.12%, making it substantially more conservative than the American code.

$$r_d = \frac{r_n}{\gamma} \quad (16)$$

$$P_f = p(g \leq 0) = P(R \leq R_d) = \Phi(-\alpha_R \beta) \quad (17)$$
$g = R - E$ and α_R: sensitivity factor provided in code

$$P(R \leq R_d) = \Phi(-\alpha_R \beta) \quad (18)$$
$$P(R \leq R_d) = \Phi(-0.8 * 3.8)$$

$P(R \leq R_d) = 0.12\%$

Calculating the partial factor γ is based on a multi-step statistical analysis, rather than a single equation like in the American method. The first step is to develop a linear relationship between the experimentally observed resistance r_e and the theoretical resistance from the design method r_t. The slope determined by the least squares regression of that linear relationship is b, seen in *Eq. 19*. A series of statistical properties are calculated based on the experimental results and theoretical predictions, as shown in *Eq. 19-24* where most variables are intermediate steps in the calculation of V_δ, which is the CoV for the error term. δ_i is the error term for test i, Δ_i is the logarithm of the error term for test i, and $\bar{\Delta}$ is the mean logarithm of the error term for all tests, and s_Δ is the standard deviation of the Δ_i terms.

$$b = \frac{\sum r_e r_t}{\sum r_t^2} \tag{19}$$

$$\delta_i = \frac{r_{e,i}}{b\, r_{t,i}} \tag{20}$$

$$\Delta_i = \ln(\delta_i) \tag{21}$$

$$\bar{\Delta} = \frac{1}{n}\sum_{i=1}^{n} \Delta_i \tag{22}$$

$$s_\Delta^2 = \frac{1}{n-1}\sum_{i=1}^{n} (\Delta_i - \bar{\Delta})^2 \tag{23}$$

$$V_\delta = \sqrt{exp(s_\Delta^2) - 1} \tag{24}$$

Fractile factors $k_{d,\infty}$ and $k_{d,n}$ are determined from tabulated values in EN1990 based on the value of n the number of samples in the database n. The following coefficients quantify the strength of the relationship between theoretical resistance function and observed values. First, the CoV for all basic variables must be determined. In the case of the effective width method for compression, the basic variables are yield strength and cross-sectional area. Therefore, V_{geom} and V_{fy} are determined as the CoV of geometrical dimensions and yield strengths for the samples in the considered experimental database. In the series of equations *Eq. 25-32*, Q_{rt} is the theoretical effects, Q_δ is the error effects, and Q is the combined effects.

$$V_{Xi} = \{V_{geom}, V_{fy}\} \quad (25)$$

$$V_{rt}^2 = \sum_{i=1}^{j} V_{Xi}^2 \quad (26)$$

$$V_r^2 = V_\delta^2 + V_{rt}^2 \quad (27)$$

$$Q = \sqrt{ln(V_r^2 + 1)} \quad (28)$$

$$\alpha_{rt} = \frac{Q_{rt}}{Q} \quad (29)$$

$$Q_{rt} = \sqrt{ln(V_{rt}^2 + 1)} \quad (30)$$

$$\alpha_\delta = \frac{Q_\delta}{Q} \quad (31)$$

$$Q_\delta = \sqrt{ln\left(V_\delta^2 + 1\right)} \quad (32)$$

The design resistance of a given section is calculated based on the theoretical resistance function given in *Eq. 33* for the EWM, where ρ is the width reduction factor. The design resistance is modified by the coefficients listed in this section, as seen in *Eq. 34*. Evidently, the partial factor is a function of the nominal resistance divided by the calculated design resistance. The nominal resistance is determined directly from the resistance function $g_{rt}(X_m)$.

$$r_t = \begin{cases} \text{if Class 1, 2, or 3} & A_g\, f_y \\ \text{if Class 4} & \rho\, A_g\, f_y \end{cases} \quad (33)$$

$$r_d = \mathrm{b} g_{rt}(X_m) \exp(-k_{d,\infty}\alpha_{rt}Q_{rt} - k_{d,n}\alpha_\delta Q_\delta - 0.5Q^2) \quad (34)$$

$$\gamma_M = \frac{r_n}{r_d} \quad (35)$$

In the Eurocode, different partial factors govern different types of failure. Because this research is concerned with cross-sectional behaviour (yielding and local buckling), the γ_{M0} factor is most relevant. For carbon steel, $\gamma_{M0} = 1.0$ is provided for the effective width method in EN1993-1-1 [62] and EN1993-1-3 [63]. For stainless steel, $\gamma_{M0} = 1.1$ is given in EN1993-1-4 [64]. When calculating the partial factor for stainless steel members per EN1990, it is common in literature to determine different partial factors for the different families of stainless steel, even though the only codified factors encompass all stainless steels [65].

3. TESTS OF HYBRID STRONG FLANGE I-SECTIONS UNDER COMPRESSION

Abstract

Hybrid I-sections are frequently designed with slender webs and thick flanges, and greater material strength in the flanges. This paper aims to understand the effect of hybridity on strong flange sections under the fundamental load case of pure compression. We present the procedure, results, and analysis for the first instances of stub column tests on hybrid stainless steel I-profiles, including those exhibiting strong flange behaviour. Thirteen compression tests are completed. The tested sections are comprised of web and flange plates made from a combination of austenitic and duplex stainless steels and carbon steel, fabricated by TIG welding. Tensile coupon tests are conducted on each constituent plate to measure material properties. Geometric imperfections for the web and flanges of each column are measured by pairing an adapted CNC machine with a linear variable differential transformer. The stub columns are compressed under a constant displacement rate while strains are measured at multiple locations using a video extensometer alongside digital image correlation. A finite element model of the compression tests is developed in Abaqus and validated against the experimental results. The influence of individual geometrical and material properties on buckling mechanisms and ultimate strength is analysed. Codified recommendations for the optimal hybrid ratio of members are reviewed for the case of compression loading. The Effective Width Method, Direct Strength Method, and Continuous Strength Method of design are evaluated based on the test results and all are found to be substantially conservative. The experimental results in this paper provide the basis to develop a new DSM equation that accounts for the behaviour of hybrid strong flange I-sections.

3.1. Introduction

Hybrid steel members – made up of two or more plates of different steel grades welded together – provide the possibility to select material properties that best meet the demands on each member element. Properly designed hybrid members can have highly desirable performance characteristics, including greater ultimate strength and the ability to influence local buckling and ductility characteristics [66].

Hybrid carbon steel members have existed in construction practice for over 50 years and have been rather extensively studied. In this time, they have been employed predominantly in bridges as I-profile girders submitted to compression and/or bending – with stronger material in the flanges to resist the high stresses furthest from the neutral bending axis. Today's body of research from over 120 publications on hybrid girders under flexure is well summarized by Terreros-Bedoya et al. in [67].

Provisions which accommodate the design of hybrid members are still rare in current design codes and tend to exclusively focus on carbon steel hybrid girders under flexure. This is, at least in part, driven by a shortage of experimental evidence needed to validate numerical models and assess the applicability of design methods. The AASHTO Bridge Design Specification [68] and EN 1993-1-5 [51] each contain rules for the design of hybrid girders. These codes give different guidelines for the allowable hybrid ratio i.e. yield strength of the flanges divided by that of the web ($f_{y,f}$ / $f_{y,w}$). AASHTO requires web elements to have a yield strength of at least 70% of the flange yield strength or 250MPa, whichever is greater [68]. This limit was developed based on research by Frost in the 1960's [15], an ASCE experimental report [17], and I-girder tests by Mozer et al. [69]. Conversely, the Eurocode recommends a hybrid ratio $\leq$2.0, and states that the value of ε used to calculate effective area of the web must be based on the f_y of the compression flange. This standard was developed based on an additional 35 years of experimental evidence and design recommendations provided by

Veljkovic & Johansson [14]. The recent publication by Terreros-Bedoya et al. [67] concludes that the optimal and safe hybrid ratio for flexural members is 1.3-1.6.

Noteworthy, compression resistance is fundamental and the worst-case loading condition to understand before addressing flexure [70]. However, the cumulative body of research on hybrid steel members under compression, as summarized in Table 4, is limited and concentrates on rather complex cross-sectional shapes. The dividing lines in Table 4 demarcate groups of directly related papers.

Table 4. Literature addressing the behaviour of hybrid steel sections under compression.

Author	Year	Evidence Type	Shape
NagarajaRao et al. [18]	1969	Test	I-section
NagarajaRao et al. [19]	1972	Test	I-section
Zhao et al. [71]	2004	Test	Bespoke
Binh et al. [72]	2004	Numerical	Bespoke
Rhodes et al. [73]	2005	Test	Bespoke
Javidian et al. [66]	2016	Test + Numerical	Bespoke
Farmani et al. [9]*	2023	Test + Numerical	Bespoke
Lalthazuala & Singh [3]*	2020	Numerical	I-section
Liu et al. [70]	2022	Test + Numerical	T-shape
Liu et al. [74]	2022	Test + Numerical	T-shape
Chen et al. [4]	2023	Test	I-section
Chen et al. [5]	2023	Numerical	I-section
Bock et al. [75]*	2023	Numerical	I-section

* includes stainless steel elements or members.

Hybrid steel members under compression were first investigated in 1969 by NagarajaRao et al. [18]. With theoretical and experimental evidence, they concluded that hybrid columns could be more cost efficient than their homogeneous counterparts within a certain slenderness range [19]. Following those tests, hybrid columns were not investigated for a period of 30 years until Zhao et al. [71] re-opened the topic to assess whether a hybrid design could be used to produce structurally efficient high-capacity columns. The authors studied a complex, bespoke design for hollow square and triangular columns (based on by Aoki & Ji [76]) – placing ultra-high strength circular tubes on the corners (f_y=1350 MPa) welded to mild steel plates on the

sides (f_y=350 MPa). Binh et al. developed a finite element (FE) model corresponding to Zhao et al.'s experimental specimens [72], and Rhodes et al. proposed the corresponding design analysis procedure [73]. The conclusive paper by Javidan et al. [66] showed that this hybrid design combining hollow sections and plates improved both the ultimate strength and ductility characteristics. Farmani et al. investigated similar tube/plate structures focusing on the fire resistance of UHSS (ultra-high-strength steel, >1200 MPa) tubes welded to plates of austenitic stainless steel [7], then analysed the effects of fire on the hybrid columns proposed by Zhao et al. [9]. Although incredibly interesting and promising, this series of papers focusses exclusively on the specific bespoke design and does not explore the potential of more practical hybrid concepts, suitable for mainstream structural engineering applications such as I-profiles. Nevertheless, the tests by Zhao et al. and the subsequent related investigations made clear that design guidelines and behavioural descriptions developed for hybrid sections needed improvements, particularly for pure compression. Importantly, the studied sections included materials with yield strength differences of approximately 3 times. This is far outside the range allowed by codes [71, 66], and much greater than the optimal ratio of 1.3-1.6 recommended by Terreros-Bedoya et al. [67] for flexural members. This disparity provides standing to assume that the optimal ratio is likely to be very different for hybrid members under compression.

In 2022, local buckling of hybrid HSS (high strength steel, *>460 MPa*) columns was studied by Liu et al. who conducted experiments on T-section stub columns with HSS in the web and assessed the applicability of three design methods [70]. They found that the Direct Strength Method (DSM) provided accurate yet conservative predictions while the Continuous Strength Method (CSM) was conservative for slender sections. Later, in 2023, Chen et al. published three studies on hybrid I-profile columns. The first study described welding effects on hybrid sections and proposed a new residual stress distribution model [28]. The second reported experiments on twelve hybrid I-section columns [4] and described a FE model which

was validated against the tests. Third, in [5], a parametric assessment focused on local buckling behaviour confirmed that the critical plate element – defined as the plate with the lowest elastic local buckling stress – governed local buckling behaviour and that interaction between web and flange plates was significant in the studied body of hybrid I-sections. Among these studies, most of the existing experimental evidence on hybrid sections in compression revolves around HSS – particularly for increasing the ductility of sections with HSS and assessing the applicability of design methods to these materials.

Despite initial costs approximately four times greater than carbon steel alternatives, stainless steel presents the advantage of excellent corrosion resistance, which can lead to lower lifecycle impacts (both financial and in CO_2 emissions accounting) compared to carbon steel equivalents [8, 77, 6]. The non-linear stress-strain properties of stainless steels affect their buckling behaviour [78]. For this reason, stainless steel I-sections were tested in compression by Yuan et al. focusing on local-overall interaction buckling [40] and Gardner et al. & Ran et al. focusing on laser welded sections [42, 44]. These studies, however, do not cover the behaviour of hybrid stainless steel members which, due to their non-linear material properties, must be considered separately from the behaviour of hybrid carbon steel. Two recent studies do focus on hybrid stainless steel sections in compression or in bending, however, neither presents experimental evidence. Bock et al. numerically modelled hybrid stainless steel sections in compression and bending and extended the CSM to the design of hybrid austenitic and duplex girders [75]. Lalthazuala and Singh proposed a new form of the DSM for hybrid stainless steel columns based on a numerical study [3], but the proposed modification focused only on design accuracy in the low slenderness range.

Last, of all the papers mentioned in this state-of-the-art, none specifically focusses on the compression behaviour of I-profiles characterised by strong flange behaviour; this is a distinct behaviour identified by Rossi & Li in 2013 based on FE models of over 1,450 hot-rolled carbon

steel I-profile stub columns [1], as is explained further in Chapter 3.2.4. Because most hybrid I-sections are designed with thick flanges made of the stronger material compared to the web, these sections can exhibit unique behaviour termed “strong flange” when the difference in plate strengths is large [11, 1].

This paper reports the findings from thirteen stub column compression tests. Among these columns are ten hybrid and three homogeneous sections. The columns include eight hybrid stainless steel I-sections and two stainless steel/carbon steel hybrids – the first experimental evidence for these categories. The local buckling behaviour of each column is studied, including those exhibiting strong flange behaviour, and the ultimate strengths are reported. The test results are used to validate a FE model and to assess applicability of the EWM, DSM, and CSM for hybrid stainless steel I-profiles under compression.

3.2. Design Methods

3.2.1. Effective Width Method

The EWM of design groups sections into four classes based on criteria which categorize their propensity to be affected by local buckling. Sections in Class 1 or 2 are those able to develop their full yield moment capacity M_p, however without sufficient ductility to allow for moment redistribution in Class 2. Local buckling will prevent Class 3 sections from developing more than their yield moment M_y. Sections in Class 4 will not reach the yield strength in any fibre of the section because of the strength reduction that results from local buckling. The slenderness classification criteria given in EN 1993-1-4 [64] for stainless steel and EN 1993-1-1 for carbon steel [62] are primarily affected by the width-to-thickness ratio of each plate composing the cross-section, although material properties and the distribution of stresses within the element also have an effect. The EWM, originally proposed by von Karman in 1932

[55], assumes that the reduced strength of any locally buckled plate can be represented by a reduced width which now reaches its full yield strength.

No modifications to the EWM are necessary to design for hybrid I-profiles, as the method already allows each plate to have its own material property parameters. In fact, EN 1993-1-5 [51] provides some EWM recommendations for hybrid girder design, which are further analysed in this paper, even though, strictly speaking, these are not applicable to hybrid members in pure compression [71, 4]. Similarly, even if the slender web of an I-profile is classified as Class 4 the code still allows the flanges (provided they themselves remain Class 1-3) to be taken at full yield strength, and it ensures that hybrid I-profiles exploit the best of both slender web and stocky flanges.

3.2.2. Direct Strength Method

The DSM was introduced by Schafer in 1998 as an alternative to the EWM, specifically for the design of cold-formed steel (CFS) thin-walled cross-sections [79]. It was originally developed to account for the distortional buckling mode and to simplify calculations for complex shapes with folds and stiffeners where traditional methods (e.g. EWM) reach their limit. The DSM is codified in AISI S100-16 [50] for cold-formed steels. However, many authors have studied its applicability to other manufacturing methods. In particular, Kwon proposed a DSM extension for welded sections in [35], Rossi for hot-rolled sections in [1], Lalthazuala for hybrid stainless steel sections in [3], and Chen found that the current DSM does not apply to hybrid HSS sections in [4]. The core assumption of the DSM is that ultimate strength is a direct function of the section's elastic critical buckling loads – local, distortional, and global buckling – and the yield load [80].

$$\lambda_l = \sqrt{P_{ne}/P_{crl}} \tag{36}$$

$$if \quad \lambda_l \leq 0.776 \quad P_{nl} = P_{ne} \tag{37}$$

$$if \quad \lambda_l > 0.776 \quad P_{nl} = \left[1 - 0.15\left(\frac{P_{crl}}{P_{ne}}\right)^{0.4}\right]\left(\frac{Pcrl}{P_{ne}}\right)^{0.4} P_{ne} \tag{38}$$

The AISI code provides *Eq. 36*-38 to calculate the nominal axial strength for local buckling P_{nl} in compression members without holes. P_{ne} is the nominal global column strength and P_{crl} is the critical elastic local buckling load. The DSM is a simpler alternative to the EWM as it is based on gross cross-sectional properties, rather than considering each individual plate's propensity for local buckling. The DSM slenderness, given in *Eq. 36,* is calculated based on the critical local buckling load. If the simplifying assumption is made that the nominal global column strength P_{ne} is equal to the yield load P_y, a valid assumption when studying the cross-section behaviour in pure compression, then the relationship between slenderness and normalized strength can be represented by a single curve – as seen later in Figure 11. I-section dimensions are labelled in the Figure 4a diagram.

Since the DSM relies on gross-section properties and a single slenderness parameter, it cannot distinguish the higher yield capacity or post-buckling strength contributions of strong, stocky flanges independently. To extend the DSM to the design for hybrid sections, the cross-sectional slenderness λ_l could still be determined numerically or analytically (e.g. a conservative simplification could assume that the critical local buckling stress σ_{crl} is governed by the most slender element, which is the solution used in this paper). When the section resistance is calculated as a function of the yield strength and gross area, the net yield strength is taken as an area-weighted average of the constituent plates to account for hybridity, as shown in *Eq. 39* where $f_{y,w}$ and $f_{y,f}$ are the yield stresses in the web and flange, respectively. However, this procedure still needs to be validated to ensure it effectively captures the true strength contribution of strong flanges.

$$P_y = \left(2\, f_{y,f}\, t_f\, b\right) + \left(f_{y,w}\, t_w\, h_w\right) \tag{39}$$

3.2.3. Continuous Strength Method

As an alternative to the method of discrete section classifications, the CSM was developed in 2008 [81]. It is based on a continuous relationship between cross-section deformation capacity and slenderness defined based on empirical evidence from stub column tests accounting for inelastic buckling, imperfections, residual-stresses and post-buckling behaviour. To design sections with the CSM, the cross-sectional slenderness $\lambda_{p,cs} = \sqrt{f_y/\sigma_{crl}}$ is first computed, based on σ_{crl} determined either numerically or analytically. To be clear, $\lambda_{p,cs}$ is different from λ_l defined in *Eq. 36* because of the difference between P_y and P_{ne} defined in the DSM. Gardner et al. propose a method to determine the local buckling stress of the whole section analytically in [49]. Considering the plates individually, however, is conservative and, in many cases, simpler. Based on the defined empirical relationship, the deformation capacity is found corresponding to the calculated slenderness.

The CSM for stainless steel design was expanded by Afshan and Gardner in 2013 [82]. The method has been adapted in the AISC 370-21 [60] and prEN 1993-1-4, although these codes do specify slightly different coefficients and applicability limits throughout the method. Stainless steel codes have adapted the CSM more readily for its more accurate consideration of strain hardening.

The CSM extension proposed by Bock [75] is used to design hybrid sections in this paper, which calculates effective section properties ($f_{y,eff}$, $\varepsilon_{y,eff}$, $E_{sh,eff}$) as an area weighted average of the properties of the constituent plates. The local buckling stress is determined from the stress-strain curve defined by a bi-linear elastic material model – based on calculated effective section properties for hybrid sections [75] – and the calculated deformation capacity. Provisions are also made to allow the use of the Ramberg-Osgood material model [60, 64]. Moreover, the use of area weighted effective properties naturally elevates the overall effective

yield stress of the hybrid section which was proven effective in [75]. However, it is yet to be fully validated for sections characterized by strong flange behaviour.

Another limitation of the CSM is that the recommendations from AISC 370-21 [60] and prEN 1993-1-4 do not include values for the material modelling constants for carbon steel. As an extension of the CSM to hybrid profiles with stainless and carbon steel, the method given in [48] could be applied to overcome this issue.

3.2.4. Strong Flange Behaviour

In 2010, Seif & Schafer's study on the local buckling of standard hot-rolled steel I-sections found that the web critical buckling stress was strongly correlated with a ratio of the profile's geometric dimensions [48], namely *LD* for "limiting dimension" defined in *Eq. 40b*. A regression was fit to empirically determine the relationship between *LD* and the web buckling coefficient k_w, *Eq. 40a*. However, the relationship quantified by *Eq. 40a* is only applicable to the range of I-profile sections included in their study defined in *Eq. 40b*. Bryan's buckling formula (*Eq. 41*) [47] could then be used to estimate the critical buckling stress of the web plate – which now accounts for the geometry of the web and its flange restraints.

$$\frac{1}{k_w} = \frac{1.5}{\left(\left(\frac{h_c}{t_w}\right)\left(\frac{2t_f}{b}\right)\right)^{2.5}} + 0.18 \tag{40a}$$

$$1.80 \leq LD \leq 10.94 \text{ with } LD = \left(\frac{h_c}{t_w}\right)\left(\frac{2t_f}{b}\right) \tag{40b}$$

h_c is the height of the section measured between the centre of the flanges.

$$\sigma_{crl} = k\frac{\pi^2 E}{12(1-\mu^2)}\left(\frac{t}{b}\right)^2 \tag{41}$$

Since hybrid I-sections typically use thick flanges made from the higher-strength material, they can display pronounced strong flange behaviour [11, 1]. This behaviour was first described in 2013 by Rossi & Li who used the FE method to simulate the behaviour of over 1,450 hot-rolled carbon steel I-profiles in pure compression [1]. They detected a clear

difference in ultimate strength depending on whether the limiting dimension was above or below 10.94.

Rossi and Li observed that sections with $LD > 10.94$ exhibited local buckling of the web and very minimal deflection of the flanges, elucidating the boundary of Seif & Schafer's *Eq. 40a*. They posited that the flange was developing (or approaching) fully plastic capacity before failure, while the web developed only its local buckling capacity i.e. 'strong flange behaviour'. *Eq. 42* was proposed in [1] to predict the ultimate strength of sections with $LD > 10.94$, where *Eq. 41* is used to calculate the elastic critical local buckling stress. In cases where $LD < 10.94$, the traditional codified DSM was applied. The method performed well for predicting the strength of the numerically modelled sections, but there was little experimental evidence available at the time to evaluate the method further.

$$P_{nl} = \left(2\ b_f\ t_f\ f_{y,f}\right) + \left(h_w\ t_w\ \sigma_{crl,w}\right) \tag{42}$$

While Rossi & Li's method describes the behaviour of strong flange I-profiles, the use of the limiting dimension does not account for the possibility of different materials in the web and flange. A method applicable to hybrid sections should independently incorporate the yield strength in both the web and the flange to account for their effects on plate slenderness and interactions between the plates. In 2024, Langone et al. demonstrated that the slenderness ratio Ω, given in *Eq. 43*, could more accurately categorize strong flange behaviour while incorporating the different material strengths in hybrid sections [11]. The *LD* and Ω equations are very similar – which is expected as they aim to capture the same behaviour.

$$\Omega = \left(\frac{h_w}{t_w}\sqrt{f_{y,f}}\right) / \left(\frac{(b_f - t_w)}{2t_f}\sqrt{f_{y,w}}\right) \tag{43}$$

$$\kappa = \frac{2\ t_f\ b_f\ f_{y,f}}{t_w\ h_w\ \sigma_{crl}} \tag{44}$$

$$if\ \lambda_l > 0.776 \begin{cases} P_{nl} = \left[1 - 0.15\left(\frac{P_{crl}}{P_{ne}}\right)^{0.4}\right]\left(\frac{Pcrl}{P_{ne}}\right)^{0.4} P_{ne} & \text{if } \Omega \leq 11.17 \\ P_{nl} = \left[\frac{1}{1-0.0208\,\kappa}\right]\left[1 - 0.15\left(\frac{P_{crl}}{P_{ne}}\right)^{0.4}\right]\left(\frac{Pcrl}{P_{ne}}\right)^{0.4} P_{ne} & \text{if } \Omega > 11.17 \end{cases} \tag{45}$$

Langone et al. then developed the strength ratio κ shown in *Eq. 44*, which is based on Rossi & Li's hypothesis that strong flange sections will develop critical buckling strength in the web and fully plastic resistance in the flanges. By positing that as the ratio of flange to web capacity increases, the extent of deviation from existing design predictions also increases, they incorporated the strength ratio into the existing DSM formulation, see *Eq. 45* which was proposed as a replacement to *Eq. 38*.

A numerical coefficient of 0.0208 was originally proposed by Langone et al. to accompany the κ parameter, and a threshold of 11.17 was set for Ω. These values were based on numerical evidence of strong flange hot-rolled carbon steel I-sections presented in [1]. In Chapter 3.8, the performance of *Eq. 45* is evaluated against the experimental evidence presented in this paper. *Eq. 45* is ultimately assessed as imperfect, but the underlying assumptions and methodology applied in [11] is maintained as a valid approach develop a modified DSM formulation.

3.3. Design and Fabrication

Thirteen stub columns were designed to investigate the effects of specific material properties and geometries on local buckling behaviour and ultimate strength. The stub columns include stainless steel grades 1.4307, 1.4462, and 1.4404 and carbon steel grade S275. This study focuses on two geometric parameters affecting local buckling and ultimate strength: the height of the web and the ratio between the web and flange thickness, being either 0.5 or 1.0. The stub columns were therefore designed by varying these parameters alongside the grades of carbon or stainless steel used. The FE method was used to compute the nominal ultimate strength of each section as a check prior to fabrication. A nominal length of 350mm was selected, ensuring local buckling was observed in each specimen. This was also checked via the FE models built prior to testing.

A diagram of the section dimensions is given in Figure 4a and geometric imperfections labels are described in Figure 4b. The complete nominal dimensions and materials for each specimen are reported in Table 5, and measured values are reported in Table 6. The measured stress-strain curves of all materials are discussed in Chapter 3.4.

Table 5. Nominal geometrical dimensions and materials for stub column specimens.

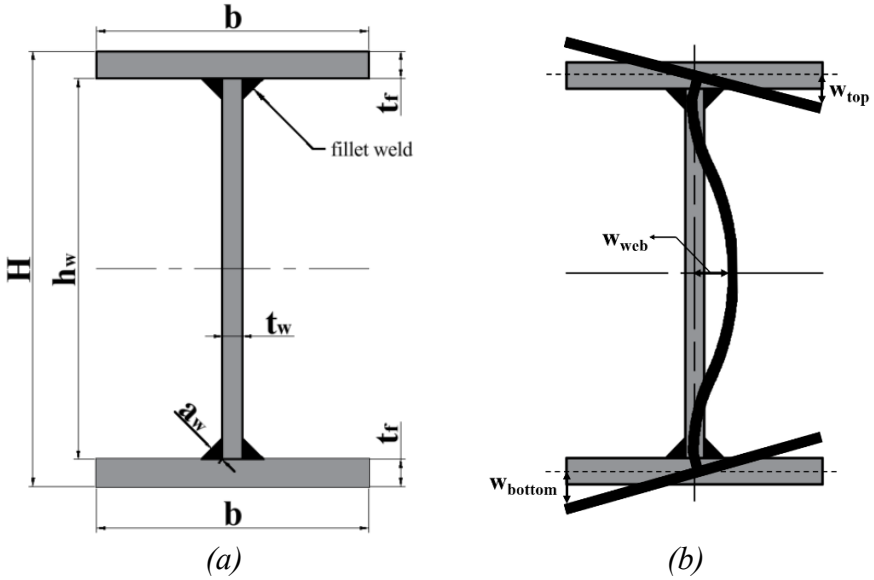
Specimen	L [mm]	h_w [mm]	b [mm]	t_w [mm]	t_f [mm]	t_w / t_f	Flange Grade	Web Grade
A1	350	200	60	3	6	0.5	1.4462	1.4307
B1	350	88	60	3	6	0.5	1.4462	1.4307
A2	350	200	60	3	6	0.5	1.4462	S275
B2	350	88	60	3	6	0.5	1.4462	S275
C1	350	394	80	3	3	1.0	1.4462	1.4307
D1	350	325	80	3	3	1.0	1.4462	1.4307
E1	350	94	60	3	3	1.0	1.4462	1.4307
C3	350	394	80	3	3	1.0	1.4462	1.4404
D3	350	325	80	3	3	1.0	1.4462	1.4404
E3	350	94	60	3	3	1.0	1.4462	1.4404
F3	350	300	90	3	6	0.5	1.4307	1.4307
G3	350	288	90	3	6	0.5	1.4307	1.4307
F4	350	300	90	3	6	0.5	1.4404	1.4404

The stub columns were designed to cover a slenderness range from 0.75 to 2.96, which includes sections theoretically reaching full cross-section plasticity and sections exhibiting strong flange behaviour. In Table 5, the columns are separated into three categories indicated by thin dividing lines. The top category is hybrid sections with different plate thicknesses in the web and flange, the middle category is hybrid sections with equal plate thicknesses, and the bottom category is homogeneous sections with different plate thicknesses. Columns are given an alphanumeric identifier with each number indicating a specific combination of materials in the web and flange, and each letter indicating a specific set of cross-section geometries. Therefore, any two columns labelled with the same letter can be compared on the basis that their only difference is material properties. Likewise, any two columns with the same number are compared knowing that their only difference is geometry.

For example, the comparison between D1 and D3 isolates a change in the web material from grade 1.4307 austenitic stainless steel to 1.4404 duplex. Similarly, the comparison between C1 and D1 isolates a change in the web height, while all other properties are held constant. The resulting differences in ultimate strength, deformation shape, and the force-displacement curve are discussed in Chapter 3.7.

Table 6. Measured dimensions and material strengths for stub column specimens.

Specimen	L [mm]	h_w [mm]	b [mm]	t_w [mm]	t_f [mm]	a_w [mm]	Flange $\sigma_{0.2}$ [MPa]	Web $\sigma_{0.2}$ [MPa]
A1	349.3	198.3	59.39	3.02	6.46	2.4	613.0	282.5
B1	349.2	87.3	59.70	2.96	6.45	1.8	613.0	282.5
A2	349.2	198.1	59.58	2.96	6.44	1.8	613.0	336.6
B2	348.8	87.1	59.86	2.96	6.47	2.4	613.0	336.6
C1	349.0	393.2	78.94	2.95	3.01	1.8	617.3	282.5
D1	348.8	323.9	78.49	2.98	3.06	2.4	617.3	282.5
E1	348.8	92.2	59.50	2.96	3.01	1.8	617.3	282.5
C3	349.2	392.7	79.13	2.99	3.01	2.4	617.3	269.6
D3	349.2	323.7	78.42	3.01	3.02	2.4	617.3	269.6
E3	348.3	92.7	59.29	3.02	3.01	1.8	617.3	269.6
F3	349.2	298.4	88.91	2.97	6.06	2.4	331.7	282.5
G3	349.3	285.2	89.39	2.95	6.03	2.4	331.7	282.5
F4	343.0	298.1	89.23	3.02	6.08	2.4	359.0	269.6



(a) *(b)*

Figure 4. Diagram of I-profile *(a)* geometric dimensions and *(b)* imperfections.

Plates were cut by waterjet to the nominal dimensions. Gas tungsten arc welding (GTAW) – also called tungsten inert gas (TIG) welding – was used to fabricate the stub columns. Inevitable distortions were induced during the welding process, and their effects on the stub column stability is addressed in Chapter 3.5 on geometric imperfections and in Chapter 3.7.3 on numerical model parameters. The column ends were milled parallel to each other to provide uniform flat surfaces to contact the compression platens. Column ends were then treated with a belt sander to further improve contact uniformity. Any remaining gaps in the column-platen contact were measured prior to each test and ensured to be less than 1 mm.

3.4. Material Properties

Tensile coupons were tested for material grades and thicknesses corresponding to those used in the stub column constituent plate elements. All coupons were cut in the longitudinal direction relative to the direction of rolling. Before testing, the dimensions of each coupon were measured at multiple locations and the average dimensions were recorded. Mill certificates were provided for each material, including the chemical compositions and the average measured properties of $R_{p0.2}$ and R_m which are included in Table 7. The tensile tests were conducted in accordance with ISO-6892-1-2019 [83] using an Instron 8804MT press. The force was recorded directly by the Instron press. The Instron 2nd generation Advanced Video Extensometer (AVE2) – with measurement accuracy of ±0.5% – measured tensile strain by tracking the distance between two points on opposite ends of the coupon gauge width. Expectedly, the video extensometer (VE) measurement was more accurate than the displacement readings from the press, particularly during initial loading, since machine compliance is excluded from these readings.

Table 7. Measured material properties from tensile coupons.

Grade	Thickness [mm]	Measured E [GPa]	Measured $\sigma_{0.2}$ [MPa]	Measured σ_u [MPa]	Code Specified E [GPa]	Code Specified $\sigma_{0.2}$ [MPa]	Code Specified σ_u [MPa]	Mill Certificate $R_{p0.2}$ [MPa]	Mill Certificate R_m [MPa]
1.4462	6.52	201.3	613.0	776.1	200	500	700	638	802
1.4462	2.99	202.3	617.3	825.7	200	500	700	631	844
1.4307	5.98	202.3	331.7	642.2	200	220	520	355	630
1.4307	2.93	194.2	282.5	663.6	200	220	520	291	622
1.4404	5.96	197.1	359.0	594.3	200	240	530	350	595
1.4404	2.99	*	269.6	622.5	200	240	530	307	602
S275	2.90	192.7	336.6	468.4	210	275	430	361	488

*The video extensometer did not accurately read the initial stiffness or elasticity for the 1.4404 3mm coupon. The measured value for the Young's Modulus was 159.5 GPa. The more accurate value of 197.1 GPa, measured in the 1.4404 6mm coupon, was therefore used to calculate the 0.2% proof stress and in the FE material model.

The material properties for Young's Modulus E , 0.2% proof stress $\sigma_{0.2}$, and the ultimate tensile stress σ_u were determined from the tensile test results for the plates included in the stub columns tested in this paper and reported in Table 7. The Young's modulus is calculated as the slope of a linear regression on the stress-strain relationship within initial domain where this relationship is linear. The strain value where this relationship departs from linearity is different in each coupon, but generally occurs between 0.0005 to 0.002 mm/mm. The 0.2% proof stress is calculated by plotting a line with the x-intercept as 0.002 mm/mm and the slope as the measured Young's Modulus. The stress value where this line intersects the measured stress-strain curve is the 0.2% proof stress. Ultimate tensile stress is taken as the greatest stress value measured during the test up to fracture. Figure 5 shows the stress-strain curve from the VE measurement for all nine tensile coupons, with the curves ending at the point of fracture or where the coupon failed to provide any further tensile resistance.

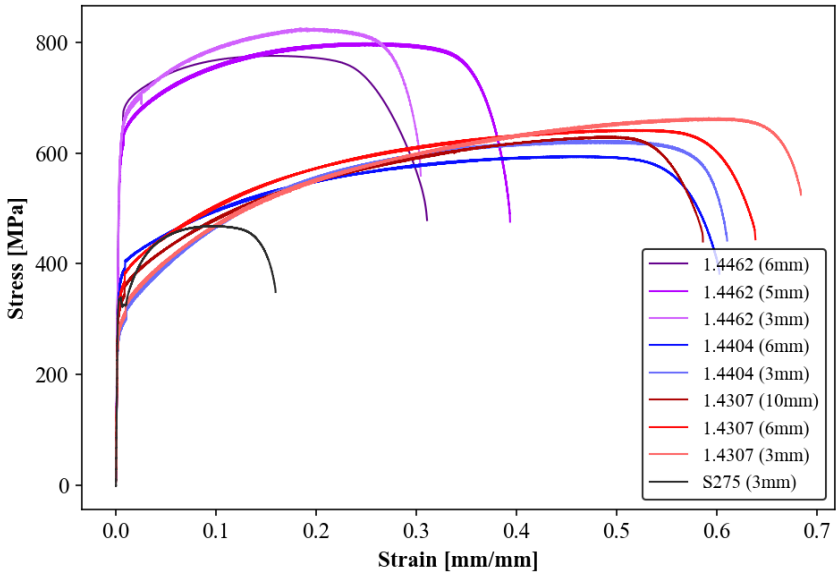


Figure 5. Stress-strain curves from eight tensile coupon tests.

The materials included in the stub column specimens were chosen as a representative sample of plausible choices for construction applications. The austenitic and duplex families are most common among stainless steels in structural applications [84] and can be employed in multiple grades. Austenitic stainless steel is preferred primarily due to excellent corrosion resistance, owing to the material's high content of chromium and nickel. Duplex stainless steels, with a microstructure of approximately equal parts austenite and ferrite, has significantly higher mechanical strength than either austenitic or ferritic grades and excellent strength-to-cost value relative to other stainless steels [8].

3.5. Initial Geometric Imperfections

Precise measurements were taken to observe the shape and magnitude of the imperfections in the web and flanges for all specimens. Imperfections organic to the plates are induced by uneven cooling after hot-rolling. The greatest share of the cross-sectional imperfections, however, is the result of distortions occurring due to welding. Figure 4b depicts how the maximum imperfection amplitudes are defined on each plate. A measurement procedure was developed to capture the geometric imperfections of the stub columns at relatively low cost. The measurement setup for web imperfections is shown in Figure 6.

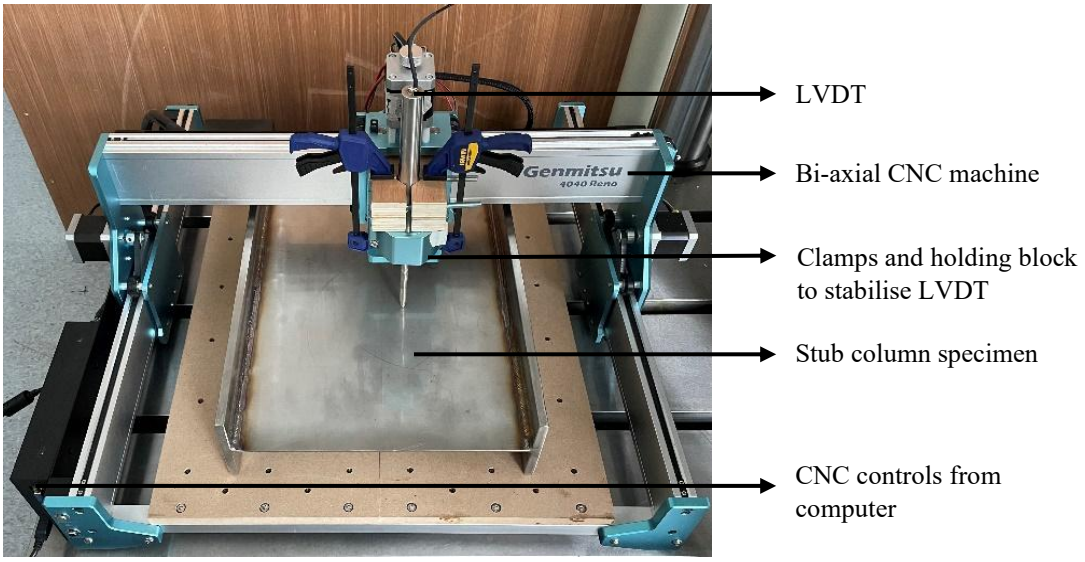


Figure 6. Measurement set-up for geometric imperfections of the web.

A Genmitsu 4040 Reno CNC machine was operated from a laptop with G-code commands. The LVDT accessory for the Instron 8804MT press was attached to the CNC machine, which was programmed to trace five evenly spaced parallel lines, each the length of the column, to survey the three plates composing each column. Displacement measurements were taken from the LVDT at a rate of 20Hz and recorded through the Instron Console. The accuracy of the CNC machine's position was controlled within ±0.1mm. Based on time readings, the displacement measurements were associated with (*x, y, z*) coordinates covering the web and flange plates. A mesh was interpolated between the five discrete rows traced along the length of each plate using the SciPy package in python. The resulting surface visualization of the web imperfection shapes and amplitudes is provided in Figure 7.

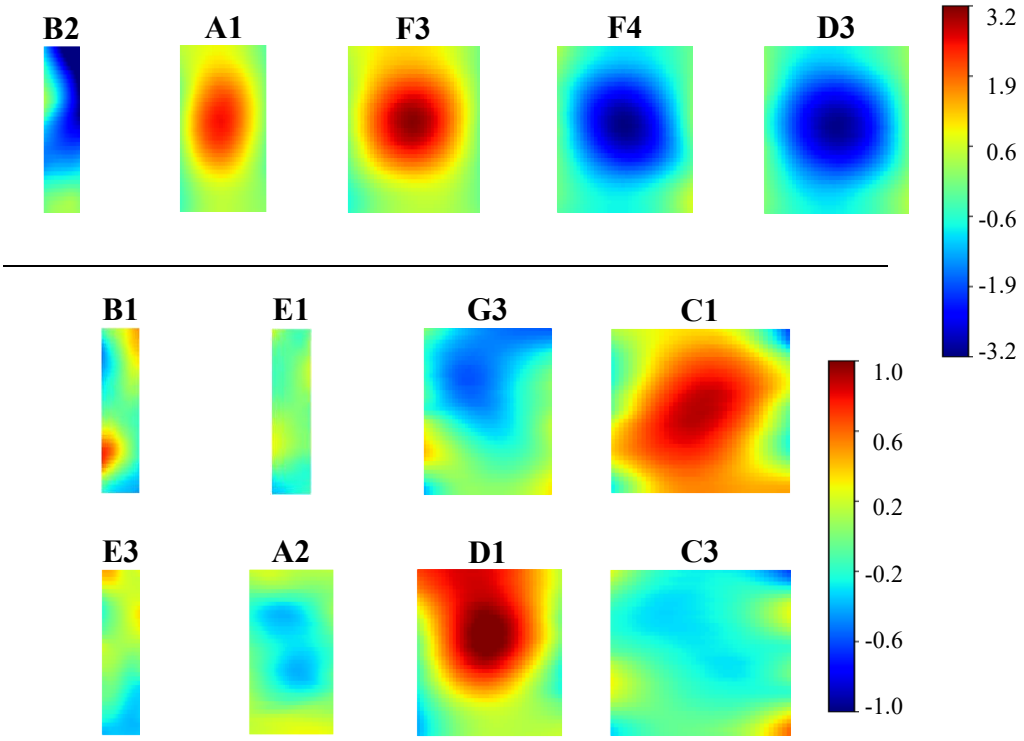


Figure 7. Interpolated surface visualization of web geometric imperfections.

The out-of-plane deformations are shown by the colour scales in Figure 7, given in millimetres. Two scales are provided to best visualize the shape of all sections given some have much larger imperfection amplitudes than others. In sections with large web height, a single half-wave shape is generally identified. In sections where the web height is too short for a full half-wave to develop (B1, B2, E1, and E3), there is less consistency in the imperfection shape and the imperfection magnitude tends to be smaller. The maximum measured geometric imperfection for each plate is reported in Table 8. The greatest measured out-of-plane displacement among the three constituent plates is taken as $w_{section}$ and is compared to the recommendation of EN 1993-1-5 to model maximum imperfection size as h_w/200 [51]. The value given in EN 1993-1-5 is found to be unconservative for many of the tested columns. However, the Eurocode guidelines were not established for sections made of different materials, or those where lower thermal conductivity (e.g. stainless steel) can cause welding distortions [85]. The maximum imperfection magnitude, $w_{section}$, is used as an input parameter to scale geometric imperfections in the FE models.

Table 8. Measured maximum geometric imperfection magnitude on each plate.

Specimen	w_{web} [mm]	$w_{top\ flange}$ [mm]	$w_{bottom\ flange}$ [mm]	$w_{section}$ [mm]	$h_w/200$ [mm]
A1	0.40	1.50	1.68	1.68	0.99
B1	0.76	1.26	1.81	1.81	0.44
A2	0.39	1.67	1.32	1.67	0.99
B2	2.66	1.57	1.55	2.66	0.44
C1	0.91	1.81	0.95	1.81	1.97
D1	1.08	1.57	1.02	1.57	1.62
E1	0.37	0.57	0.44	0.57	0.46
C3	0.62	1.65	1.90	1.90	1.96
D3	3.14	2.12	2.23	3.14	1.62
E3	0.47	0.58	0.73	0.73	0.46
F3	3.15	1.66	1.48	3.15	1.49
G3	0.58	1.39	1.54	1.54	1.43
F4	3.19	1.19	2.26	3.19	1.49

3.6. Stub Column Test Procedure

Thirteen stub column tests were completed using an Instron 8804MT press and load cell with 600kN static load capacity. The load was applied in displacement control at a rate of 0.2mm/s, allowing the investigation of post-ultimate strength behaviour. The use of rates between 0.1-0.3mm/min is customary in studies for quasi-static steel compression tests [86, 87, 88, 74, 30]. The Instron press measured the end-shortening of the column. Strains were measured in one of the flanges at mid-height by the VE with measurement accuracy of ±0.5%. The VE measured the distance between two points drawn on the flange and compared them to the measurement before loading to compute strains. Finally, a strain field on the entire web was measured using digital image correlation (DIC). Two Allied Vision Technologies cameras were fitted with 25mm focal length Kowa lenses and set up in stereo configuration 1300mm from the stub column, facing the web. The images produced have resolution of 4122 by 2176 pixels. Prior to testing, the specimens were spray painted in matt white with a black speckle pattern on the web for DIC measurement. The minimum target size of the black speckles based on the camera resolution and the distance to the object was 0.54mm. A full diagram of the test setup is shown in Figure 8.

The stub columns were geometrically centred on the loading press and put into contact with both the loading and support platens. The original contact locations of the column with the platens were marked. Before loading, a detailed diagram of the column contacts with both platens was created to quantify the deviations from an assumption of perfectly uniform contact. After the calibration of DIC and VE cameras, a pre-load of 3kN was established before balancing the actuator. The critical assumption of fixed-fixed end conditions held true beyond the ultimate strength for all specimens – verified as the columns did not slip from the original contact locations marked on the platen.

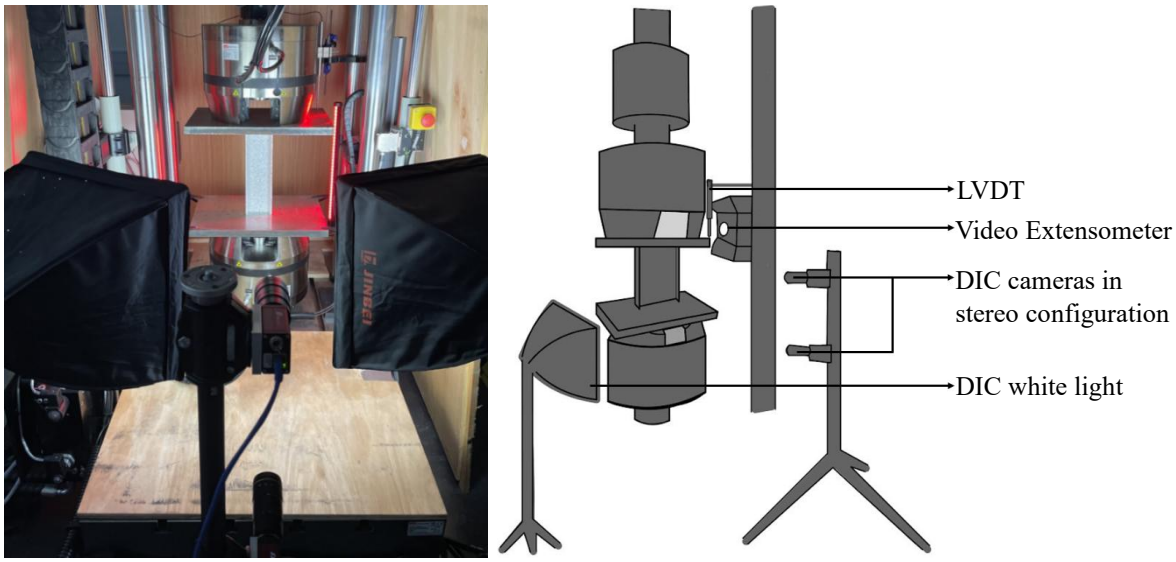


Figure 8. Photo and diagram of stub column experimental set-up.

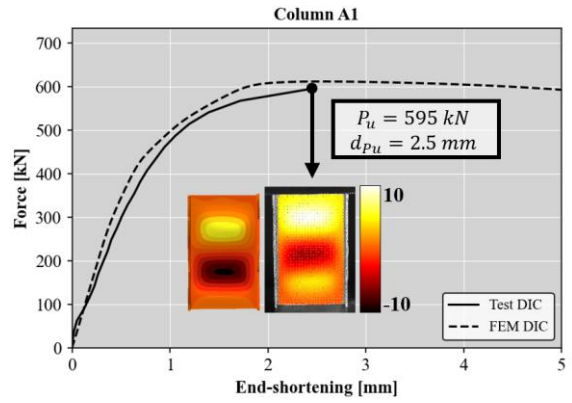
3.7. Tests and Numerical Validation

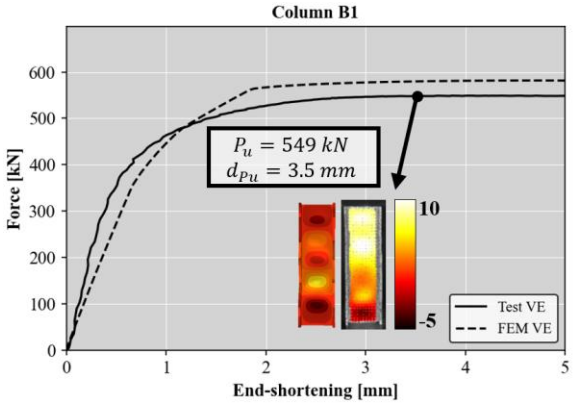
All stub columns were compressed beyond the point of their ultimate strength. Among the thirteen stub columns, one failed with local-global interaction buckling, and the remaining twelve underwent local buckling with substantial flange resistance followed by local plastification. The variation in the local buckling mechanisms is primarily influenced by differences in the geometry or materials of the plates.

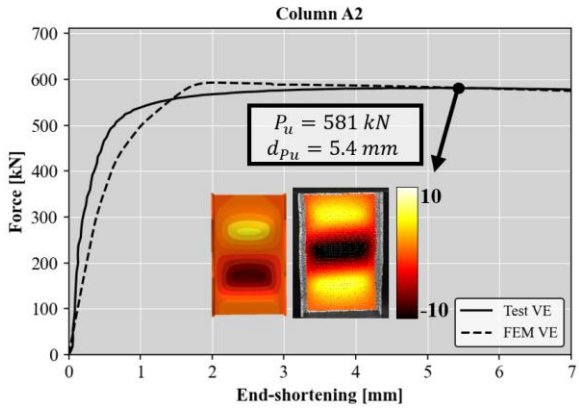
3.7.1. Test Results

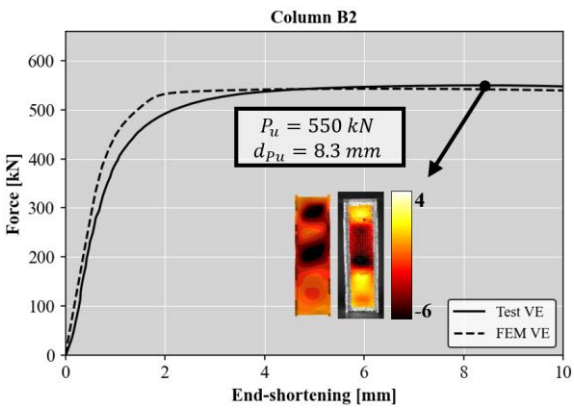
The force-displacement curves for all thirteen stub column tests are reported in Figure 9. Force measurements were taken from the Instron press data. End shortening is measured by two methods. First, strain readings taken by the VE from the mid-length of the flange and scaled it up to the full length of the column estimate the end-shortening. The VE has the advantage of eliminating errors from the load string compliance, but this method to calculate end-shortening assumes a perfectly uniform distribution of stresses and, since it is measuring along a line parallel to the flange, is inaccurate if there is any non-axial motion in the flanges. DIC also measured end-shortening, but the image data is sensitive to small changes in lighting (sunlight), surrounding temperature (localised heat), and inaccurate once (if) the paint chips or flakes. Therefore, engineering judgment was applied to determine which of these two measurements most accurately capture the behaviours of interest, as indicated in the legends of Figure 9. Both the VE and DIC readings are more reliable before reaching the ultimate force as flange rotations and paint chipping generally begin after that point.

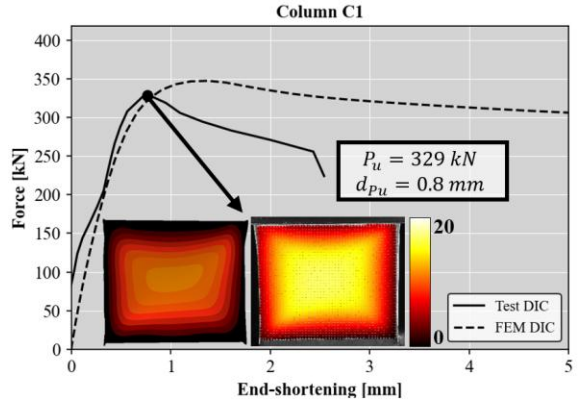
The plots in Figure 9 also include the force-displacement curves from the FE model corresponding directly to the end shortening measurement method used for that column, which will be discussed further in Chapter 3.7.3. The ultimate load sustained by the columns and the measured level of end-shortening at this point are labelled. Finally, graphics of the column FE model (left) and DIC measurements (right) at the point of ultimate force are provided within the graph for each column. The colour gradient corresponds to the measured out-of-plane displacements to visualize the buckling shape and deformation magnitudes at ultimate force. Equivalent colour scales are used to enable direct comparison between the FE model prediction and DIC measurements.

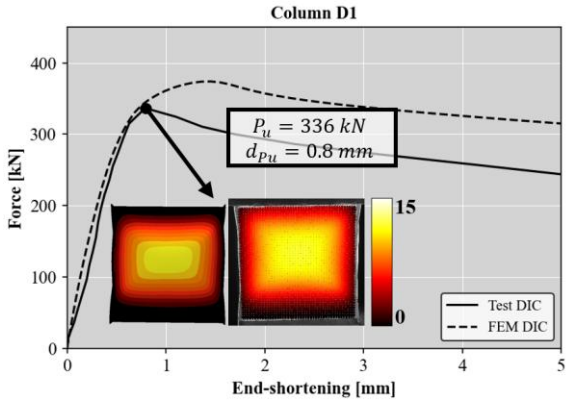

Column A1
$P_u = 595\ kN$
$d_{Pu} = 2.5\ mm$
10
-10
Test DIC
FEM DIC
Force [kN]
End-shortening [mm]

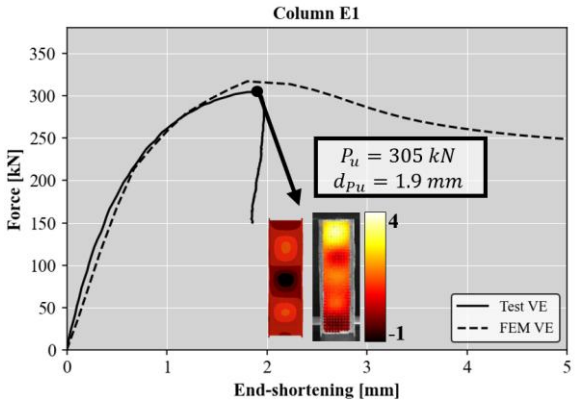

Column B1
$P_u = 549\ kN$
$d_{Pu} = 3.5\ mm$
10
-5
Test VE
FEM VE
Force [kN]
End-shortening [mm]

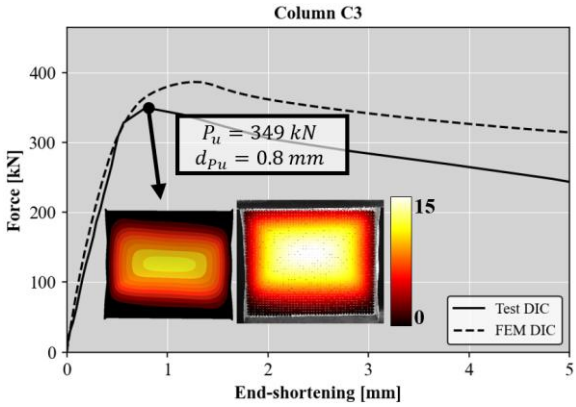

Column A2
$P_u = 581\ kN$
$d_{Pu} = 5.4\ mm$
10
-10
Test VE
FEM VE
Force [kN]
End-shortening [mm]


Column B2
$P_u = 550\ kN$
$d_{Pu} = 8.3\ mm$
4
-6
Test VE
FEM VE
Force [kN]
End-shortening [mm]


Column C1
$P_u = 329\ kN$
$d_{Pu} = 0.8\ mm$
20
0
Test DIC
FEM DIC
Force [kN]
End-shortening [mm]


Column D1
$P_u = 336\ kN$
$d_{Pu} = 0.8\ mm$
15
0
Test DIC
FEM DIC
Force [kN]
End-shortening [mm]


Column E1
$P_u = 305\ kN$
$d_{Pu} = 1.9\ mm$
4
-1
Test VE
FEM VE
Force [kN]
End-shortening [mm]


Column C3
$P_u = 349\ kN$
$d_{Pu} = 0.8\ mm$
15
0
Test DIC
FEM DIC
Force [kN]
End-shortening [mm]

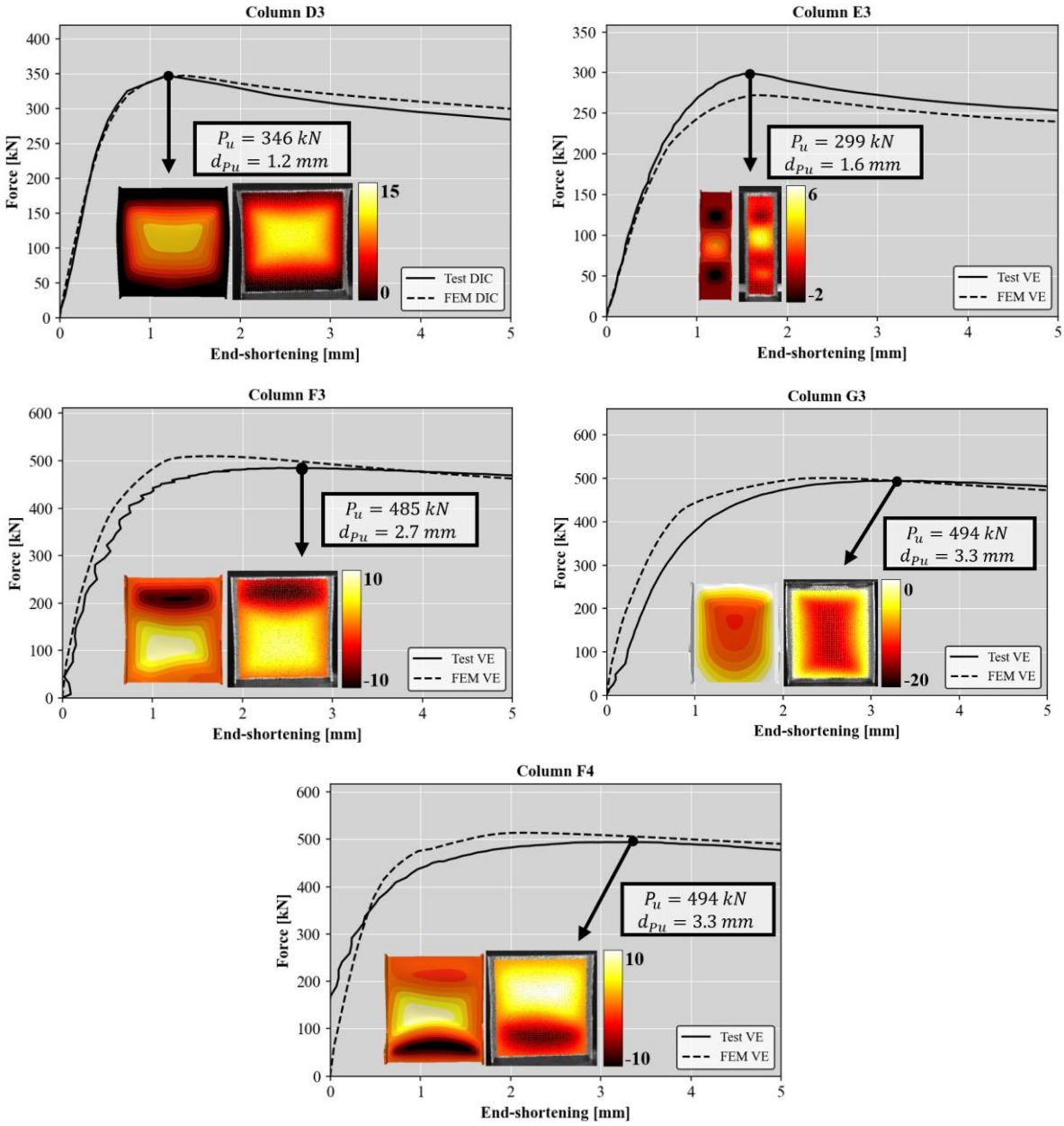


Figure 9. Force-displacement curves from stub column tests and FE models. Graphics within each plot show FE model results (left) and DIC measurements (right) for out-of-plane deformations in millimetres at the point of ultimate force.

3.7.2. Buckling Mechanisms

All stub columns initially locally buckled in the web. Localized flange rotations developed, generally occurring after the point of ultimate force, in sections with large web deformations (i.e. C1, D1, E1, C3, D3, E3, and F3) to accommodate the increasingly deformed shape. This observation supports the hypothesis that when I-profile flanges are substantially stronger than the web plate (strong flange), the web may locally buckle with minimal flange

deformation and the section ultimate strength can be approximated as the sum of the web plate local buckling capacity and the flange fully plastic capacity [1]. The number of buckling half waves developed in each column was primarily determined by the aspect ratio of the web plate, consistent with Timoshenko & Gere's description of plate buckling [54]. Variations to the theoretical web buckling shape were observed, however, due to influences including the column initial imperfections and imperfect initial contact between the column and platens.

Figure 10 shows the deformed shape of all stub columns after the compression tests. FE model results at equivalent levels of end-shortening are included in Figure 10 with the colour gradient representing the out-of-plane deformations in millimetres.

The influence of flange strength on buckling behaviour is most clearly demonstrated by the differences between columns B1, E1, and E3. First, column B1 is the only specimen to exhibit local-global interaction buckling. It developed five local buckling half-waves in the web – each with small out-of-plane deformation. This was caused by the B1 flanges (6mm thick of 1.4462) providing substantial resistance, resembling fixed-fixed end conditions on the web buckling mode. This is contrasted with column E1 – which has identical materials and only thinner flanges, 3mm, than B1 – where the flanges provide less resistance. In column E1, three buckling half-waves formed, the middle half-wave developed large out-of-plane deformations, and eventually the flanges rotate at the location of the web buckle to accommodate the deformation. Column E3 – which has identical geometry as E1 but a slightly weaker 1.4404 web – exhibited the same buckling mechanism as column E1. The reduction in web strength was not substantial enough to affect the buckling shape.

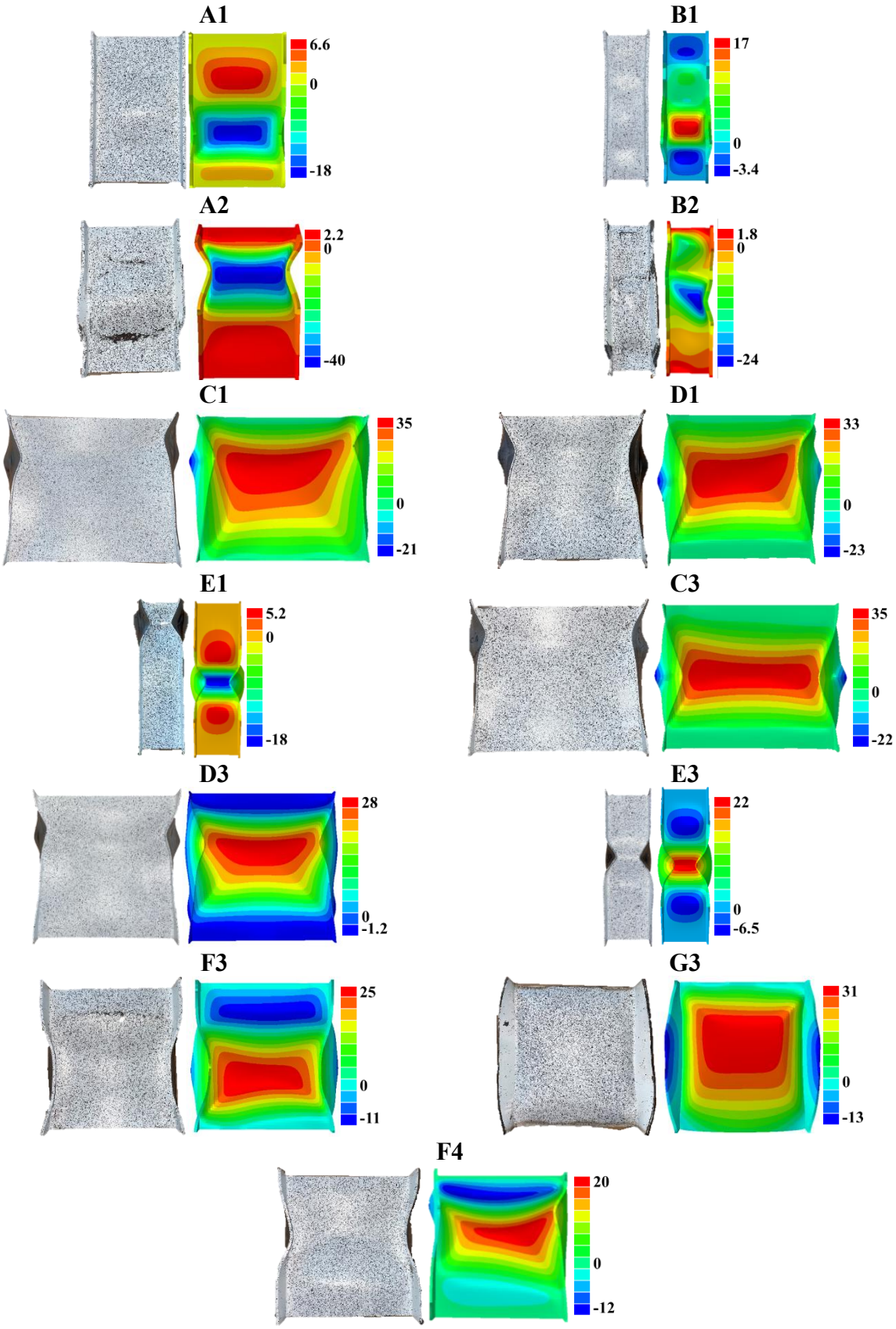


Figure 10. Comparison of stub column deformed shape with FE model results. Colour scale of FE model represents the out-of-plane displacements in millimetres.

The comparison of columns A1 and B1 (1.4307 in the web) to A2 and B2 (S275 in the web) isolates the change in web material from stainless steel to carbon steel. The measured proof strength $\sigma_{0.2}$ of the S275 is approximately 20% greater than that of the 1.4307. This difference, expectedly, did not substantially change the observed buckling behaviour and did not increase the ultimate strength of the sections with carbon steel webs. In the logic of the EWM, the buckling strength of the carbon steel webs is reduced because they have lager f_y than the 1.4307 stainless steel, leading to smaller values of the material factor ε, and therefore more slender classifications – or smaller reduction factors ρ. A1 and A2 both have Class 4 webs, but the reduction factor ρ is smaller for A2. The B1 web is Class 2, while the B2 web is Class 3. Columns A2 and B2 are not able to make efficient use of the greater material strength in their web because the increased f_y leads to instability.

The comparison of columns C1 to D1 (1.4307 in the web) and C3 to D3 (1.4404 in the web) isolates the effect web height reduction. These four columns exhibit very similar buckling shapes. The effect of the web height on ultimate force is small in these columns and overshadowed by other factors including initial imperfections. It is clear, however, that D1 and D3 are more efficient than C1 and C3 as they achieve similar ultimate strengths despite having smaller cross-sectional areas.

Relative to column D3, F4 has a smaller web height h_w, smaller width-to-thickness ratio in the flange plates, and a much lower material strength in the flange – all of which make the plates in this section less susceptible to local buckling. As expected, the lower slenderness of F4 caused it to locally buckle at higher forces. Column D3 achieved an ultimate strength that is 62% of its fully plastic capacity while column F4 achieved 78%, as seen in Figure 11. F3 and G3 – which both have the increased flange thickness of 6mm, like F4 – reached ultimate strengths that were 80% and 83%, respectively, of their fully plastic capacity.

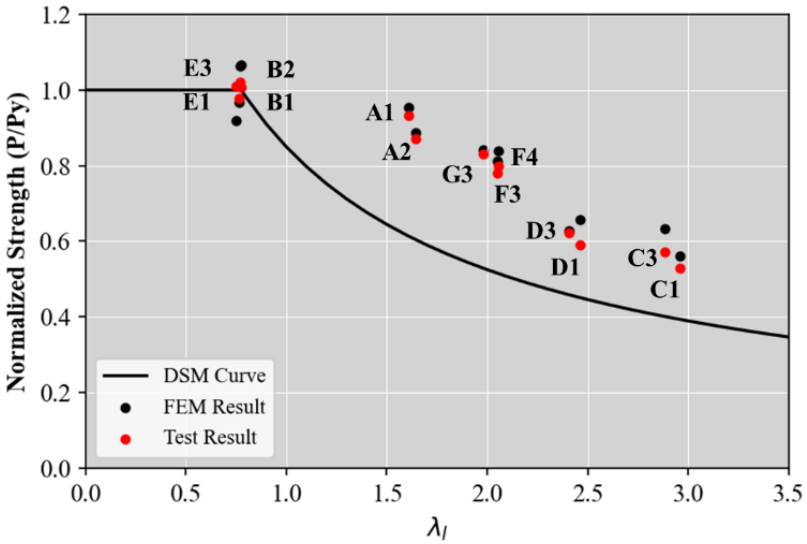


Figure 11. Normalized strength vs. slenderness for stub column tests and FE model results.

In Figure 11, the normalised strength of each section – the observed ultimate strength divided by the fully plastic strength determined per *Eq. 39* based on measured properties– is plotted against the sectional slenderness λ_l , given in *Eq. 36*. The observation that the stub columns test results are plotted above the DSM curve is evidence of strong flange behaviour – the tendency for sections with sufficiently strong flanges to exhibit higher ultimate strengths than existing design methods account for.

3.7.3. Numerical Modelling and Validation

Finite element models were developed using Abaqus Standard [12] to numerically represent the stub column compression experiments and investigate the sensitivity of ultimate capacity to primary parameters such as geometric imperfection, weld geometry and residual stress model. The stub columns were modelled using 4-node shell elements with reduced integration (S4R), which have been repeatedly shown successful for this type of model [75, 89, 3, 5]. The loading and bearing platens were modelled as non-deforming plates. All degrees of freedom (DOF) were locked on the bottom bearing plate (no motion). The upper loading plate had all DOF locked except for motion along the loading axis (free *z*-axis translation). At

locations where the column was measured to be in-contact with the plates, a fixed connection is represented by giving the column ends and the platen coinciding nodes.

A mesh convergence study was conducted to appropriately trade-off result precision against computational time. The selected mesh density is a 5mm square mesh throughout the stub column and 15mm mesh in the bearing and loading plates. The fillet weld connecting the web and flange plates is not represented with any additional elements. Representation of the weld was removed because the overlapping area of elements in the web and flange accounted for areas approximately equal to the area of the fillet weld. Additionally, the effect of the weld representation was found to be small relative to other parameters in a sensitivity assessment.

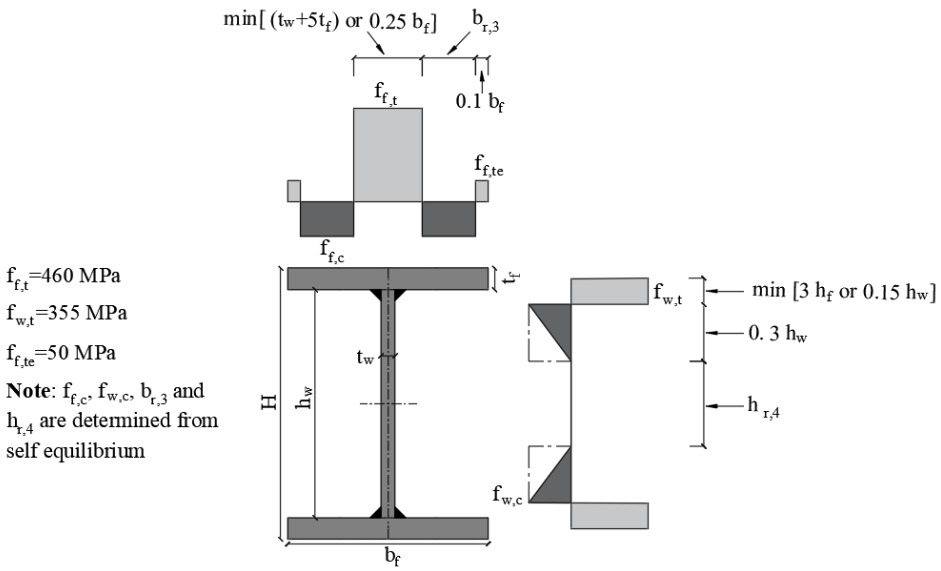


Figure 12. Residual stress profile from [28] used in FE models.

The material constitutive models were defined by the two-stage Ramberg-Osgood model specified in the Design Manual for Stainless Steel [90]. The model parameters for E, f_y , and f_u were taken from the measured values reported in Chapter 3.4. All other parameters in the model were defined using the equations provided in the codes. The shape of geometric imperfections was taken as the first elastic buckling mode shape determined by linear perturbation buckling analysis [5, 43]. This shape is then scaled to the maximum measured imperfection magnitude, as reported in Table 8.

Residual stresses induced by welding and uneven cooling also contribute to premature yielding and a reduction in structural stiffness [91]. The longitudinal residual stresses were modelled as an equilibrium rectangular block stress distribution, with magnitudes obtained from [28] based on the profile originally developed by [92]. This residual stress model [28], originally developed for high-strength steel, is adopted for stainless steel due to the similarities in their mechanical responses, i.e., both materials exhibits pronounced nonlinearity and high yield strength. The validity of this approach is further supported by a sensitivity analysis conducted in [93] which compared the residual stress model from [28] to another model and showed negligible variation in the resulting strength predictions. Figure 12 shows the profile of the residual stresses used in the numerical model.

Table 9. Comparison of ultimate loads from tests and numerical results.

Specimen	$N_{u,test}$ [kN]	$N_{u,FE}$ [kN]	$N_{u,test}$ / $N_{u,FE}$
A1	595*	611	0.98
B1	549	582	0.94
A2	581	593	0.98
B2	550	543	1.01
C1	329	349	0.94
D1	336	375	0.90
E1	305	317	0.96
C3	349	387	0.90
D3	346	349	0.99
E3	299	272	1.10
F3	485	510	0.95
G3	494	501	0.99
F4	494	514	0.96
Average			**0.97**
S.D.			**0.05**

* Test A1 was terminated at 595 kN to prevent exceeding the press capacity. If the test ran to completion, it is estimated that the ultimate force would be an additional 1%.

Ultimate strength values from the FE models are compared with the test results in Table 9 and show generally strong agreement. The alignment of the force-displacement curves from the FE model and test results in Figure 9 and the accurate representation of deformed shapes

in Figure 10 also demonstrate the FE model is capturing the relevant characteristics of the tested stub columns.

The FE model provides the opportunity to investigate which specific parameters in each column are influencing ultimate strength and buckling behaviour. The FE model was built incrementally to individually introduce new parameters and observe their effects. As expected, incorporation of geometric imperfections of the measured magnitudes resulted in a substantial decrease in the predicted ultimate strength. Addition of the initial residual stresses slightly reduced the ultimate strength and caused an earlier departure from linearity in the force-displacement curve. A parametric assessment of the material model parameters found that ultimate strength was much more sensitive to f_y than f_u or n, the non-linearity parameter for stainless steel. These relationships were expected and well covered in previous literature.

The FE model also proved to be sensitive to the representation of initial contact imperfections. In the test setup, it was observed that small gaps (<1mm) between the column and the platens were present at some locations. Measurements of the size and location of these gaps were made before running the test. Contact imperfections were represented in the FE model by de-coupling nodes in the platen and column, which were otherwise defined as coinciding to represent a perfectly fixed end condition. Incorporation of the measured asymmetrical contact imperfections resulted in reductions to the ultimate strength and allowed for the accurate representation of asymmetrical buckling development, as seen in columns C1 and D1.

3.8. Evaluation of Design Methods

3.8.1. Codified Design Methods

The stub column specimens were evaluated for their nominal design strength according to the Effective Width Method (EWM) from EN1993-1-5 [51], the Direct Strength Method (DSM) from AISI S100-16 [50], and the Continuous Strength Method (CSM) from prEN 1993-

1-4. The design strength was calculated using the measured geometric dimensions of the columns. The measured 0.2% proof stresses reported in Chapter 3.4 are used in place of the nominal f_y in the design equations.

Modifications of each codified design method were made to accommodate the design of hybrid sections, as previously discussed in Chapter 3.2. None of the EWM, DSM, or CSM is currently stated as applicable to the design of hybrid stainless steel sections under compression. To account for this, the section yield stress is calculated as an area weighted average of $\sigma_{0.2}$ in the constituent plates in the EWM and DSM, see *Eq. 39*. For the EWM, this is the only change to the codified procedure required to design for hybrid stainless steel. In the DSM, an analytical solution for λ_l is used which conservatively assumes that σ_{crl} is controlled by the most slender plate, i.e. the web. In the CSM, material modelling constants for carbon steel were determined by the method given in [48], slenderness applicability limits were not observed, and σ_{crl} is determined analytically and controlled by the web as well. The CSM extension for hybrid sections proposed by Bock et al. [75] was used to account for the different materials within one section.

Table 10. Comparison of test ultimate loads with EWM, DSM, and CSM design formulae.

Specimen	$P_{u,test}$ [kN]	P_{EWM} [kN]	Test/ EWM	P_{DSM} [kN]	Test/ DSM	P_{CSM} [kN]	Test/ CSM
A1	595	544	1.10	365	1.64	405	1.47
B1	549	545	1.01	513	1.07	555	0.99
A2	581	539	1.08	375	1.55	207	1.59
B2	550	562	0.98	528	1.04	230	1.46
C1	329	231	1.42	229	1.44	268	1.85
D1	336	252	1.33	242	1.39	264	1.84
E1	305	298	1.02	277	1.10	301	1.01
C3	349	232	1.50	230	1.52	210	1.66
D3	346	245	1.41	240	1.44	231	1.50
E3	299	296	1.01	275	1.09	285	1.73
F3	485	403	1.20	306	1.58	300	1.00
G3	494	405	1.22	308	1.61	394	1.48
F4	494	438	1.13	319	1.55	564	0.98
Average			**1.19**		**1.39**		**1.43**
S.D.			**0.17**		**0.22**		**0.31**

Comparison of the EWM and DSM nominal design performance based on measured properties found that both methods are quite conservative. For this sample of test columns, the EWM was more accurate and more precise than the DSM. In the AISI Standard, both methods are given the same resistance factor for reliability [50] i.e. $\phi = 0.85$. For eight of the thirteen test sections, the DSM and EWM provide nearly identical predictions. In the remaining five sections (A1, A2, F3, G3, F4), the experimentally observed strength is approximately 60% greater than the DSM prediction but only 20% greater than the EWM prediction. Notably, the five sections for which the DSM is overconservative relative to the EWM are the only five sections that exceed the upper limit of the limiting dimension (see *Eq. 40b*). This provides strong evidence that local buckling behaviour – and the resulting strength reduction – is categorically different in strong flange sections than conventional I-sections [1]. Further, this distinction in behaviours is poorly accounted for by the DSM. The method proposed by Rossi & Li in [1] was also evaluated and performed, as expected, very similarly to the EWM.

The CSM predictions were the least accurate for the tested columns. Notably, the CSM sets a limit on the plate slenderness $\lambda_{p,cs} < 1.6$ which is exceeded by five of the thirteen tested stub columns. However, CSM equations are proposed in literature which do not have this limit – as Duan et al. proposed for stainless steel stub columns [94]. The CSM is giving consistently over-conservative strength estimates primarily because of the assumption that the cross-section critical local buckling stress is controlled by the web plate. The code permits that a numerical method or the robust analytical method given in [49] be used to determine less conservative values for this variable. The conservative treatment of σ_{crl} is made here for consistency as it is also made in the DSM evaluation.

3.8.2. Alternative Design Methods

The design method proposed by Langone et al. [11] was evaluated and performed marginally better than the codified DSM, leading to an average of 1.32 and standard deviation of 0.15. The correction factor based on κ given in *Eq. 44* does not increase strength predictions by a large enough magnitude to substantially improve design accuracy. However, the methodology of identifying sections which may exhibit strong flange behaviour, then using an empirical trend to quantify the increased strength prediction remains promising.

Repeating the methodology found in [11] based on the experimental evidence in this paper, the linear function of κ fit by least squares regression now suggests a coefficient of 0.0816 rather than 0.0208 as was used in *Eq. 45*. The linear regression considered only strong flange sections, which are only reported in this paper and the tests by Chen et al. [4] and Salem et al. [45]. Applying the 0.0816 coefficient into the modified DSM from *Eq. 45* substantially improved the average observed-to-predicted ratio to 1.05 and decreases the scatter (standard deviation of 0.07).

Applying the updated coefficient for κ in *Eq. 45* based on the experimental evidence provides very accurate design performance for this sample of tests. However, it is necessary to evaluate this method more rigorously before confidently proposing it as an alternative. The linear trend leading to the coefficient of 0.0816 has an R^2 value of only 0.62 – indicating a weak relationship between the independent and dependent variables. Given the sample size of experimental evidence is only 14 tests for strong flange I-sections, more data is required to determine if this trend is meaningfully strong, or even linear in shape. The slenderness ratio Ω performs generally as intended to distinguish tests characterised by a strong flange behaviour, but the small sample size of 14 is not sufficient for a highly confident validation. In a companion paper [95], the validated FE model is applied to simulate 1325 stub column

compression tests to study a range of strong and not strong flange I-sections. The results of this numerical analysis provide a much stronger basis to evaluate a modified DSM equation.

3.9. Conclusions

This study conducted tests to understand the fundamental loading case of compression for hybrid I-sections which, in application, are often designed with strong flanges. Thirteen stub columns were tested to investigate the effect of hybridity and geometrical proportions on compression behaviour. The tests also provide the first experimental evidence of stainless-steel hybrid I-profile behaviour, with or without strong flanges.

The stub column tests provide substantial evidence that I-sections characterised by strong flanges exhibit distinctly different behaviour from conventional, more uniformly proportioned sections. Interaction between the capacity of the flanges and the web buckling mode is demonstrated by controlled experiments changing the flange thickness between sections. Sections with greater flange thickness also generally exhibited greater structural efficiency. Critically, sections with increased flange strength developed ultimate strengths much greater than the predictions from existing design methods. Geometry proved to have a greater effect on local buckling behaviour than material properties – which is consistent with the existing equations for section slenderness classification. High strength materials are not efficiently employed when the greater material strength leads to local buckling strength reductions driven by the increase of slenderness. Stub column ultimate strength and buckling behaviour is accurately reflected in the validated FE model. Agreement between experimental results and the numerical model strengthens the findings in Chapter 3.7 about the effect of material, geometric, and initial imperfection parameters on stiffness and ultimate strength.

Among the tested columns, the observed ultimate strengths normalized by fully plastic strength achieved by hybrid sections was negligibly different from homogenous sections when

controlling for sectional slenderness λ_l. Further, columns in this study with hybrid ratios up to 2.29 showed no indications of reduced structural efficiency. This provides standing to assume that the optimal hybrid ratio of 1.3-1.6 recommended by Terreros-Bedoya et al. [67] for flexural members (to achieve post-critical resistance states that maximize the web's capacity) should be replaced for hybrid compression members by a different – more complete – ratio encompassing thickness and yield strength for both the web and the flanges to distinguish between behaviours and more adequately evaluate member efficiency.

The DSM, EWM, and CSM were evaluated based on the experimental results, and all were found to be conservative. In particular, the DSM and CSM give very low strength predictions for sections exhibiting strong flange behaviour. These methods define a slenderness for the whole cross-section, which makes them poorly suited to hybrid designs or sections with elements of very different slenderness. Modifications to these methods are needed to make them applicable to the full range of material and geometric possibilities that are beneficial in structural applications. In a companion paper, the authors use the validated FE model to generate evidence of strong flange behaviour for a more complete range of material and geometric possibilities [95]. That research, developed using the experimental results in this paper, concludes by providing a modified DSM formulation which is sufficient to design for strong flange behaviour of I-sections.

3.10. Acknowledgements

The fabrication of experimental specimen for this research was done by Whittaker Engineering of Stonehaven, UK. They were excellent partners in manufacturing and the communication of technical information. Gregory Langone is an Engineer Officer in the U.S. Army and a recipient of the John & Daria Barry Scholarship which generously supports his studies. Usman Ali is a doctoral candidate whose research and studies are funded by the Marie

Skłodowska-Curie Doctoral Network (MSCA-DN) SeaChem project, EU Grant No. 101073471. Majid Shamlooei (majid.shamlooei@unitn.it) contributed to the preliminary development of the finite element model.

4. NUMERICAL MODELLING AND DESIGN OF STAINLESS STEEL I-SECTIONS WITH STRONG FLANGES

Abstract

This research focusses on cross-sectional geometries of I-profiles characterised by strong flange behaviour, which is not well accounted for by existing design methods. Experimental data selected from a paper by the same authors is first used to validate a finite element model of stainless steel I-section stub column tests. Following validation, a large parametric study is conducted to evaluate the influence of geometric and material parameters on the I-profile ultimate strengths. Four grades of stainless steel (EN 1.4062, EN 1.4462, EN 1.4307, and EN 1.4404) are studied from two distinct families, austenitic and duplex, covering a wide range of cross-sectional slenderness. A total of 1325 FE models are built, more than 1000 of which are for strong flange sections. The performance of the codified Effective Width Method (EWM), Direct Strength Method (DSM), and Continuous Strength Method (CSM) is evaluated against the numerical results. The comparison indicates that element interaction and local buckling strength reductions cause I-sections with slender webs and stocky flanges to exceed the strength predictions of the codified design methods. A modified DSM is then developed by introducing two new parameters, Ω and α, to distinguish between behaviours and better account for strong flange effects. The proposed DSM provides strength predictions with greater accuracy and less variation than any of the codified methods. A reliability assessment provides evidence that the new DSM equation achieves the codified target for acceptable probability of failure when applied with the existing resistance factor for the DSM.

4.1. Introduction

I-profile members are commonly used in frames due to ease of connections as beams, columns, or beam-columns. The compression behaviour of I-profile members is well

understood, specifically in the context of hot-rolled steel. The prevailing design philosophy in hot-rolled section design is often to avoid local buckling entirely [96, 97] using section classification methods based on the width-to-thickness ratios of the member elements [64, 53, 60, 98]. The avoidance of local buckling, however, removes the opportunity to benefit from post-buckling reserve strength, which can be significant in some sections. More materially efficient design typically leads to sections with thinner webs [48], both for members in bending and in compression.

While catalogued mild-steel hot-rolled I-profiles generally avoid local buckling, welded or built-up I-profiles with stocky flanges and slender webs can exceed traditional width-to-thickness limits. Research on carbon steel posited that in cases where the I-profile web is more slender than the flanges, it develops only its local buckling capacity while the flanges develop substantial post-buckling reserve strength and approach their full plastic capacity with minimal deformation before failure [1]. This phenomenon is termed strong flange behaviour. Based on the limited evidence available prior to this paper, the codified forms of the EWM make reasonable, conservative strength predictions for strong flange sections, while the DSM gives substantially over-conservative nominal strengths [1, 11].

The behaviour of stainless steel I-profiles under similar strong flange conditions remains largely unexplored. Given the differences in material properties between stainless and carbon steel – such as the wider strain hardening domain and a nonlinear stress-strain relationship – stainless steel sections may demonstrate even more pronounced post-local-buckling strength reserve and, therefore, have much larger resistance than what any of the codified methods currently account for. This paper covers the local buckling and post-buckling strength reserve in stainless steel I-profiles under compression to fill this gap. Recently completed stub column tests by Langone and Ali et al. [99] on stainless steel I-profiles enables validation of finite element (FE) models to study a wide range of geometric and material possibilities influencing

the strong flange behaviour. The results of the parametric assessment are then used to propose a modified form of the DSM specifically accounting for the strong flange behaviour of I-profiles. Last, a reliability assessment is conducted using the sample of numerically generated evidence to compute resistance factors per AISC 370-21 [60].

4.1.1. Tests and Design of Fabricated I-sections

Strong flange I-sections under pure compression was first studied by Rossi and Li in 2013 [8], where they developed a FE model validated on tests of hot-rolled I-section. Ultimate strengths from the FE model were compared with DSM predictions. Rossi and Li identified a distinct difference in the behaviour of sections once a ratio of geometrical dimensions exceeded a critical threshold, termed LD for limiting dimension. Sections that exceeded this threshold were categorized as exhibiting strong flange behaviour.

For hot-rolled I-profile sections with $LD = \frac{h_w}{t_w}\frac{2t_f}{b_f} > 10.94$, i.e., those likely to exhibit strong flange behaviour, Rossi and Li proposed a simple method to predict the ultimate strength P_u, given in *Eq. 46*, where the variables t_w and t_f are the thicknesses of the web and flange, respectively, b_f is the width of the flange, h_w is the web height, and $f_{y,f}$ is the flange yield stress and $f_{cr,w}$ is the elastic critical local buckling stress can be determined from *Eq. 47* based on classical plate buckling theory [54], where E is the modulus of elasticity, μ is Poisson's ratio, k_w is the web buckling coefficient determined by *Eq. 48*, proposed by Seif and Schafer in [48], to account for the influence of flange geometry on the end conditions for web buckling analysis. In *Eq. 48*, h_c represents the height measured from the center of the top flange to the centre of the bottom flange. The LD threshold is especially significant for fabricated sections, which often feature slender webs and stocky flanges that go beyond the geometric range of the hot-rolled catalogue sections. While the DSM gave substantially overconservative predictions for sections with $LD > 10.94$, Rossi and Li's equation provided more accurate results.

$$P_u = 2\, b_f\, t_f\, f_{y,f} + h_w\, t_w\, f_{cr,w} \tag{46}$$

$$f_{cr,w} = k_w \frac{\pi^2 E}{12(1-\mu^2)} \left(\frac{t_w}{h_w}\right)^2 \tag{47}$$

$$\frac{1}{k_w} = \frac{1.5}{\left(\left(\frac{h_c}{t_w}\right)\left(\frac{2t_f}{b_f}\right)\right)^{2.5}} + 0.18 \tag{48}$$

The compression response of stainless steel stub columns has been extensively studied over the last three decades, covering both austenitic and duplex alloys, and multiple cross-section geometries such as I-sections [43, 30, 100, 44, 40, 42] square hollow sections (SHS) [100, 101, 102, 103], rectangular hollow sections (RHS) [101, 102, 104], channel sections [105, 106] and oval hollow sections [107]. The general body of research on stainless steel stub columns contributed to the development of codified design methods such as CSM, DSM, and EWM. Among these studies, Saliba and Gardner [43] investigated the cross-section stability of lean duplex welded I-sections and recommended to incorporate the modified slenderness limits proposed in [108] into the Eurocode (EC). Studies [43, 100, 102] showed that the codified EWM conservatively predicted the strength of stainless steel sections and modifications to the EWM for improved strength predictions are proposed in [30, 100, 94].

In 2023, Chen et al. [4] showed that hybrid sections, i.e., made of two different steel grades in the web and flanges, were particularly susceptible to strong flange behaviour. They concluded that the unbuckled portion of the slender web plate continues to contribute to post-buckling strength, allowing I-profile stub columns to sustain additional load after buckling. Additionally, Salem et al. [45] investigated the post-local buckling strength of welded I-profiled sections. Part of their tests focused on pure compression, including some sections with strong flanges. They concluded that the web width–to–thickness ratio had a more significant effect on the member capacity compared to the flange width–to–thickness ratios. Gardner et al. [44] tested nine laser-welded stub columns made of different stainless steel grades, including one strong-flange section of EN 1.4571. They concluded that the CSM is more accurate and

less conservative compared to the EWM prediction for the tested specimens which primarily fell in the low slenderness range. Since Gardner's sample largely consisted of conventional I-section geometries, with only one section categorized in the strong flange group, these recommendations cannot be equally reliable for this particular group.

In 2024, Langone et al. [11] further researched the strong flange behaviour of I-profiles under compression and proposed a modified DSM equation applicable to hybrid sections and more accurate than Rossi & Li's method based on preliminary evidence. Langone et al.'s method introduced two new parameters: the slenderness ratio (*SlR*) to categorize which sections would exhibit strong flange behaviour, and strength ratio (*StR*) to quantify the magnitude of the effect on ultimate strength. In 2025, Langone and Ali et al. [99] conducted stub column tests on homogeneous and hybrid stainless steel I-profiles exhibiting strong flange behaviour. These tests more than doubled the body of experimental evidence for strong flange behaviour and provided sufficient evidence to characterize the local buckling mechanisms and plate interactions for these sections.

The experimental data collected from the literature, limited to welded I-profile sections under pure compression, is summarized in Table 11 and covers carbon steel, high-strength steel, stainless steel, hybrid high-strength steel, and hybrid stainless steel. Some studies where a full set of nominal and measured section properties could not be obtained were excluded. These experimental results are shown with the numerical results from Chapter 4.3.1 in Figure 17.

Table 11. Studies containing stub column tests on fabricated stainless steel I-sections.

Author	Ref.	Material	Author	Ref.	Material
Langone et. al., 2025	[99]	SS*	Saliba, 2013	[43]	SS
Gardner, 2016	[44]	SS	Yuan, 2015	[40]	SS
Ran, 2022	[42]	SS	Kuwamura, 2003	[41]	SS
Chen, 2023	[4]	HSS*	Su, 2021	[39]	HSS
Zhou, 2013	[38]	HSS	Rasmussen, 1992	[36]	HSS
Salem, 2005	[45]	CS	Davids, 1989	[37]	CS

CS: Carbon Steel, HSS: High-Strength Steel, SS: Stainless Steel, * includes hybrid sections, different grades in web and flange.

4.2. Numerical Modelling

The first step of this research was to perform a numerical analysis of fabricated I-sections under compression using the commercial finite element analysis (FEA) software ABAQUS 2019 [12]. First, a validation model was developed, and its results were compared against experimental results presented in Langone and Ali et al. [99], which includes both homogeneous and hybrid stub columns. This paper solely focuses on homogeneous stainless steel columns exhibiting strong flange behaviour. Therefore, the three homogeneous stainless steel specimens in [99], made from EN 1.4307 and EN 1.4404 grades, were selected to conduct the validation for this paper. Table 12 provides their measured geometries, and a schematic of the stub column dimensions is given in Figure 13.

In [99], the nominal length of all specimens was set to 350mm to ensure full development of local buckling in each specimen. Homogeneous specimens were designed with webs having a significantly higher width-to-thickness ratio compared to the flanges to ensure that strong flange behaviour would be observed in the cross-sections.

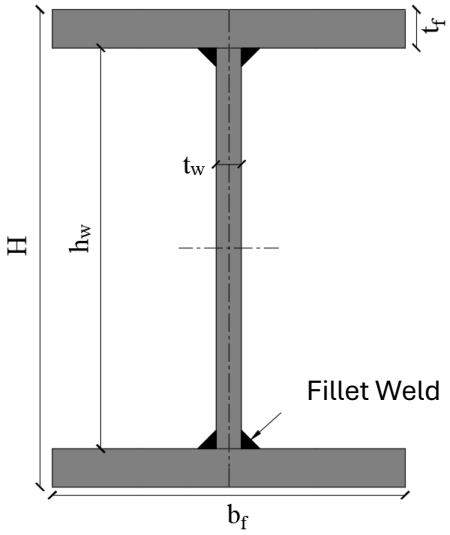


Figure 13. Schematic of the stub column's cross section and notations.

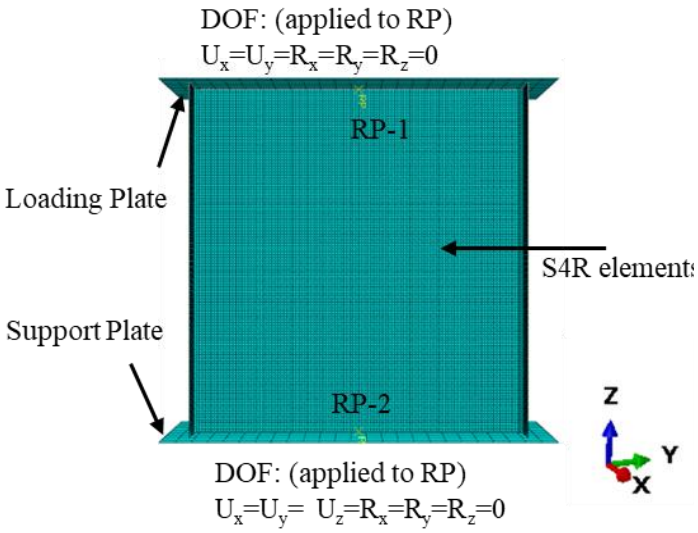


Figure 14. Schematic of the FE model of the stub column test.

Table 12. Materials and measured dimensions of the three tested specimens from [99].

ID	L	h_w	b_f	t_w	t_f	a_w	Flange Grade	Web Grade
	[mm]	[mm]	[mm]	[mm]	[mm]	[mm]		
G3	349.3	285.2	89.39	2.95	6.03	2.4	1.4307	1.4307
F3	349.2	298.4	88.91	2.97	6.06	2.4	1.4307	1.4307
F4	343.0	298.1	89.23	3.02	6.08	2.4	1.4404	1.4404

A description of specific components of the FE model is provided in [99] where the model was applied to analyse buckling modes and the force-displacement response of tested stub columns. The described components include the mesh, boundary conditions, constitutive material model, initial geometric imperfections, residual stress model, and representation of welds [99]. The stub column test model applied static point loading in increments using the static RIKS method [12].

4.2.1. Validation Model

A distinct FE model was developed for each of the stub columns tested in [99]. The parameters in each model which were unique and based on measured characteristics of the tested specimen were the column dimensions, geometric imperfection (GI) magnitude, material properties and non-linearities, and contact imperfections. Sensitivity analysis showed that as

the section approached P_u, the geometric nonlinearity, which was introduced as GI, significantly influenced the column behaviour as reduction in stiffness caused sections to deviate from their ideal stress strain response and reach lower ultimate capacities.

Because stainless steel is a particularly ductile material, it exhibits pronounced nonlinear stress strain behaviour due to its significant strain hardening after the yield point. This enables the sections to carry loads greater than the yield load (P_y) when local buckling does not excessively reduce the column strength. Due to this pronounced material nonlinearity the loss of stiffness that occurs once the FE model reaches the critical elastic buckling capacity is gradual compared to carbon steel alternatives. Thus, the reduction of stiffness and ultimate capacity is smaller for stainless steel sections. In the tests and FE models, the stub columns were compressed to levels of end-shortening far exceeding the point of ultimate strength to capture the post buckling response.

Validation of the FE model was conducted in [99] by comparing load versus end-shortening curves and buckling modes against test results. For the three homogeneous stainless steel stub columns, we show this comparison in Figure 15. Approximate parity between the model and test results is achieved for the initial column stiffness, ultimate strength, and post-buckling response.

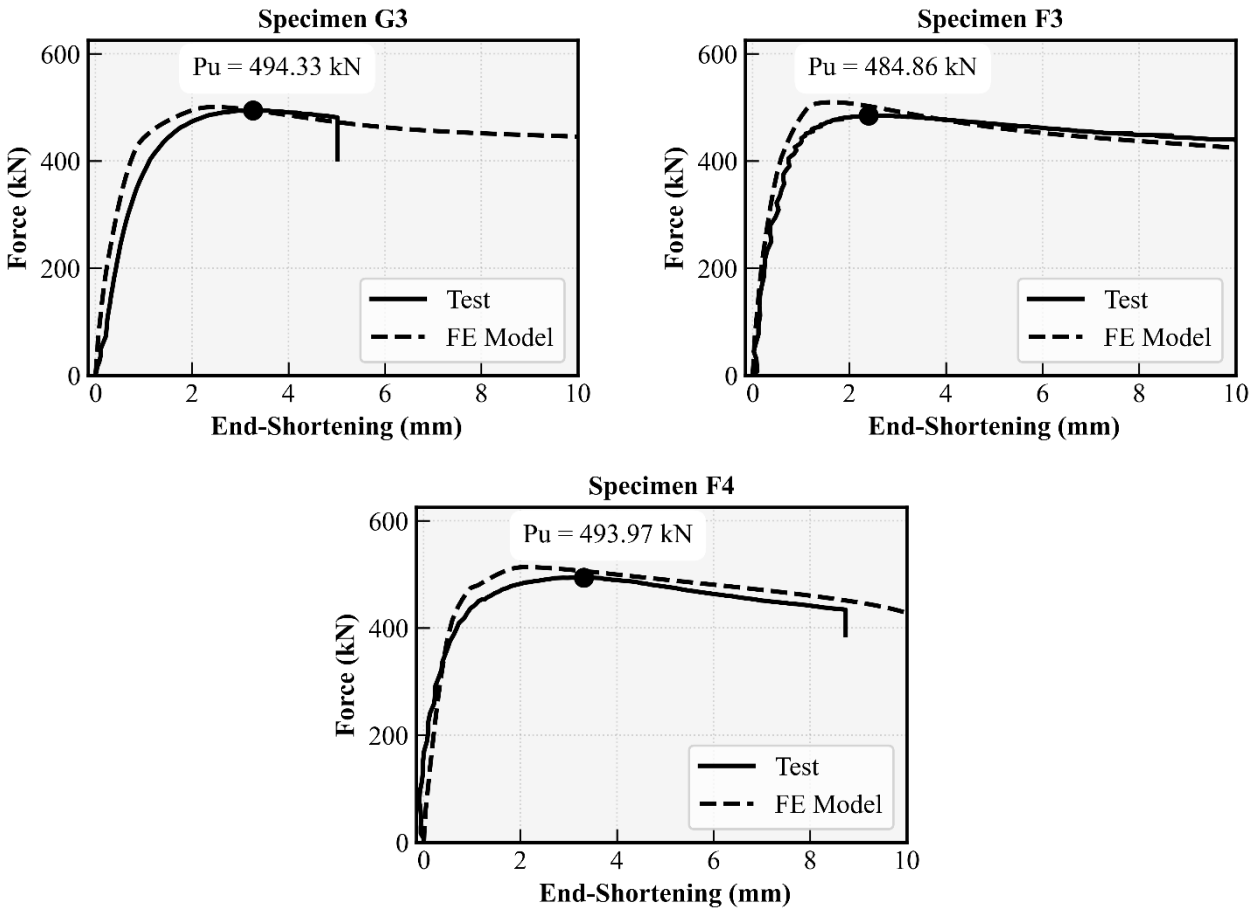


Figure 15. Load versus end-shortening curves for the three tested specimens.

Figure 16 compares the out-of-plane deformations at the point of ultimate force measured by Digital Image Correlation (DIC) from the test against the FE model prediction for these selected three sections. Specimens G3 and F3 are made of the same material, and their only nominal geometric difference is a slightly smaller web height in G3. Specimen F4 has the same nominal geometry as F3, with the difference being the material change from EN 1.4307 to EN 1.4404. Images taken throughout the test by two cameras in stereo configuration were processed to measure the experimental deformations on the web of each specimen, as described in [99]. The plotted DIC results produce a field of out-of-plane deformation values which are in good agreement with the FE model predictions for all three columns. In case of specimen G3, a single half-wave buckle is formed in the web of the section, in contrast to specimens F3 and F4, which show two buckling waves in the web at P_u followed by slight rotations of the

flanges in the opposite directions to accommodate the web deformation and end-shortening. The different buckled shapes observed for G3 and F3 are attributed to variations in contact asymmetries at the column-platen interface caused by small gaps, as discussed previously in [99].

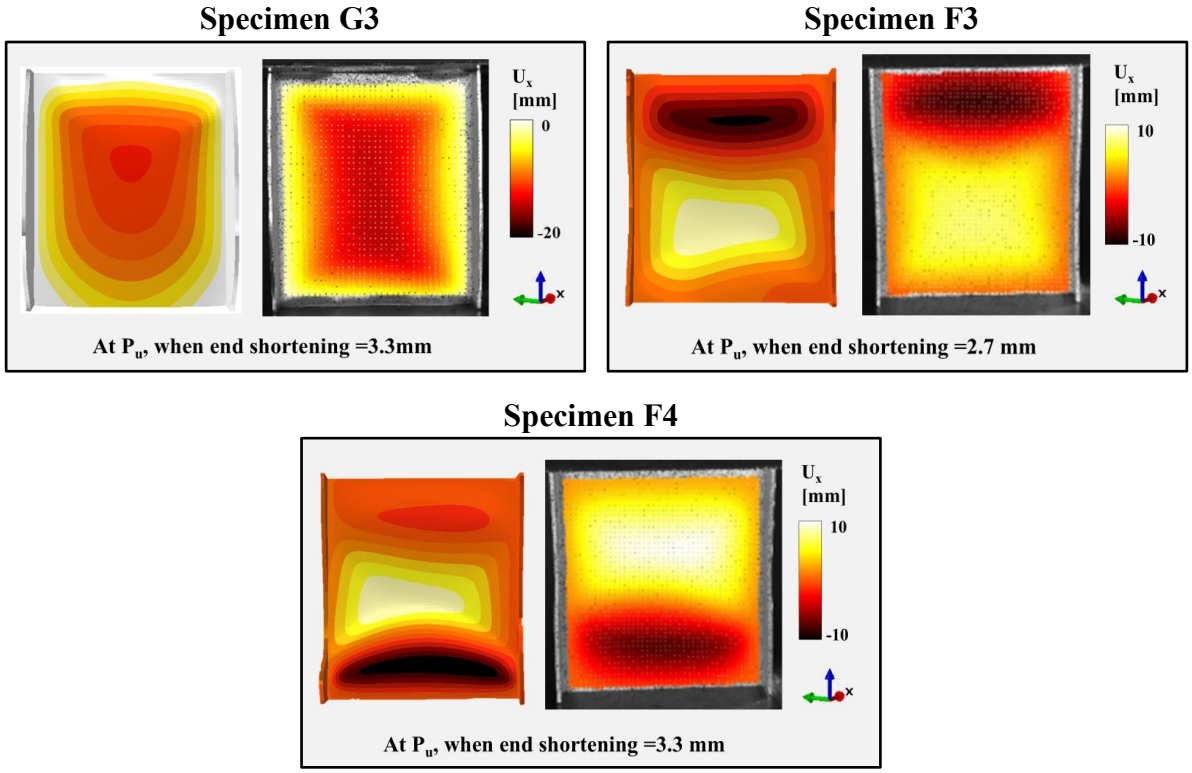


Figure 16. Comparison of buckled shapes in FE models and DIC results.

The comparison between the FE models and the tests shows good agreement, for these three sections, accurately capturing the ultimate loads and reasonably approximating the buckling modes. Table 13 presents a comparison between the ultimate loads obtained from the three modelled stub columns $P_{u,FE}$ and those measured in the tests $P_{u,test}$. The FE predictions are slightly higher than the experimental results with a standard deviation of 0.02. The load versus end-shortening and buckled modes confirm that the FE model can be used for further parametric assessment, with key parameters being the stainless-steel grades and geometries.

Table 13. Comparison of ultimate loads from tests and numerical results [99].

Specimen	$N_{u,test}$ [kN]	$N_{u,FE}$ [kN]	$N_{u,test}$ / $N_{u,FE}$
F3	485	510	0.95
G3	494	501	0.99
F4	494	514	0.96
Average			**0.97**
S.D.			**0.02**

4.3. Parametric Study

The parametric study is comprised of 1325 simulated stub column compression tests. These columns were designed by varying the material and geometric parameters listed in Table 14. All sections in the parametric study are materially homogeneous, using one of four grades from two stainless steel families (austenitic and duplex stainless steel). For duplex grades, there are 560 sections with EN 1.4062 and 155 with EN 1.4462. For austenitic grades, there are 450 sections with EN 1.4404 and 155 with EN 1.4307. Fewer sections are modelled for EN 1.4462 and EN 1.4307 because they have similar material properties to the other grade in their family and are shown to lead to nearly the same structural response. The length of the cross section is chosen to be 1.2 times the height of the web, as proposed by Chen et al. [4] and proven effective to capture local buckling of the web in our sensitivity assessment, or 500 mm (for a small subset of cross-sections), ensuring that global buckling would not occur.

4.3.1. Numerical Model Results

In selecting the parameters to incrementally change, it was ensured that a wide range of slenderness values with different geometries was considered. Series of sections are developed within which all parameters except for one were kept constant. The varied parameter is then studied to capture its effect on the cross-sectional response. In some cases, the ratio between (h_w/b_f) or (t_f/t_w) is the parameter held constant, requiring one parameter to change simultaneously with the other to maintain the constant ratio.

Table 14. Materials and geometric domains of I-sections included in the parametric study.

Stainless Steel Grades	EN 1.4062 EN 1.4462 (Duplex Family) EN 1.4404 EN 1.4307 (Austenitic Family)
Geometric Parameters	h_w: 80 to 710 mm, b_f: 60 to 340 mm t_w: 3 to 7mm, t_f:5 to 14 mm

The material properties for the parametric study are the nominal material properties obtained from the Design Manual for Stainless Steel [90], as reported in Table 15. Full material models are developed using the Ramberg-Osgood equations, then converted into true stresses for Abaqus. Residual stresses were modelled as a rectangular stress block distribution, with stress magnitudes based on [93]. Tensile and compressive residual stresses were in self-equilibrium within each plate element. The GI in the parametric assessment models is introduced using the same approach as in the validation model: taking the first buckling eigenmode from linear perturbation analysis. The magnitude of the amplification factors ω are those specified in Eurocode [51]. The end support conditions were the same as in the validation model, meaning all DOFs were fixed for the rigid plates, except for vertical translation on the top plate. Contact between the column and platens is represented as an ideal fixed-fixed connection by giving coinciding nodes to the elements in contact.

Table 15. Nominal material properties for FE modelling.

Stainless Steel Grade	**Material Properties**		
	E [GPa]	$\sigma_{0.2}$ [MPa]	σ_u [MPa]
EN 1.4062	200	530	700
EN 1.4462	200	500	700
EN 1.4307	200	220	520
EN 1.4404	200	240	530

Unlike the validation models, where end-shortening was measured using strains captured at reference points placed on the outer face of the flange to represent test measurements by a video extensometer, the parametric FE models calculate the end shortening through the vertical

downward movement of a reference point defined at the centre of the top rigid plate. This method is ideal for models with complete fixed contact.

Figure 17 depicts the ultimate capacities obtained from numerical models, normalized by their yield loads $P_y = A\,f_y$ where A and f_y are the cross-sectional area and yield strength. Figure 17 also includes the data from the literature given in Table 11. The data set from the literature contains very few cross-sections with stocky flanges and slender webs. Sections with $\Omega > 6.5$ are classified as having strong flange behaviour based on criteria developed in Chapter 4.3.3. The limited experiments which do demonstrate strong flange behaviour come from [4, 45] which focus on high-strength steel or carbon steel, or from Langone and Ali et al. [99] recently adding experimental evidence for strong flange behaviour of stainless steel cross-sections.

The non-dimensional slenderness $\lambda = \sqrt{P_{ne}/P_{cr}}$ is defined per the DSM in AISI S100-16 [50], where P_{cr} and P_{ne} are the elastic critical buckling load and the global buckling capacity of the section. P_{cr} is recommended to be computed via the finite strip method (using CUFSM), the FE method, or empirical relations proposed in [48, 49], while P_{ne} is calculated using *Eq. 57*. For numerically modelled sections P_{cr} was determined using the FE method, whereas for literature data P_{cr} was determined based on f_{cr} calculated from *Eq. 47* for the most slender plate where the buckling factor k is conservatively taken as 4.0 for internal compression members and 0.43 for outstand elements.

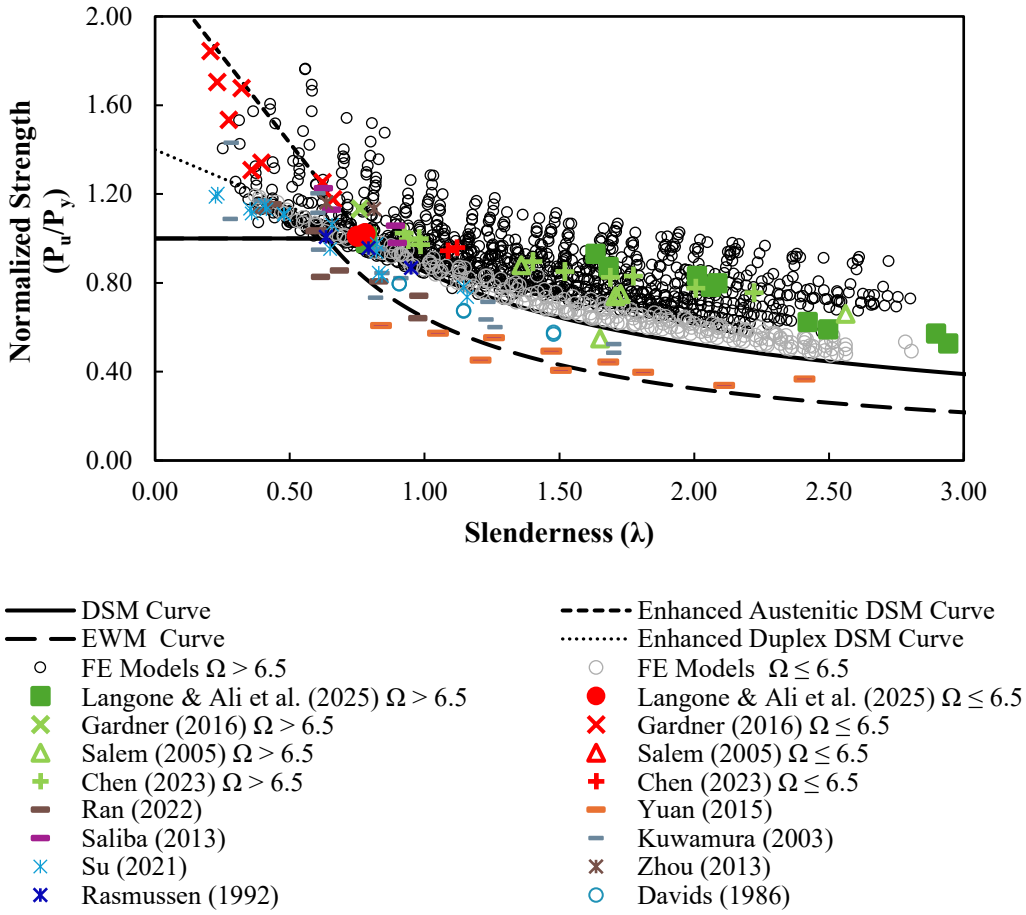
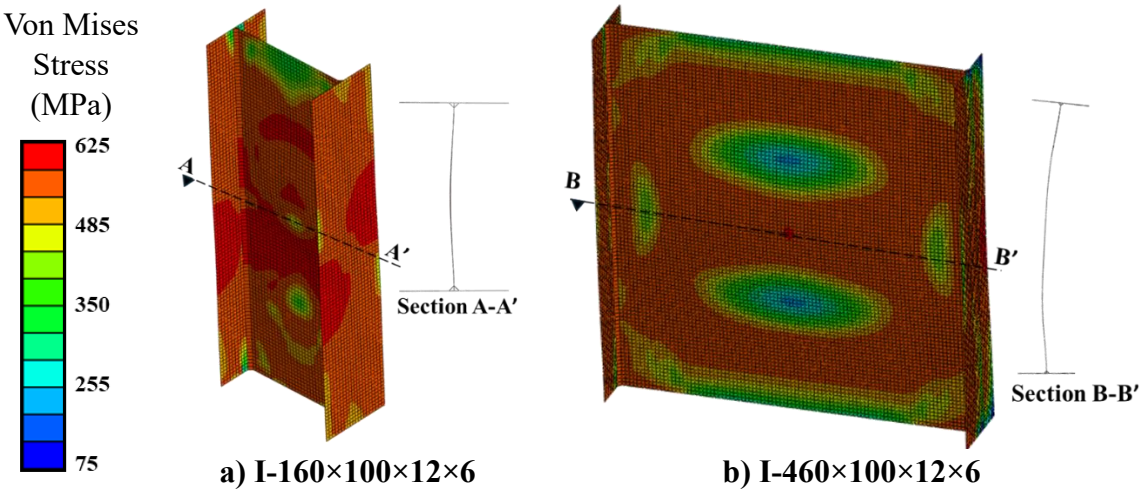


Figure 17. Normalized strength versus slenderness results from experiments in literature overlayed on the results from the FE model parametric assessment.

Figure 17 presents the FE and literature dataset along with four curves: the DSM curve from *Eq. 59*, the EWM curve from *Eq. 54-56*, and the enhanced DSM curves proposed for duplex and austenitic stainless steel from [109], which account for strain hardening effects of stainless steel. Based on the numerical results, the scattered nature of the data for $\lambda > 0.776$ can be attributed to two distinct behaviours of the stub column. One group of sections closely follows the codified DSM curve which is accurate or slightly unconservative in its current form, while the other group of data noticeably deviates from the codified DSM curve and reaches higher than expected normalized strengths. The variation in prediction accuracy for these two groups is attributed to their modes of failures, prompting their categorization into two distinct groups.

Figure 18 shows two typical behaviours observed in the FE study. Section I-460×100×12×6 exhibits strong flange behaviour whereas Section I-160×100×12×6 shows a conventional I-section compression response. Both cross-sections are made up of lean duplex stainless steel EN 1.4062 with a nominal yield strength of 530 MPa. While austenitic stainless steel offers higher ductility and, therefore, greater deformation capacity, the overall failure behaviour and structural response remain largely comparable across these materials. Figure 18 shows the Von Mises stresses developed in the two sections at their respective ultimate strengths P_u.

In section I-160×100×12×6, most of the flanges along with a significant portion of the web have yielded at P_u reaching stresses greater than 530 MPa. Additionally, P_{cr} is significantly higher than both P_u and P_y, causing the section to fail shortly after yielding. This indicates that local buckling does not occur in the elastic range and is not governing the failure. Instead, the section undergoes plastic deformation, with its capacity limited by material yielding. Most importantly, the web, being the most slender element in the cross section, does not buckle before the ultimate load is reached. The section cut A-A' of I-160×100×12×6 shows minimal deformation at the mid-span of the column at the point of ultimate strength.



a) I-160×100×12×6 δ = 2.86 mm (at P_u)

b) I-460×100×12×6 δ = 2.06 m (at P_u)

Figure 18. Schematic of Von Mises stresses for two sections under compression at P_u.

In Section I-460×100×12×6, by contrast, the flange yields while large portions of the web fail to reach 530 MPa. Local buckling of the web initiates at P_{cr}, after which the section exhibits post-buckling reserve strength and partial yielding in the cross-section. However, local buckling prevents fully plastic behaviour across the section, resulting in an ultimate load capacity noticeably lower than P_y. In spite of this, the post-buckling reserve enables the section to sustain additional load beyond the critical elastic buckling point. At higher end-shortening values, a larger portion of the web yields, accompanied by further plastification and rotation of the flanges in the opposite direction. This failure behaviour differs notably from that of the first case, which suggests that a unified classification could lead to conservative predictions.

It is important to note that plate strength reductions due to local buckling are well understood and quantified, for example, in the EWM. Strong flange behaviour of I-sections is therefore of greatest concern when "whole-section" or "non-dimensional" slenderness definitions are used, like in the case of the DSM and CSM, as these methods.

The critical distinction between existing methods and the observed behaviour of I-460×100×12×6 is the extent to which this section reaches higher ultimate forces despite locally buckling. This is caused by two factors. First is the development of stresses beyond f_y due to strain hardening in compact flanges, and potentially in portions of the bucked web. The second is and the extent to which strong flanges provide restrained end conditions for the web which increases the buckling capacity beyond design predictions. This case of element interaction is not accounted for in the EWM. Stronger flanges provide more resistance on the end of the web, leading to a web buckling solution which behaves closer to ideal fixed end conditions rather than a pinned end assumption [48, 49]. Design methods that consider plate strengths independently from the whole section cannot account for these interactions which are more pronounced in strong flange I-sections. On balance, however, accounting for the slenderness

instabilities of each plate has a much larger effect on the ultimate strength prediction than does accounting for element interaction.

The remainder of this paper, therefore, aims to develop a modification to the DSM which quantifies the capacities of strong flange I-sections. This modification will maintain the simplicity of the DSM's whole cross-section approach (which was a primary motivation for its development), account for plate slenderness instabilities with the precision of the EWM, and provide an opportunity to account for element interactions.

4.3.2. Development of the Strong Flange Parameters

The DSM in its current codified form, does not adequately capture the distinct behaviour of strong flange sections. To address this limitation, two parameters, given in *Eq. 49-50*, are introduced into the existing DSM equations which serve to classify strong flange sections and quantify their strength prediction adjustment. The proposed DSM modification incorporating κ and Ω is given in Chapter 4.4.4 (*Eq. 62*) with $\lambda_l = \sqrt{P_{ne}/P_{crl}}$ as the cross-sectional slenderness defined for the cases governed by local buckling.

$$\kappa = \frac{t_f\, b_f}{t_w\, h_w}{\lambda_l}^2 = \alpha{\lambda_l}^2 \tag{49}$$

$$\Omega = \left(\frac{h_w}{t_w}\sqrt{f_{y,f}}\right) / \left(\frac{(b_f - t_w)}{2t_f}\sqrt{f_{y,w}}\right) \tag{50}$$

An extensive range of material and geometric parameters was investigated to best capture the strong flange behaviour effect on ultimate strength. Based on the analysis from Chapter 4.3, it was established that two fundamental effects combine to produce strong flange behaviour: strength reductions due to slenderness instability and interaction of connected elements. Thus, the parameters κ and Ω are derived from approximations of the flange and web plate effective strength and slenderness.

The parameter κ is derived starting from the first premise that strong flange behaviour will be more pronounced in sections where there is a large difference between the effective strengths developed in the plates. The prediction from [1] that strong flange sections develop full yield capacity in the flange and only the critical elastic buckling capacity in the web is used to estimate the effective strength of each plate. This prediction is further supported by analysis of the EWM strength predictions for web and flange plates in strong flange sections. The numerical evidence given in Chapter 4.3.1 confirms that this prediction is a reasonable approximation of the developed effective strengths in high slenderness sections with strong flanges. To incorporate this parameter into the DSM, the flange yield stress $f_{y,f}$ is conservatively approximated as the column global compressive stress f_{ne}, as calculated in the DSM. This enables algebraic manipulation to put the equation in terms of λ_l – which is a term already used in the DSM equation – and a combination of four geometric dimensions, expressed as α. The development of the parameter κ is summarized in *Eq. 51*.

$$\frac{Flange\ Strength}{Web\ Strength} \approx \frac{f_{y,f}\, t_f\, b_f}{\sigma_{cr,w}\, t_w\, h_w} \approx \frac{t_f\, b_f}{t_w\, h_w} \frac{f_{ne}}{f_{crl}} = \frac{t_f\, b_f}{t_w\, h_w} \lambda_l{}^2 = \alpha \lambda_l{}^2 = \kappa \tag{51}$$

When the ratio of numerically computed strength to DSM predicted strength (P_u/P_{DSM}) is plotted against κ, two separate clusters of points are revealed. The upper cluster shows the direct relationship between P_u/P_{DSM} and κ expected for strong flange sections. The lower cluster shows generally no relationship, as expected for conventional I-sections that avoid local buckling or have plates of similar slenderness. The parameter Ω was developed to segregate these two clusters of points. The basis of Ω is that sections with plates of similar slenderness will not exhibit strong flange behaviour. Thus, Ω is the width-thickness ratio of the divided by the square root of web yield strength, all divided by the same for the flange. Algebraically rearranged for simplicity, Ω is defined by *Eq. 50*. The parameter Ω provides a simplified comparison for the web and flange slenderness. A preliminary threshold of $\Omega = 6.5$ was selected by visual inspection as the basis for further analysis. As seen in Figure 19, the $\Omega = 6.5$

threshold is very successful at classifying which sections may exhibit strong flange behaviour. With the κ and Ω parameters defined, the next sections address incorporating these parameters into a modified DSM equation.

4.3.3. Development of the Modified DSM

The relationship between P_u/P_{DSM} and κ was quantified to establish an empirically derived correction factor for the strength prediction of strong flange I-sections. The modified DSM general form, given in *Eq. 52*, shows the logic that for sections which may exhibit strong flange behaviour ($\Omega >$ threshold), then the existing DSM prediction will be multiplied by a correction factor, which is a function of κ.

$$P_{nLG} = \begin{cases} if\ \lambda_l \leq 0.776 \{ P_{ne} \\ if\ \lambda_l > 0.776 \begin{cases} (\lambda_l^{-0.8} - 0.15\lambda_l^{-1.6})P_{ne} & if\ \Omega \leq \text{Threshold} \\ \left(Correction\ Factor * (\lambda_l^{-0.8} - 0.15\lambda_l^{-1.6})\right)P_{ne} \leq P_y & if\ \Omega > \text{Threshold} \end{cases} \end{cases} \quad (52)$$

$$Correction\ factor = 1 + \frac{0.38\ \alpha^{0.8}\ {\lambda_l}^{1.6}}{1+0.12\ \alpha\ {\lambda_l}^2} \quad (53)$$

The dataset for this empirical analysis was the population of the 1325 numerically modelled stub columns for which $\Omega > 6.5$ (i.e., those which may exhibit strong flange behaviour). The y-intercept for the relationship was forced through 1.0. Eleven different equations forms were considered as potential best representations of the data for a design method. Table 16 provides the considered correction factor equations and their design performance. The first three equations in the dataset, labelled with "LB", are fit to a collection of points identified at 0.1 intervals along the x-axis forming the lower bound of the strong flange data cluster. Thus, they have low R^2 values when tested against the full dataset, but fewer unconservative observations in the nominal analysis. The remaining equations are assessed based on their fit to the full strong flange dataset. In all equations, the coefficients are determined by a least squares regression.

Table 16. Evaluation of correction factor equations based on data fit and design performance.

Fitted Curve Equation	R^2	ϕ	$\frac{P_u}{P_{mDSM}}$	$\frac{P_u}{\phi P_{mDSM}}$	Section Count	
					$P_u < P_{mDSM}$	$P_u < \phi P_{mDSM}$
$1 + 1.09\,(1 - e^{-0.38\kappa})^{2.06}$ [LB]	0.159	1.031	1.160	1.13	34	114
$1 + \,(1 - e^{-0.48\kappa})^{2.57}$ [LB]	0.099	1.034	1.166	1.13	32	166
$1 + \,(1 - e^{-0.42\kappa})^{2}$ [LB]	0.245	1.025	1.150	1.12	37	107
$1 + 1.14\,(1 - e^{-0.24\kappa})^{0.78}$	0.753	0.935	1.062	1.14	397	91
$1 + \,(1 - e^{-0.34\kappa})^{0.87}$	0.752	0.936	1.062	1.13	395	88
$1 + \,(1 - e^{-0.73\kappa})^{2}$	0.654	0.946	1.073	1.13	337	101
$-0.98\,e^{-0.408\,\kappa} + 1.98$	0.748	0.938	1.064	1.13	386	85
$0.2\,\kappa + 1$	0.441	0.981	1.106	1.13	184	123
$-0.63\,e^{-0.62\,\kappa} + 0.05\,\kappa + 1.63$	0.751	0.937	1.063	1.13	388	85
$1 + 0.34\,\kappa^{0.57}$	0.743	0.935	1.063	1.14	397	107
$1 + \frac{0.38\,\kappa^{0.8}}{1+0.12\,\kappa}$ **(Selected)**	0.753	0.936	1.062	1.13	397	90

The strength reduction factor ϕ is calculated using each of the tested equations for the correction factor in *Eq. 52*. A full explanation of the reliability assessment is provided in Chapter 4.5. Equations were also evaluated based on the R^2 value for this dataset, average prediction accuracy, and the number of unconservative observations. The preferred correction factor equation is one that has a strong fit to the data, leads to a strength reduction factor reasonably close to 1.0, and is most algebraically simple. Based on these criteria, the final equation in the table is selected for high achieving strong data fit and prediction accuracy at greater simplicity. The selected fitted curve is plotted amongst the numerical and test data in Figure 19.

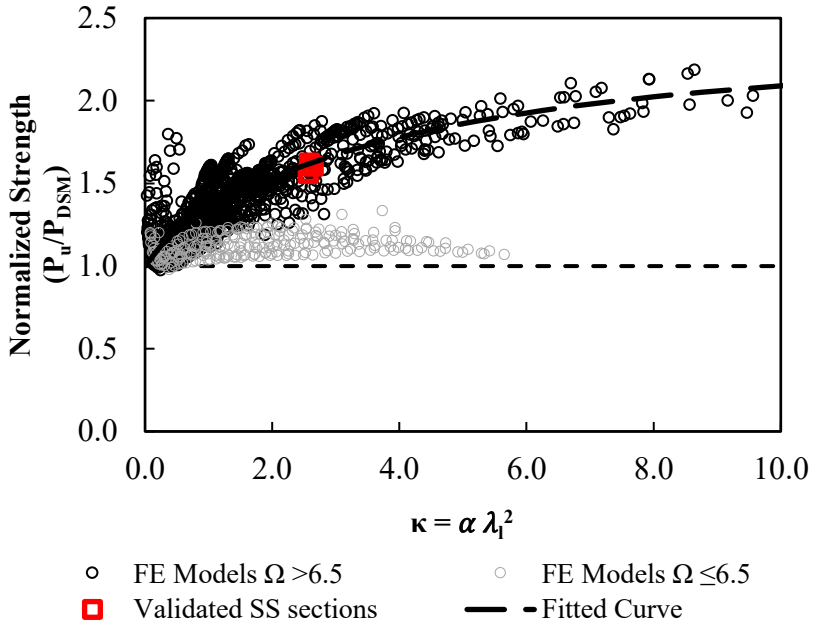


Figure 19. Regression analysis to establish empirical relationship between P_u/P_{DSM} and κ.

After selecting the correction factor equation, the Ω parameter is re-evaluated to select the optimal threshold value for the design method. The threshold value of Ω separating strong flange from conventional I-sections was set by evaluating performance of the modified DSM at 28 possible values of Ω in the range $5 \leq \Omega \leq 15$. Trade-offs were considered between the resistance factor, design accuracy, and conservativeness. The effect of the Ω threshold on these three parameters is shown in Figure 20.

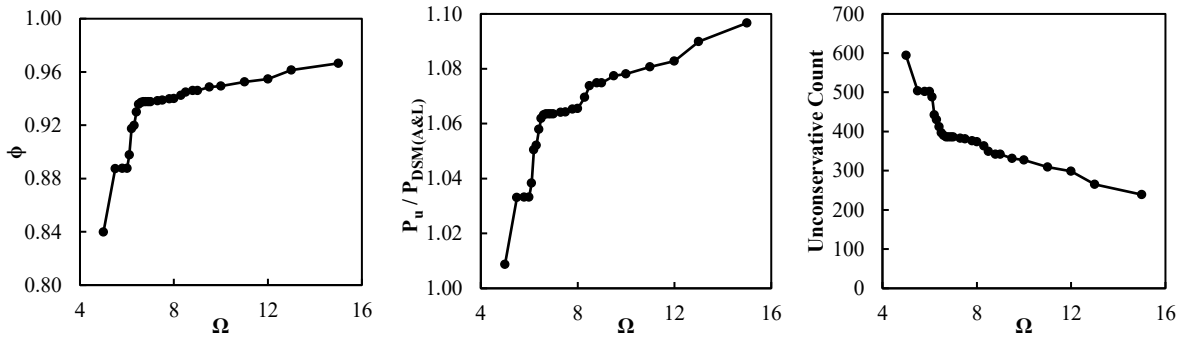


Figure 20. The effect of the Ω threshold on resistance factor, average accuracy, and conservativeness.

Based on this analysis, $\Omega = 6.5$ was kept as the optimal threshold. This is the point at which the slope of each graph becomes less steep. That is, a threshold of $\Omega = 6.5$ achieves the

greatest possible accuracy without causing a rapid decrease in conservativeness. Figure 19 visually demonstrates that the threshold of $\Omega = 6.5$ is effective for separating the clusters of points associated with strong flange and conventional behaviours. With this conclusion, the correction factor equation and Ω threshold is entered into the modified DSM, producing the final proposed equation (*Eq. 62*) which is assessed in Chapter 4.4 against three codified methods.

4.4. Design Method Assessments

In this section, the applicability of codified design methods, including EWM, DSM, and CSM, is assessed for the dataset obtained from FE modelling of homogeneous stainless steel stub columns. A modified form of the DSM is proposed to improve prediction accuracy for strong flange sections, and the method's performance is assessed.

4.4.1. Effective Width Method

The EWM is widely accepted in international design standards [53, 64, 60, 98] where the cross sections are classified based on the width-to-thickness ratio of each plate comprising it. In this paper, the EWM from prEN 1993-1-4:2023 is assessed. For non-slender cross-sections, the ultimate capacity is $P_{EWM} = Af_y$. For slender sections (Class 4), a reduction factor ρ is considered to account for local buckling by reducing the gross cross-sectional area to an effective area $A_{eff} = \rho A$. The effective width factor ρ depends on the plate width-to-thickness ratio, boundary conditions, stress distribution, and material properties. *Eq. 54-56* are used to determine the strength reduction factors for each member element where $\varepsilon = \sqrt{235/f_y}$ is the material coefficient, b and t are the width and thickness of the plate, and Ψ is the stress ratio based on loading and boundary conditions.

$\lambda_p$is the plate slenderness:

$$\lambda_p = \sqrt{\frac{f_y}{f_{cr}}} = \frac{b/t}{27.7\ \varepsilon\sqrt{k}} \tag{54}$$

Internal compression elements:

$$\rho = \begin{cases} 1.0 & for\ \lambda_p \le 0.328 + \sqrt{0.100 - 0.003\Psi} \\ \frac{0.655\lambda_p - 0.003(3+\Psi)}{{\lambda_p}^2} \le 1.0 & for\ \lambda_p > 0.328 + \sqrt{0.100 - 0.003\Psi} \end{cases} \tag{55}$$

Outstand compression elements:

$$\rho = \begin{cases} 1.0 & for\ \lambda_p \le 0.639 \\ \frac{0.655\lambda_p - 0.01}{{\lambda_p}^2} \le 1.0 & for\ \lambda_p > 0.639 \end{cases} \tag{56}$$

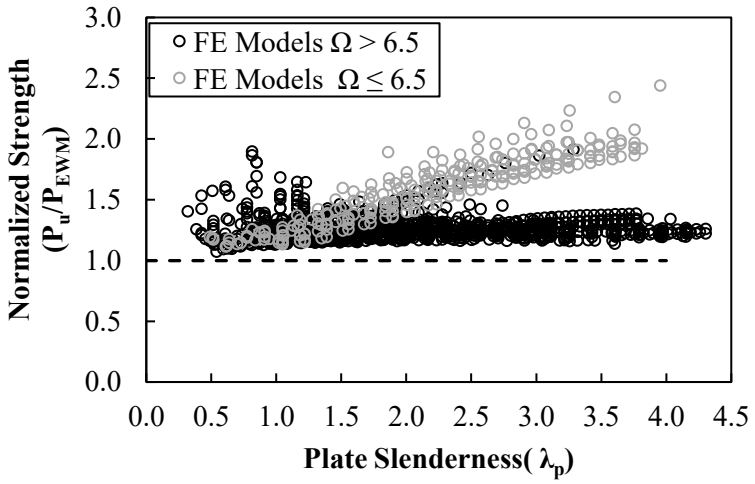


Figure 21. Normalized FE model strength-to-EWM predictions versus slenderness.

EWM performance is evaluated by comparing the numerically obtained compression capacities against Eurocode predictions. Figure 21 shows the ratio of numerically computed strength to EWM predicted strength against the slenderness of the most slender plate of the cross-section λ_p. The EWM is accurate and slightly conservative for predicting the capacity of strong flange cross-sections. The average normalized capacity P_u/P_{EWM} for the group of sections with strong flanges is approximately 20% better predicted than that of the conventional I-section group. Additionally, the CoV for strong flange section group is 0.08, which, despite the conservative bias, reflects less scatter and more uniformity in the predictions compared to the 0.17 CoV observed in the other group. The overall conservative nature of the EC predictions

is partly because the EWM does not allow strengths to exceed the yield capacity, as it neglects strain hardening.

4.4.2. Direct Strength Method

DSM was introduced to design cold-formed steel (CFS) sections exhibiting local, distortional or global buckling or a combination of those [79]. Unlike the EWM, the DSM considers the overall cross-section slenderness termed λ_l for local buckling. The DSM formulation proposes that member's ultimate strength be represented as a direct function of its nominal yield strength and the slenderness for the relevant buckling mode, as given by *Eq. 57-58*. If one failure mode is not present under specific loading, then it is ignored in design [110]. Therefore, the distortional buckling mode is not considered here due to the absence of such buckling modes in these I-profile stub columns. In the DSM equations (*Eq. 57-58*), λ_G and λ_l are the global and local buckling slenderness, $P_{cr\,e}$ and $P_{cr\,l}$ are the capacities under elastic critical global buckling and local buckling, and P_{ne} and P_{nLG} are the global buckling capacity and the combined local-global buckling capacity, respectively. The elastic critical global buckling load $P_{cr\,e}$ is determined from the analytical expression $\pi^2 EI/(KL/r_y)^2$ where K is the effective length factor, r_y is the minimum radius of gyration, and L is the length of the column.

$$P_n = \min(P_{ne}, P_{nLG})$$

$$\frac{P_{ne}}{P_y} = \begin{cases} 0.658^{\lambda_G^2} & \text{if } \lambda_G \le 1.5 \\ 0.877^{\lambda_G^{-2}} & \text{if } \lambda_G > 1.5 \end{cases} \qquad \lambda_G = \sqrt{\frac{P_y}{P_{cr\,e}}} \tag{57}$$

$$\frac{P_{nLG}}{P_{ne}} = \begin{cases} 1.0 & \text{if } \lambda_l \le 0.776 \\ (1 - 0.15\lambda_l^{-0.8})\lambda_l^{-0.8} & \text{if } \lambda_l > 0.776 \end{cases} \qquad \lambda_l = \sqrt{\frac{P_{ne}}{P_{cr\,l}}} \tag{58}$$

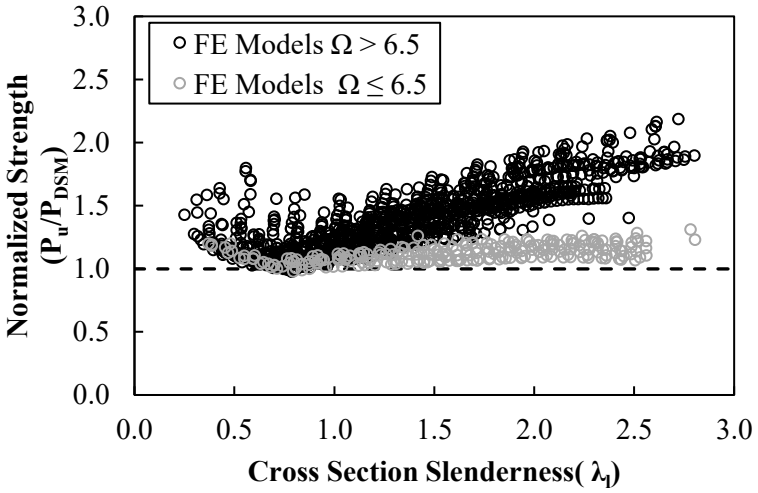


Figure 22. Normalized FE model strength-to-DSM predictions versus slenderness.

Figure 22 shows the ratio of numerically computed strength-to-DSM predicted strength plotted against the cross-sectional slenderness λ_l. The ratio P_u/P_{DSM} for conventional I-sections are on average 25% more accurate than those with strong flanges. Significant variation is observed in the prediction accuracy for strong flanges sections. The CoV for the strong flange section group is 0.18, which is 315% higher than that of the conventional group. When comparing the numerically computed strengths normalized by the DSM and EWM strengths for the whole dataset, the averages are quite close as shown in Table 17. However, for sections with strong flanges, the EWM prediction average is 1.26 compared to 1.40 for the DSM prediction. This suggests that the DSM method is too conservative when predicting the capacities of the sections with strong flanges, contrary to the EWM which was too conservative for non-strong flange sections.

4.4.3. Continuous Strength Method

CSM is a deformation-based design method that was introduced in 2008 [81] to capture the continuous resistance predictions across varying cross-section slenderness. It is comprised of two main components, *a)* base curve and *b)* constitutive material model. The codes [111, 64]

propose two different equations for the base curves, one to use with the bi-linear material model and the other to use with the rounded two-stage Ramberg-Osgood material model.

Unlike the EWM, the CSM considers the effects of strain hardening and element interaction to predict the ultimate capacity of stainless-steel compression members. Various researchers have applied the CSM to the design of non-slender stainless-steel sections as originally proposed [112, 82, 113] and have also extended the method to slender steel sections [114]. The relationship between the cross-sectional slenderness $\lambda_{p.cs} = \sqrt{P_y/P_{cr}}$ and the normalized deformation capacity $\varepsilon_{csm}/\varepsilon_y$ is given by *Eq. 59*. Importantly, here $\lambda_{p.cs}$ is different than the DSM slenderness λ_l. The strain hardening modulus E_{sh} is defined as $\frac{f_u - f_y}{C_2\ \varepsilon_u - \varepsilon_y}$, ε_u and ε_y are the strains at ultimate strength and yield strength points, and f_u and f_y are the ultimate tensile stress and yield stress. For austenitic and duplex stainless steel grades, C_1 is taken as 0.1 and C_2 as 0.16. The cross-sectional compression resistance P_{CSM} is determined with *Eq. 61*.

$$\frac{\varepsilon_{csm}}{\varepsilon_y} = \begin{cases} \frac{0.25}{\lambda_{p.cs}^{3.6}} \leq \min\left(15, \frac{C_1\ \varepsilon_u}{\varepsilon_y}\right) & \lambda_{p.cs} \leq 0.68 \\ \left(1 - \frac{0.222}{\lambda_{p.cs}^{1.050}}\right) \frac{1}{\lambda_l^{1.050}} & \lambda_{p.cs} > 0.68 \end{cases} \tag{59}$$

$$f_{csm} = f_y + E_{sh}\ \varepsilon_y \left(\frac{\varepsilon_{csm}}{\varepsilon_y} - 1\right) \tag{60}$$

$$P_{CSM} = \begin{cases} \frac{\varepsilon_{csm}}{\varepsilon_y}\ A\ f_y & \frac{\varepsilon_{csm}}{\varepsilon_y} < 1 \\ A\ f_{csm} & \frac{\varepsilon_{csm}}{\varepsilon_y} \geq 1 \end{cases} \tag{61}$$

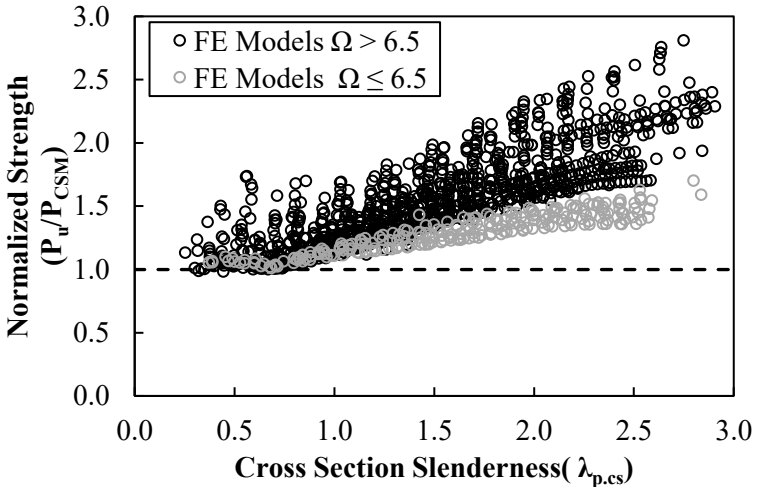


Figure 23. Normalized FE model strength-to-CSM predictions versus slenderness.

The numerically computed strengths normalized with the CSM predictions, are plotted against $\lambda_{p.cs}$ in Figure 23. The results indicate that the current form of the CSM is more conservative than EWM or DSM when predicting the capacities of the given dataset, yet accurate enough to predict the strength of cross-sections in the conventional behaviour category. When the two groups are examined separately, the CSM provides more accurate predictions for sections with conventional behaviour category in the low slenderness range, while it becomes overly conservative for those with strong flanges. The CoV for sections with strong flange group is 0.23, nearly twice as high as of the conventional I-section group, indicating greater scatter and substantially lower strength predictions.

4.4.4. Modified DSM Proposal

The codified form of the DSM is not sufficiently accurate to predict the capacities of sections with strong flanges. Therefore, a modification is necessary to enhance its predictive performance. In Chapter 4.3.2, the parameter Ω was established to define the transition between different section behaviours. The proposed $DSM_{(A\&L)}$ equation, given in *Eq. 62*, applies Ω to identify sections likely to exhibit strong flange effects. The parameter $\alpha = \frac{t_f\, b_f}{t_w\, h_w}$ is applied,

along with the previously established parameter λ_l, to quantify the magnitude of the strong flange effect.

$$P_{nLG} = \begin{cases} if\ \lambda_l \leq 0.776\ \{ P_{ne} \\ if\ \lambda_l > 0.776 \begin{cases} \left(\lambda_l^{-0.8} - 0.15\lambda_l^{-1.6}\right)P_{ne} & \text{if } \Omega \leq 6.5 \\ \left(\left(1 + \frac{0.38\ \alpha^{\ 0.8}\ \lambda_l^{\ 1.6}}{1+0.12\ \alpha\ \lambda_l^{\ 2}}\right)\left(\lambda_l^{-0.8} - 0.15\lambda_l^{-1.6}\right)\right)P_{ne} \leq P_y & \text{if } \Omega > 6.5 \end{cases} \end{cases} \quad (62)$$

The proposed modification limits the section capacity to P_y. Figure 24 reports the performance of the proposed $DSM_{A\&L}$ method evaluated against the numerically computed dataset. The results show that the CoV for the strong flange section is reduced by 40% compared to the original DSM prediction, indicating significantly less scatter and more precise capacity predictions. The average ratio $P_u/P_{DSM(A\&L)}$ show that this new design modification improves the average accuracy of predictions by at least 21%. For sections categorized as strong flange sections, the average of the numerically computed strength normalized by the codified DSM strength prediction is approximately 1.40. This is substantially improved to 1.05 when normalized by $DSM_{(A\&L)}$ strength prediction.

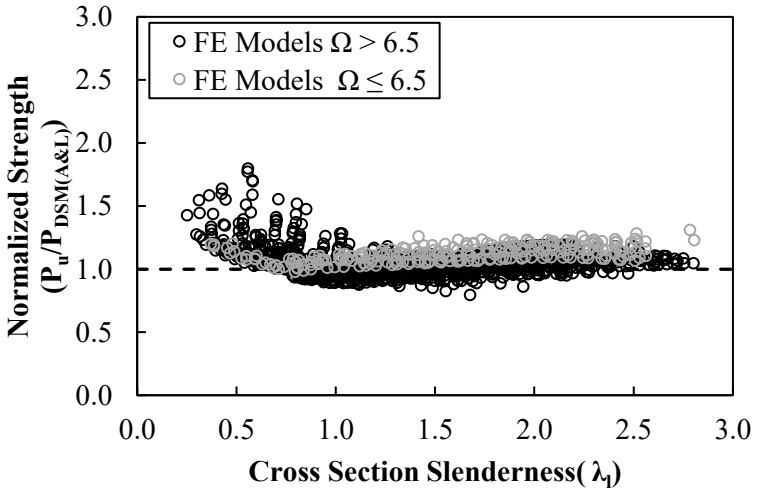


Figure 24. Normalized FE model strength-to-$DSM_{(A\&L)}$ predictions versus slenderness.

Table 17 summarizes the numerically computed strengths normalized with the predictions from the evaluated design methods. It shows that the $DSM_{(A\&L)}$ provides the most precise predictions, with the lowest CoV among all methods. While the EWM provides precise,

slightly conservative predictions for strong flanges sections, it is more conservative for the sample of conventional behaviour sections. The CSM is very conservative, particularly for strong flange and high slenderness sections. The codified DSM is accurate for conventional sections, but overconservative for strong flanges sections.

Table 17. Numerically computed strengths normalized by nominal strengths from four design methods.

Normalized Predictions	Sections	Sample Size	Average	CoV
$\frac{P_u}{P_{EWM}}$	$\Omega \leq 6.5$	241	1.582	0.169
	$\Omega > 6.5$	1082	1.263	0.081
	All sections	1323	1.321	0.145
$\frac{P_u}{P_{DSM}}$	$\Omega \leq 6.5$	241	1.122	0.057
	$\Omega > 6.5$	1082	1.398	0.180
	All sections	1323	1.347	0.187
$\frac{P_u}{P_{CSM}}$	$\Omega \leq 6.5$	241	1.281	0.114
	$\Omega > 6.5$	1082	1.477	0.239
	All sections	1323	1.441	0.231
$\frac{P_u}{P_{DSM(A\&L)}}$	$\Omega \leq 6.5$	241	1.122	0.057
	$\Omega > 6.5$	1082	1.047	0.110
	All sections	1323	1.061	0.105

4.5. Reliability Assessment

The performance of the proposed design equations was assessed in accordance with the reliability assessment guidelines in the commentary to Chapter B of AISC 370-21 [60]. The Load and Resistance Factor Design (LRFD) approach is applied throughout this analysis. The resistance factor ϕ required for the DSM$_{(A\&L)}$ is calculated as a function of two parameter types: (1) established basic variables describing material and geometric characteristics of steel members and (2) performance data for the design method evaluated against a sample of numerical or experimental evidence.

The equation to calculate ϕ is given in *Eq. 63*, where M_m and F_m are the average ratio between measured and specified minimum values for mechanical properties and geometrical

properties, respectively. P_m is the ratio of numerically computed failure loads from the relevant dataset to the design method predicted failure loads. β is the target reliability index, set at 2.6 for members which entails targeting a 0.47% probability of failure. V_Q is the variation of load effects, based on assuming a dead-to-live load ratio of three. V_R is the variation of resistance, which is a function of the variation of mechanical properties, geometrical properties, and design prediction errors, as seen in *Eq. 64*.

$$\phi = \frac{1.481\, M_m F_m P_m}{exp\left(\beta\sqrt{{V_R}^2+{V_Q}^2}\right)} \tag{63}$$

$$V_R = \sqrt{{V_M}^2 + {V_F}^2 + {V_P}^2} \tag{64}$$

Most parameters in the equation are provided in the code based on meta-assessments drawing from large samples of experimental data on stainless steel members. For the average and CoV of mechanical properties (M_m and V_M), different values are given in the code for the austenitic and duplex families of stainless steel. P_m and V_P must be calculated based on comparison of the design method against the numerically computed ultimate strengths.

Table 18. Reliability assessment parameters for stainless steel members.

β	M_m	F_m	P_m	V_R	V_M	V_F	V_P	V_Q
2.6	1.25 (A) 1.10 (D)	1.00	Data Dependant	$\sqrt{{V_M}^2 + {V_F}^2 + V_P}$	0.08 (A) 0.04 (D)	0.05	Data Dependant	0.19

Mechanical properties have different averages and CoVs in different families of stainless steel.
(A) indicates austenitic stainless steel and (D) indicates duplex.

Because the code provides different basic variables for different stainless steel, it is possible to calculate different resistance factors for each family. However, when resistance factors for design methods are specified in the stainless steel code [60], one overall ϕ factor is provided. In this paper, the overall factor is calculated by taking the more conservative basic variable for each parameter and applying these to the full dataset. That is, taking 1.10 for M_m and 0.08 for V_M. Figure 25 shows the resistance factor results of $DSM_{(A\&L)}$ evaluated at 28 different threshold values for Ω. The same general trend that was shown in Figure 20 is

preserved when calculating the resistance factor for individual stainless-steel families, and the "Overall" curve is the most conservative, as expected.

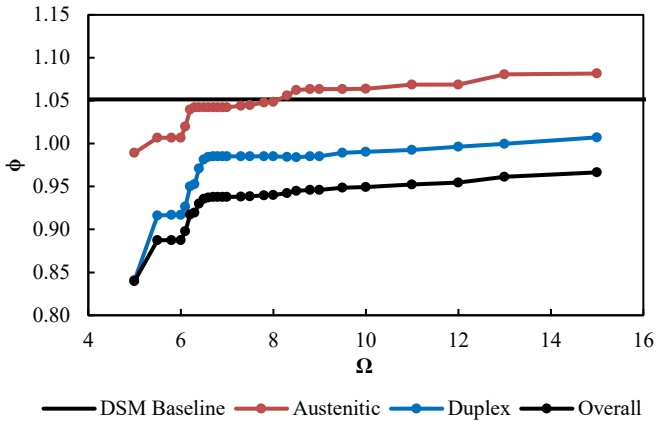


Figure 25. Resistance factor ϕ versus Ω threshold for multiple stainless steel families.

The DSM baseline set at $\phi = 1.05$ in Figure 25 was determined by calculating the resistance factor per *Eq. 63* for the codified DSM based on our numerical dataset. As a basis of comparison, the LRFD resistance factor $\phi = 0.85$ is given for the DSM in AISI S100-16 (2020) Section E3 [50] on compression members susceptible to local buckling interacting with yielding and global buckling. The "Overall" ϕ value of 0.963 was calculated for the $\text{DSM}_{(\text{A\&L})}$ at the selected Ω threshold of 6.5, which it as significantly lower than the calculated DSM baseline for this dataset, but still safely above the 0.85 value given in the code.

The average ratio of numerically computed-to-predicted strengths and number of unconservative observations for the nominal $P_{DSM(A\&L)}$ and design strength $\phi P_{DSM(A\&L)}$ are reported in the final row of Table 16, containing the selected correction factor equation. The calculated ϕ value of 0.963 was used to determine the design strengths. Unconservative observations are counted as sections for which the numerically computed ultimate strength is less than the calculated design strength. The nominal prediction has an average of 1.06 with 397 unconservative observations. The factored design strengths produce to an average of 1.13 with 90 unconservative observations.

The number of unconservative observations in the design strength analysis is unusually high, representing a 6.8% probability of failure compared to the target probability of 0.47%. This observation is related to the finding that the ϕ values calculated based on this dataset for both P_{DSM} and $P_{DSM(A\&L)}$ are higher than the codified resistance factor. High calculated values of ϕ are a substantial influence leading to the high number of unconservative observations. This observation is caused by the uniqueness in the 1325 observation numerical dataset.

The plots in Figure 26 report the distribution of numerically computed strengths divided by the predicted strength. The reliability assessment calculated a required ϕ of 0.963 while the AISI code recommends ϕ of 0.85. One of the core assumptions invoked in reliability assessment is that variation in load and resistance effects is normally distributed [50, 60]. This is generally a safe assumption for sufficiently large datasets. While the dataset used in this research is very large, the numerically computed-to-predicted strength errors have a right skew. The histograms in Figure 26 are overlayed with normal distributions defined by the mean and standard deviation of the data.

In the nominal case $P_{DSM(A\&L)}$ returns an average error term P_m of 1.062 with a standard deviation of 0.111. The nominal strength prediction is unconservative for 30% of the dataset. The design strength with ϕ as 0.963 returns an average of 1.13 and standard deviation of 0.118, with 6.8% unconservative observations. Finally, the design strength with codified ϕ of 0.85 return mean of 1.25 and 0.13 standard deviation, and only 0.15% unconservative results.

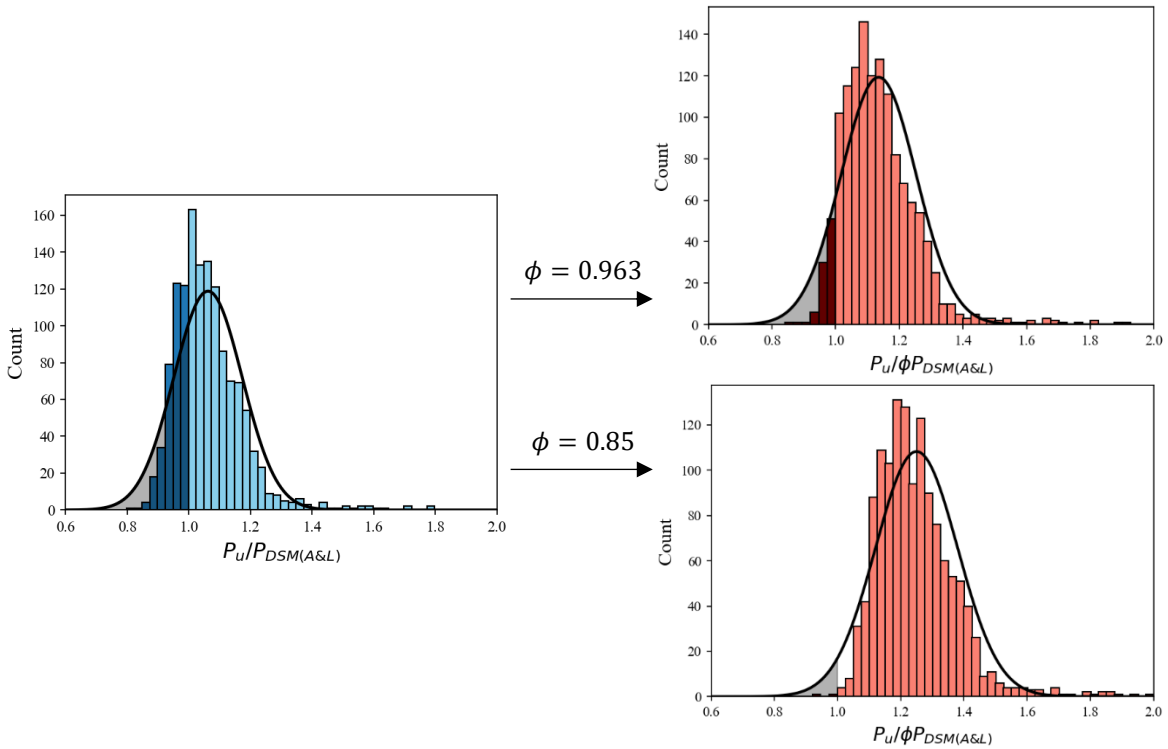


Figure 26. Distribution of numerically computed-to-predicted strength ratios based on two ϕ values.

The observed probability of failure will vary based on changes in the dataset that a design method is evaluated against. This reliability analysis, however, does show strong evidence that the proposed $DSM_{(A\&L)}$ method may be applicable with the same resistance factor that is currently used in the American code for the DSM [50]. The dataset nearly fulfils the assumption of normally distributed variation, with the slight skew caused mostly by sections in the low slenderness range that develop loads far above yield capacity. The 0.15% probability of failure when using the codified ϕ of 0.85 is safely below the targeted probability of failure – approximately 0.47% in the case of a standard normal cumulative distribution – based on the β of 2.6 given in American code [60] for members.

4.6. Conclusions

This research demonstrates that certain geometries of I-profile cross-sections exhibit behaviours not well accounted for by existing design methods. This is particularly true when members have plates of different slenderness and the design method considers a whole-section

definition of slenderness. Whole cross-section definitions of slenderness, used in the DSM and CSM, were found to produce over-conservative predictions for ultimate strength when I-section flanges were substantially stronger and less slender than the web plate.

A detailed FE model was developed and validated against experimental results in a companion paper by the authors [11]. The validated model was then extended to conduct a comprehensive parametric study considering a wide range of geometric parameters and four stainless steel grades, two austenitic and two duplex. A total of 1325 stub column compression tests were modelled, including both strong flange and conventional I-sections.

Strength predictions from three codified design methods – the EWM, DSM, and CSM – are compared with the numerical results. Plots in Chapter 4.4 demonstrate that strong flange behaviour is a characteristic affecting design accuracy in all three methods. Among these methods, the current EWM predicts the capacity of strong flanges sections most accurately. The DSM and CSM give conservative predictions with high variation for the strength of strong flange I-sections, and the DSM is generally accurate for non-strong flange sections.

A modified DSM is developed to identify sections likely to exhibit strong flange behaviour and predict the effect on ultimate strength (*Eq. 62*). Two new parameters, Ω and α are included in the new $DSM_{(A\&L)}$ formulation to classify and quantify this behaviour. The proposed $DSM_{(A\&L)}$ is evaluated against the numerical data and is shown to provide predictions with the greatest accuracy and lowest variation among the considered methods. A reliability assessment indicates that the existing DSM codified ϕ value of 0.85 applied with the new $DSM_{(A\&L)}$ equation leads to an acceptable probability of failure across the full range of slenderness. The proposed $DSM_{(A\&L)}$ preserves most of the simplicity of the codified DSM, while introducing two simple parameters that are sufficient to account for the effects of strong flange behaviour in stainless steel I-sections under pure compression.

4.7. Acknowledgements

Usman Ali is a doctoral candidate whose research and studies are funded by the Marie Sklodowska-Curie Doctoral Network (MSCA-DN) SeaChem project, EU Grant No. 101073471. Gregory Langone is an Engineer Officer in the U.S. Army and a recipient of the John & Daria Barry Scholarship which generously supports his studies. The authors also gratefully acknowledge Majid Shamlooei (majid.shamlooei@unitn.it) for his contribution to the initial FE model development.

5. DISCUSSION & CONCLUSION

5.1. Treatment of Stainless Steel Families in Reliability Assessment

Progress in steel manufacturing and design methods through the 1990s has driven increased adoption of high strength and stainless steel members [6, 115]. These materials have unique structural characteristics which require re-evaluation of design methods and reliability assessments to ensure applicability. These re-evaluations have been substantially addressed for stainless steels [65, 116] and high strength steels [117, 118, 119]. Nonetheless, there are features of how the existing reliability methods deal with different families (e.g. austenitic and duplex) of a similar material that ought to be clarified for the assessment of stainless steel structures.

In American and European reliability standards, different values are given for basic variables defining properties of austenitic and duplex stainless steels. In both standards, the coefficient of variation and average ratio of measured-to-specified values for material strengths and geometrical dimensions are used as generalizable parameters to describe the reliability of all structures of a given material family. The values used in these codes are compiled in Table 19. The mean values for yield stress are not directly applied in the Eurocode, but the concept of over-strength applied in [65] by Afshan et al. provides an equivalent variable based on meta-analysis of the available test data. The parameter values in the Eurocode column are all taken from [65].

Table 19. Basic reliability parameters for austenitic and duplex stainless steels.

		Austenitic		**Duplex**	
		AISC	**EN**	**AISC**	**EN**
Yield Stress	Mean	$M_m = 1.25$	$O.S. = 1.30$	$M_m = 1.10$	$O.S. = 1.10$
	CoV	$V_m = 0.08$	$V_{fy} = 0.06$	$V_m = 0.04$	$V_{fy} = 0.03$
Geometry	Mean	$F_m = 1.00$	n/a	$F_m = 1.00$	n/a
	CoV	$V_F = 0.05$	$V_{geom} = 0.05$	$V_F = 0.05$	$V_{geom} = 0.05$

Although American and European reliability methods provide different basic variables for the mechanical properties of these material families, one universal resistance factor or

partial factor pertaining to all stainless steel families is specified in the design codes. One way to achieve a general solution for all stainless steel families is to take the more conservative value among the possible materials for each variable, as was done in Chapter 4.5. The more conservative selection is the lower value for the mean parameters and the higher value for variance parameters. When this is done, a lower, more conservative value for the resistance factor ϕ in the American code is calculated which is broadly applicable to stainless steels. This result is demonstrated Figure 25 where the resistance factor that applies to all stainless steel families is systematically lower than that calculated for just austenitic or duplex members.

The procedure used to calculate broadly applicable resistance factors for multiple material families in the AISC design code is not explicitly defined. This makes it difficult to assess the extent to which the provided resistance factors are conservative. The evidence from Chapter 4.5 indicates that a designer who uses only austenitic stainless steels may be able to justify increasing the codified resistance factor by approximately 10% due to the higher reliability of the austenitic family. In the modern stainless steel industry, where structural applications face limited viability due to up-front capital costs approximately four times greater than carbon-steel alternatives, a 10% increase in structural efficiency would represent a significant contribution to lowering costs.

The issue of how to represent basic variables for different families of stainless steel applies generally in the same way for the Eurocode reliability method. The Eurocode has an additional complication, however, because EN1990 includes a clause that permits reliability assessments for individual stainless steel families to be conducted while counting the sample size of a larger database – intended to prevent needlessly increasing the partial factor because of small sample sizes. The purpose of this clause is that when the variance of a design method is too high, it can be because multiple underlying behaviours/materials are being addressed. Thus, splitting these behaviours/materials into two separate populations can allow a more

precise model for each distinct population to be developed. In the case of stainless steels, designers split austenitic and duplex families into separate categories to represent their distinct basic variables. When this is done, however, the clause in EN1990 D8.2.2.5(4) allows the fractile factor k_n to be based on the total number of tests in the dataset (before it was split into multiple categories). Generally, sample size directly determines the fractile factors $k_{d,\infty}$ and $k_{d,n}$, with larger sample sizes leading to smaller, less conservative partial factors γ. This clause introduces an arbitrary factor into the reliability analysis without providing criteria for when this is permitted.

The category splitting clause in EN1990 does not resolve the problem of how to represent basic variables, because it still requires the average measured-to-predicted strengths ratio to be calculated separately for each family. The clause only specifies that the sample size for the dataset does not need to be constrained to the set of evidence for that specific family. Critically, insufficient guidance is given for what the "full" dataset should be defined by. Can it include tests for all stainless steel families? What about carbon steel, high-strength steel, or other materials? The guidance attached to this clause ought to be specified more tightly, or removed entirely, to prevent arbitrary factors from reducing the consistency of reliability results.

5.2. Conceptual Contextualization for Design Methods

Investigation into the strong flange behaviour of I-sections was inspired primarily by observations that the DSM strength predictions for a certain group of similar sections were consistently over-conservative. Throughout this research project, three design methods were investigated (DSM, CSM, and EWM) and all three fell short of accurately describing I-section ultimate strength behaviours when considering a wide range of geometries. While Chapters 3 and 4 focused on analysing these methods to distil a more suitable design equation, it is useful

here to point out the conceptual differences between the codified design methods and what is learned from this context.

Slenderness in the DSM and CSM is defined as a single parameter which represents the whole cross-section. This is not entirely consistent with the underlying theory of plate buckling [54]. In the case of plated members, it is instead that local buckling instability from slenderness arises within an *individual* plate element and is primarily governed by the plate width-to-thickness ratio. Schafer and Gardner understood this well when developing the DSM and CSM, respectively. That theoretical understanding was not included in the DSM and CSM, however, because the definition of cross-sectional slenderness as $\lambda = \sqrt{P_y/P_{cr}}$ matches most empirical evidence well and a designer can ensure the estimation is conservative by allowing the most slender element in the cross-section to govern. This conservative estimation, however, causes increasingly inaccurate predictions when the difference in slenderness between plate elements is very large. The EWM is distinctly different from the CSM and DSM, because it defines a slenderness for each individual plate and requires the designer to account for the potential of different strength reduction factors in every plate. Conceptually, the EWM is clearly better suited to design for strong flange behaviour because it can apply to a wider range of geometric possibilities.

The treatment of slenderness as a continuous or discrete parameter is another difference between these methods. In the EWM, slenderness is defined in four distinct classes corresponding to four distinct behaviours. In Class 1, sections can develop their full plastic hinge resistance. In Class 2, sections develop plastic moment resistance with rotation capacity limited by buckling. In Class 3, the extreme fibres of the member can reach the yield stress but buckling prevents plasticity from further developing. In Class 4, local buckling occurs before attaining the yield stress in at least one element of the cross-section. The EWM requires that a reduction factor be applied for cross-sections with one or more Class 4 element. Classification

limits are empirically determined and are different for all materials. Importantly, the empirical data indicates that the relationship between strength and slenderness is more continuous than stepwise. Nonetheless, the EWM uses a conservative stepwise equation to design based on this relationship. The DSM similarly recommends no strength reductions for Classes 1-3 in pure compression and defines a curve representing strength reductions which is similar to the way the EWM treats Class 4 sections. The CSM, in contrast, defines a continuous relationship between slenderness and deformation capacity which removes the stepwise definition entirely.

In Chapter 4, an extensive range of material and geometric parameters was investigated to best capture the effect of strong flange behaviour on ultimate strength. In this investigation, it was determined that two fundamental effects combine to produce strong flange behaviour: strength reductions due to slenderness instability and interaction of connected elements. The codified DSM is particularly poorly suited to address these behaviours, because it has no mechanism to account for the characteristics of individual plates. The calculation of cross-sectional slenderness λ_l in the DSM is skewed when one plate is extremely slender, and the other is stocky. There is also no mechanism in the DSM to predict that strong flanges may increase the buckling capacity of the web through interaction by providing more fixed end conditions. Between these two effects, slenderness instabilities have the larger influence on ultimate strength.

Because design methods are mathematical abstractions of physical reality which quantify a parameter of interest, they always need to trade-off accuracy and simplicity. Among the three codified methods investigated for their applicability to strong flange behaviour, the EWM is the most accurate and least simple. The EWM is generally precise and conservative to design for strong flange behaviour, as is detailed in the Chapter 4.4.1. As expected, the DSM and CSM are more simple and less accurate, to similar extents. One of the two principal justifications for establishing the original DSM was to reduce design labour for members with multiple elements

and stiffeners. Thus, a successful DSM modification had to account for the different effective strengths in each plate without sacrificing too much of the original method's simplicity. The modified DSM proposed in Chapter 4.4.4 achieved this by preserving the core methodology and incorporating only two additional parameters which are calculated as simple ratios of geometrical dimensions.

5.3. Research Impact and Efficiency Gains

Pure compression loading, which has been the focus of this research project, will remain the minority use case for I-section members – both hot rolled W-shapes and built-up plate girders. This is simply because the I-profile is particularly well suited to resist the stresses that develop under flexural loading. The breadth of possible applications combined with recent research advancements on hybrid and strong-flange sections indicates that these types of sections offer benefits which warrant further consideration for multiple use cases.

The principal advantage of hybrid and strong flange I-sections is the potential for increased structural efficiency (i.e., the load a structure can hold divided by the weight of the structure itself) when properly designed. Structures such as bridge piers and high-rise buildings include large, fabricated compression members (or combined compression and flexure) with high demand for efficiency. Steel bridge piers, while less common than concrete, must support large axial compression loads spanning long vertical distances which requires maintaining low self-weight. In cases where columns are designed to resist combined compression and flexure due to lateral forces, the I-profile shape can be employed to provide flexural resistance. It also provides ease of fabrication as it is rather easy to connect I-profiles with bolted or welded connections. Deep webs, which increase the likelihood of strong flange behaviour, can be used to increase flexural stiffness, for instance in bridges. Architectural columns in high-rise buildings or industrial structures also face high compressive loads and can be employed in

moment frames to resist lateral loads. Structurally efficient I-shapes can be useful in this application to provide flexural resistance against wind loads while requiring minimal cross-sectional area to support large compression forces. The application of hybrid sections, generally, to meet the demands of lower-story columns in high-rise buildings inspired the previous study by Zhao et al. [71].

Hybrid and strong flange members are more complex than homogenous sections and require increased design labour. For this reason, these sections are more likely to be adopted in higher cost, customizable projects where the increased design cost can be justified by greater opportunity for reductions in material and construction costs. Bridge piers, high-rise building columns, and industrial facility columns are all examples of the types of projects where a hybrid or strong flange design is more likely to be cost-justified.

The increased capacity of strong flange and hybrid designs quantified in this research project makes these types of members particularly useful in cases where the controlling limit state is ultimate strength. This is particularly true for strong flange I-sections which are slender and susceptible to local buckling in the webs, which makes them less suitable for some serviceability limits. Relevant ultimate strength-controlled applications include certain seismic resistant and non-inhabited structures. Cranes and communication or observation towers, for example, can include large, fabricated members with the potential for cost saving from optimized design in use cases generally controlled by the ultimate strength limit state.

Seismic moment frames are given the primary task of resisting cyclic lateral loads but can also be under compression loads in the case of multi-story buildings. These structures tend to require strong connections, bracing members, and beam-columns capable of withstanding combined loading, or some combination of these features. Seismic frame systems prioritize high ductility to maximize energy dissipation, particularly when ultimate strength is the prioritized limit state. Slender elements, including strong flange I-sections, which may

plastically deform before reaching ultimate strength, are poorly suited compared to compact members for high ductility requirements. Hybrid sections, however, have been shown to improve the ductility of systems with high strength steels, making them potentially very useful for seismic applications [66].

5.4. Limitations and Future Work

The viability of hybrid and stainless steel compression members in novel applications will rely on continued research, particularly in key areas identified in this section. First, the design methods for hybrid stainless steel members must be further investigated to ensure accurate strength predictions. The parametric assessment and subsequent development of the $DSM_{A\&L}$ in Chapter 4 are based on strong flange I-sections that are materially homogeneous, and therefore the conclusions do not necessarily extend to hybrid sections. The finite element model in Chapter 4 was developed only on homogeneous sections to first investigate the effects of geometry in isolation, leaving the isolation of material effects to future work. The proposed $DSM_{A\&L}$ represents the yield load of the section P_y as an area weighted average of the yield strength of the web and flange plates. This simplification is applied in other hybrid section design proposals [75, 3], but may be undermined by the development of substantially different effective strengths in web and flange elements for hybrid sections exhibiting strong flange behaviour. The design accuracy that results from representing sectional yield strength in this simplified manner must be closely inspected in the future work.

In addition to establishing accurate and user-friendly design methods, future research must address concerns for the constructability, corrosion, and thermal expansion of hybrid sections and strengthen the case for these sections in terms of life cycle cost. Hybrid sections face the difficulty of welding together multiple grades of steel. Because welding parameters (welding speed, voltage, and current) are optimized for the type and grade of steel in use,

welded joints of hybrid sections are likely to be more susceptible to mechanical and corrosion failures in the heat affected zone [120]. Further challenges arise in sections which connect multiple families of steel, such as difficulties to weld stainless steel and carbon steel [121] and issues of durability due to the materials having different coefficients of thermal expansion. Because stainless steel hybrid sections will ultimately be used in construction applications for their corrosion resistance, it will be imperative to demonstrate that welded connections in hybrid sections are minimally more vulnerable to corrosion when compared to alternative homogenous fabricated or hot-rolled continuous sections.

Finally, there are multiple limitations associated with the experimental and numerical investigations which are important the bear in mind when developing structures for construction applications. Beginning with the test setup, compression tests are often compromised by the difficulty of achieving uniform contact between the specimen and compression plates, resulting in substantial reductions in the measured stiffness and ultimate load. In construction applications, this is of less concern because the base of the column is likely welded or cast into other structural elements on each end allowing transfer of loads which is closer to the ideal condition. The parametric assessment in Chapter 4 assumes perfect fixed-fixed end conditions for the column, likely slightly over-estimating the column capacity compared to a real word connection which may have defects. The experimental tests on the other hand, have ends constrained only by friction and therefore are expected to underestimate the capacity of the same section in a real column with welded connections. This is the modelling assumption which produced by far the greatest effect on column capacity in this research. The residual stress profile of hybrid stainless steel sections is an additional modelling assumption, because there is currently no published literature reporting the profile shape magnitudes and for this type of section. The effect of residual stresses on column capacity is,

however, very small – likely causing variation from the modelled results of approximately ±1%.

5.5. Conclusion

This research project investigates the behaviour of stainless steel I-sections to expand an underdeveloped section of the literature on the fundamental load case of pure compression. Fabricated, or built-up, sections are primarily studied because these sections are more customizable and comprise a wider range of geometrical and material combinations. Strong flange I-sections, with webs substantially more slender than the flanges, are studied to understand why these sections exceeded the ultimate strength predictions from multiple codified design methods. The compression behaviour of hybrid stainless steel I-sections is studied, including the first experiments in this category, to inspect the effects of this material on column post-local buckling behaviour and ultimate strength.

The relevant history and theoretical background for this research is provided in Chapter 2. The development of hybrid I-profile girders is described, including an explanation of why the corpus of literature on compression loading is sparce compared to flexural loading. A database of fabricated I-section compression tests is compiled which shows that minimal evidence is available for hybrid or strong flange I-sections. Theoretical explanations are provided for plate buckling and element interactions within members. The development of methods to quantify strength reductions due to local buckling is recounted. Finally, initial hypotheses are advanced to explain how plate interactions and local buckling can explain the behaviour of strong flange I-sections.

Thirteen stub column tests are conducted to understand the fundamental loading case of pure compression for hybrid and strong flange I-sections, as reported in Chapter 3. Interaction between the capacity of the flanges and the web buckling mode is demonstrated by controlled

experiments changing the flange thickness between sections. Sections with thicker flanges generally exhibited greater structural efficiency. Geometry proved to have a greater effect on local buckling behaviour than material properties, and high strength materials were not efficiently employed when the greater material strength caused local buckling strength reductions driven by the increase of slenderness. The hybrid ratio for girders recommended in literature of 1.3-1.6 [67] is exceeded in multiple sections, providing evidence that hybrid compression members should be governed by a more complete ratio encompassing thickness and yield strength for both the web and the flanges to distinguish between behaviours and more adequately evaluate member efficiency.

A detailed FE model is validated against the experimental results presented in Chapter 3 and accurately reflects both ultimate strength and buckling behaviour. In Chapter 4, the validated model is used to conduct a parametric study with 1325 simulated stub column tests, incrementally changing individual parameters to evaluate a wide range of possible geometric combinations and four stainless steel grades. The parametric study results are used the evaluate the design performance of three codified methods: the EWM, DSM, and CSM. The EWM is slightly conservative for strong flange sections and the most complex of the considered methods, while the DSM and CSM give highly varied and over-conservative predictions.

A modified DSM is developed which can identify sections likely to exhibit strong flange behaviour and quantifies the expected effect on ultimate strength. The proposed $DSM_{(A\&L)}$ formulation is given in Chapter 4.4.4, *Eq. 62*. Two parameters, Ω and α, calculated based on ratios of geometric and material properties are incorporated into the $DSM_{(A\&L)}$ to design for strong flange behaviour while maintaining a degree of simplicity. The proposed method achieves the greatest accuracy and lowest variation among the considered methods. A reliability assessment of the proposed $DSM_{(A\&L)}$ indicates that it can achieve a satisfactory

probability of failure for strong flange and conventional I-sections under compression when applied with the resistance factor provided in code for the existing DSM.

The improved accuracy of ultimate strength predictions achieved by the $DSM_{(A\&L)}$ in *Eq. 62* and increases the structural efficiency for strong flange I-sections, in some cases by a factor of two. Modifications to reliability assessment methods are proposed to allow even further efficiency gains to be achieved. The advancements in this research, and by other contemporaries, invites further use of hybrid and strong flange members in bride piers, industrial facilities, architectural columns, and more. The improved understanding of hybrid and strong flange section behaviour prevents over-design, directly contributing to reduced cost, reduced waste, and increased performance.

6. REFERENCES

[1] B. Rossi and Y. Li, “Extension of the DSM to welded H profile cross-sections,” in *Research and Applications in Structural Engineering, Mechanics and Computation*, 2013, pp. 1291-1296.

[2] B. Rossi and K. Rasmussen, “Carrying Capacity of Stainless Steel Columns in the Low Slenderness Range,” *Journal of Structural Engineering,* vol. 139, no. 6, 28 May 2012.

[3] R. Lalthazuala and K. Singh, “Structural behaviour of hybrid stainless steel stub columns under axial compression,” *Structures,* vol. 27, pp. 128-140, October 2020.

[4] S. Chen, J.-z. Liu and T.-M. Chan, “Investigations into the local buckling and post-buckling behaviour of fixed-ended hybrid I-section stub columns with slender web,” *Thin-Walled Structures,* vol. 184, 2023.

[5] S. Chen, J.-z. Liu and T.-M. Chan, “Local buckling behaviour of high strength steel and hybrid I-sections under axial compression: Numerical modelling and design,” *Thin-Walled Structures,* vol. 191, October 2023.

[6] L. Gardner, “The use of stainless steel in structures,” *Progress in Structural Engineering and Materials,* vol. 7, 21 February 2005.

[7] M. A. Farmani, A. Heidarpour and X.-L. Zhao, “Thermal creep of austenitic stainless steel plate material under transient heating conditions,” *Thin-Walled Structures,* vol. 171, February 2022.

[8] B. Rossi, “Discussion of the use of stainless steel in construction in view of sustainability,” *Thin-Walled Structures,* vol. 83, pp. 182-189, October 2014.

[9] M. A. Farmani, A. Heidarpour and C. Woo, “Thermal creep of hybrid steel columns comprising ultra-high strength steel tubes and stainless steel plates under transient fire conditions,” *Thin-Walled Structures,* vol. 185, 2023.

[10] H. Yuan, F. Han and M. Theofanous, “Experimental behaviour of hybrid carbon steel – stainless steel bolted connections subjected to electrochemical corrosion,” *Thin-Walled Structures,* vol. 199, June 2024.

[11] G. Langone, M. Shamlooei, U. Ali, X. Ruan and B. Rossi, “Extension of the direct strength method to fabricated I-profiles under compression,” in *Nordic Steel Construction Conference*, Lulea, Sweeden, 2024.

[12] Dassault Systems Simulis Corp, “ABAQUS/CAE User's Manual,” Providence, RI, 2022.

[13] D. Makweche, “Beam behaviour of hybrid steel sections,” 2007.

[14] M. Veljkovic and B. Johansson, “Design of hybrid steel girders,” *Journal of Constructional Steel Research,* vol. 60, no. 3-5, pp. 535-547, 2004.

[15] R. Frost and C. Schilling, “Behavior of Hybrid Beams Subjected to Static Loads,” *Journal of the Structural Division ASCE,* vol. 90, no. 3, June 1964.

[16] D. A. Nethercot, “Buckling of Welded Hybrid Steel I-Beams,” *Journal of the Structural Division,* vol. 102, no. 3, 1976.

[17] Joint American Society of Civil Engineers-AAHSO Committee, “Design of Hybrid Steel Beams,” *Journal of the Structural Division ASCE,* vol. 94, no. 6, June 1968.

[18] N. R. NagarajaRao, P. Marek and L. Tall, “Hybrid steel columns, May 1969 (72-37),” Fritz Laboratory Reports, 1969.

[19] N. R. NagarajaRoa, P. Marek and L. Tall, “Welded hybrid steel columns,” *Welding Journal Research Supplement,* pp. 462-472, September 1972.

[20] R. Chacon, M. Bock and E. Real, “Longitudinally stiffened hybrid steel plate girders subjected to patch loading,” *Journal of Constructional Steel Research,* vol. 67, no. 9, pp. 1310-1324, September 2011.

[21] S. Shimizu, J. Zhang, N. Nakada, N. Tanaka and H. Nakai, “Effect of Stiffeners in Hybrid Steel Plate Girders,” *Steel Construction Engineering,* vol. 10, no. 37, pp. 43-50, 2003.

[22] R. Chacon, E. Mirambell and E. Real, “Hybrid steel plate girders subjected to patch loading, Part 1: Numerical study,” *Journal of Constructional Steel Research,* vol. 66, no. 5, pp. 695-708, May 2010.

[23] R. Chacon, E. Mirambell and E. Real, “Hybrid steel plate girders subjected to patch loading, Part 2: Design proposal,” *Journal of Constructional Steel Research,* vol. 66, no. 5, pp. 709-715, 2010.

[24] M. Shokouhian and Y. Shi, “Flexural strength of hybrid steel I-beams based on slenderness,” *Engineering Structures,* vol. 93, pp. 114-128, June 2015.

[25] A. S. Kulkarni and L. M. Gupta, “Experimental Investigation on Flexural Response of Hybrid Steel Plate Girder,” *KSCE Journal of Civil Engineering,* vol. 22, pp. 2502-2519, September 2018.

[26] Q. Zhao, Z. Guo, X. Shen and B. Briseghella, “Test study on residual stress distribution of hybrid steel u-rib stiffened plates,” *Journal of Constructional Steel Research,* vol. 121, pp. 261-267, 2016.

[27] A. Ghadami and Broujerdian, “Flexure–shear interaction in hybrid steel I-girders at ambient and elevated temperatures,” *Advances in Structural Engineering,* vol. 22, no. 6, pp. 1501-1516, 2019.

[28] S. Chen, J.-z. Liu and T.-M. Chan, “Material properties and residual stresses of welded high strength steel and hybrid I-sections,” *Engineering Structures,* vol. 276, February 2023.

[29] M. S. Y. Shokouhian and M. Head, “Interactive buckling failure modes of hybrid steel flexural members,” *Engineering Structures,* vol. 125, pp. 153-166, 2016.

[30] K. Jiang, Zhao and Ou, “Stainless steel built-up section stub columns: Testing, numerical modelling and design,” *Thin-Walled Structures,* vol. 191, October 2023.

[31] G. Shi, W. Zhou and C. Lin, “Experimental Investigation on the Local Buckling Behavior of 960 MPa High Strength Steel Welded Section Stub Columns,” *Advances in Structural Engineering,* vol. 18, no. 3, pp. 423-437, November 2016.

[32] G. Shi, W. Zhou, Y. Bai and C. Lin, “Local buckling of 460 MPa high strength steel welded section stub columns under axial compression,” *Journal of Constructional Steel Research,* vol. 100, pp. 60-70, September 2014.

[33] D.-K. Kim, C.-H. Lee, K.-H. Han, J.-H. Kim, S.-E. Lee and H.-B. Sim, “Strength and residual stress evaluation of stub columns fabricated from 800 MPa high-strength steel,” *Journal of Constructional Steel Research,* vol. 102, pp. 111-120, November 2014.

[34] G. Shi, Z. Zhang, L. Zhou, L. Yang and W. Zhou, “Experimental and numerical investigation on Local–Overall interactive buckling behavior of welded I-Section steel columns,” *Thin-Walled Structures,* vol. 151, June 2020.

[35] Y. B. Kwon, N. G. Kim and G. Hancock, “Compression tests of welded section columns undergoing buckling interaction,” *Journal of Constructional Steel Research,* vol. 63, no. 12, pp. 1590-1602, December 2007.

[36] K. Rasmussen and G. Hancock, “Plate slenderness limits for high strength steel sections,” *Journal of Constructional Steel Research,* vol. 23, no. 1-3, pp. 73-96, 1992.

[37] A. J. Davids and G. J. Hancock, “Compression Tests of Short Welded I-Sections,” *Journal of Structural Engineering,* vol. 112, no. 5, 1986.

[38] F. Zhou, L. Tong and Y. Chen, “Experimental and numerical investigations of high strength steel welded h-section columns,” *International Journal of Steel Structures,* 2013.

[39] A. Su, Y. Sun, Y. Liang and O. Zhao, “Membrane residual stresses and local buckling of S960 ultra-high strength steel welded I-section stub columns,” vol. 161, 2021.

[40] H. Yuan, Y. Wang, L. Gardner, X. Du and Y. Shi, “Local–overall interactive buckling behaviour of welded stainless steel I-section columns,” *Journal of Constructional Steel Research,* vol. 111, pp. 75-87, 2015.

[41] H. Kuwamura, “Local Buckling of Thin-Walled Stainless Steel Members,” *Steel Structures,* pp. 191-201, 2003.

[42] H. Ran, Z. Chen and Y. Ma, “Experimental and numerical studies of laser-welded slender stainless steel I-section columns,” *Thin-Walled Structures,* vol. 171, 2022.

[43] N. Saliba and L. Gardner, “Cross-section stability of lean duplex stainless steel welded I-sections,” *Journal of Constructional Steel Research,* vol. 80, pp. 1-14, January 2013.

[44] L. Gardner, Y. Bu and M. Theofanous, “Laser-welded stainless steel I-sections: Residual stress measurements and column buckling tests,” *Engineering Structures,* vol. 127, pp. 536-548, November 2016.

[45] A. Salem, M. El Aghoury, F. El Dib and M. Hanna, “Post local buckling strength of bi-axially loaded slender I-section columns,” *Thin-Walled Structures,* vol. 43, no. 7, pp. 1003-1019, July 2005.

[46] W. E. Ayrton and J. Perry, “On struts,” *The Engineer,* 1886.

[47] G. H. Bryan, “On the Stability of a Plane Plate under Thrusts in its own Plane, with Applications to the “Buckling” of the Sides of a Ship,” *Proceedings of the London Mathematical Society,* Vols. s1-22, no. 1, pp. 54-67, 01 November 1890.

[48] M. Seif and B. W. Schafer, “Local buckling of structural steel shapes,” *Journal of Constructional Steel Research,* vol. 66, no. 10, pp. 1232-1247, October 2010.

[49] L. Gardner, A. Fieber and Macorini, “Formulae for Calculating Elastic Local Buckling Stresses of Full Structural Cross-sections,” *Structures,* vol. 17, pp. 2-20, February 2019.

[50] AISI, “S100-16: North American Specification for the Design of Cold-Formed Steel Structural Members,” American Iron and Steel Institute, 2020.

[51] CEN (Committee of European Normalization), Eurocode 3: Design of steel structures - Part 1-5: General rules - Plated structural elements. (EN 1993-1-5), Brussels, 2006.

[52] General Administration of Quality Supervision Inspection and Quarantine, “Technical code of cold-formed thin-wall steel structures,” in *GB50018, Chinese Standard*, Beijing, 2002.

[53] Joint Technical Committee BD-082, Cold-formed Steel Structures, “AS/NZS 4600:2005 Cold-formed steel structures,” Sydney, 2005.

[54] S. Timoshenko and J. Gere, Theory of Elastic Stability, 2nd ed., New York: McGraw-Hill Book Company, 1961.

[55] T. von Karman, E. E. Sechler and L. H. Donnell, "The Strength of Thin Plates in Compression," *Journal of Fluids Engineering,* vol. 54, no. 2, pp. 53-56, 1932.

[56] G. Winter, "Performance of Thin Steel Compression Flanges," in *Third Congress, Intenational Association for Bridge and Structural Engineering*, Liege, 1948.

[57] American Iron and Steel Institute, Specification for the Design of Light Gage Steel Structural Members, New York, NY, 1946.

[58] G. Winter, "Stress Distribution in and Equivalent Width of Flanges of Wide, Thin-Wall Steel Beams," National Advisory Committee for Aeronautics, Washington, D.C., 1940.

[59] N. Lind and M. P. J. Ravindra, "A Review of the E view of the Effective Width F e Width Formula," in *International Specialty Conference on Colf-Formed Steel Structures*, 1971.

[60] American Institute of Steel Construction (AISC), "ANSI/AISC 370-21: Specification for Structural Stainless Steel Buildings," 2021.

[61] CEN (Committee of European Normalization), Eurocode: Basis of structural design (EN1990), Brussels, 2002.

[62] CEN (Committee of European Normalization), Eurocode 3: Design of steel structures, Part 1-1: General rules and rules for buildings (EN 1993-1-1), Brussels, 2005.

[63] CEN (Committee of European Normalization), Eurocode 3: Design of steel structures - Part 1-3: General rules - Supplementary rules for cold-formed members and sheeting (EN1993-1-3), Brussels, 2006.

[64] CEN (Committee of European Normalization), Eurocode 3: Design of steel structures - Part 1-4: General rules and supplementary rules for stainless steels (EN 1993-1-4), Brussels, 2006.

[65] S. Afshan, P. Francis, N. Baddoo and L. Gardner, "Reliability analysis of structural stainless steel design provisions," *Journal of Constructional Steel Research,* vol. 114, pp. 293-304, November 2015.

[66] F. Javidan, A. Heidarpour, X.-L. Zhao and J. Minkkinen, "Application of high strength and ultra-high strength steel tubes in long hybrid compressive members: Experimental and numerical investigation," *Thin-Walled Structures,* vol. 102, pp. 273-285, May 2016.

[67] A. Terreros-Bedoya, I. Negrin, I. Paya-Zaforteza and V. Yepes, "Hybrid steel girders: Review, advantages and new horizons in research and applications," *Journal of Constructional Steel Research,* vol. 207, 2023.

[68] American Association of State Highway and Transportation Officials, AASHTO LRFD Bridge Design Specificiations, 4th Edition ed., Washington DC, 2007, pp. 6.84-6.85.

[69] J. Mozer, R. Ohlson and C. Culver, "Horizontally curved highway bridges: Stability of curved plate girders," 1971.

[70] J.-z. Liu, S. Chen and T.-M. Chan, "Experimental and numerical investigations of hybrid high strength steel welded T-section stub columns with Q690 flange and Q460 web," *Thin-Walled Structures,* vol. 177, 2022.

[71] X.-L. Zhao, D. V. Binh, R. Al-Mahaidi and Z. Tao, "Stub column tests of fabricated square and triangular sections utilizing very high strength steel tubes," *Journal of Constructional Steel Research,* vol. 60, no. 11, pp. 1637-1661, November 2004.

[72] D. V. Binh, B. Al-Mahaidi and X.-L. Zhao, “Finite Element Analysis (FEA) of Fabricated Square and Triangular Section Stub Columns Utilizing Very High Strength Steel Tubes,” *Advances in Structural Engineering,* vol. 7, no. 5, 2004.

[73] J. Rhodes, X.-L. Zhao, B. V. Binh and R. Al-Mahaidi, “Rational design analysis of stub columns fabricated using very high strength circular steel tubes,” *Thin-Walled Structures,* vol. 43, no. 3, pp. 445-460, March 2005.

[74] J.-z. Liu, S. Chen and T.-M. Chan, “Testing, numerical modelling and design of Q690 high strength steel welded T-section stub columns,” *Engineering Structures,* vol. 259, May 2022.

[75] M. Bock, M. Gkantou, M. Theofanous, S. Afshan and H. Yuan, “Ultimate behaviour of hybrid stainless steel cross-sections,” *Journal of Constructional Steel Research,* vol. 210, November 2023.

[76] T. Aoki and B. Ji, “Experimental study on buckling strength of tri-tube steel members,” in *Proceeding of the Third International Conference on Coupled Instabilities in Metal Structures*, Lisbon, Portugal, 2000.

[77] B. Karabulut, G. Ferraz and B. Rossi, “Lifecycle cost assessment of high strength carbon and stainless steel girder bridges,” *Journal of Environmental Management,* vol. 277, January 2021.

[78] G. van den Berg, “The effect of the non-linear stress–strain behaviour of stainless steels on member capacity,” *Journal of Constructional Steel Research,* vol. 54, no. 1, pp. 135-160, April 2000.

[79] B. W. Schafer and T. Pekoz, “Direct Strength Prediction of Cold-formed Steel Members Using Numerical Elastic Buckling Solutions,” in *CCFSS Proceedings of International Specialty Conference on Cold-Formed Steel Structures*, 1998.

[80] B. Schafer, “Review: The Direct Strength Method of cold-formed steel member design,” *Journal of Constructional Steel Research,* vol. 64, no. 7-8, pp. 766-778, 2008.

[81] L. Gardner, “The continuous strength method,” *Proceedings of the Institution of Civil Engineers - Structures and Buildings,* vol. 161, no. 3, pp. 127-133, June 2008.

[82] S. Afshan and L. Gardner, “The continuous strength method for structural stainless steel design,” *Thin-Walled Structures,* vol. 68, pp. 42-49, July 2013.

[83] Internation Organization for Standardization, “ISO 6892-1: Metallic materials - Tensile testing. Part 1: Method of test at room temperature,” 2019-11.

[84] K. Cashell and N. Baddoo, “Ferritic stainless steels in structural applications,” *Thin-Walled Structures,* vol. 83, pp. 169-181, October 2014.

[85] K. Tseng and C. Chou, “Effect of pulsed gas tungsten arc welding on angular distortion in austenitic stainless steel weldments,” *Science and Technology of Welding and Joining,* vol. 6, no. 3, pp. 149-153, 2001.

[86] J.-H. Zhang and B. Young, “Compression tests of cold-formed steel I-shaped open sections with edge and web stiffeners,” *Thin-Walled Structures,* vol. 52, pp. 1-11, March 2012.

[87] H. Fang, T.-M. Chan and B. Young, “Behavior of Octagonal High-Strength Steel Tubular Stub Columns,” *Journal of Structural Engineering,* vol. 145, no. 12, 2019.

[88] Y. Sun, Y. Liang and O. Zhao, “Testing, numerical modelling and design of S690 high strength steel welded I-section stub columns,” *Journal of Constructional Steel Research,* vol. 159, pp. 521-533, August 2019.

[89] M. Theofanous and L. Gardner, “Experimental and numerical studies of lean duplex stainless steel beams,” *Hournal of Contructional Steel Research,* vol. 66, no. 6, pp. 816-825, June 2010.

[90] SCI (Steel Construction Institute), “Design Manual for Structural Stainless Steel, 4th Edition,” SCI, Berkshire, 2017.

[91] M. Abambres and W.-M. Quach, “Residual stresses in steel members: a review of available analytical expressions,” *International Journal of Structural Integrity,* vol. 7, no. 1, pp. 70-94, February 2016.

[92] H. Y. Ban, “Research on the overall buckling behavior and design method of high strength steel columns under axial compression,” Tsinghua University, Beijing, 2012.

[93] H. Yuan, Y. Wang, Y. Shi and L. Gardner, “Residual stress distributions in welded stainless steel sections,” *Thin-Walled Structures,* vol. 79, pp. 38-51, June 2014.

[94] S. Duan, S. Fen, G. Shu, L. Jiang, J. Tong and Y. Wu, “Numerical study and design of S35657 stainless steel welded stub columns,” *Journal of Constructional Steel Research,* vol. 214, March 2024.

[95] U. Ali, G. Langone and B. Rossi, “[Submitted] Numerical modelling and design of stainless steel I-sections with strong flanges,” *ASCE Journal of Structural Engineering,* 2025.

[96] X. Yun, L. Gardner and N. Boissonnade, “Ultimate capacity of I-sections under combined loading – Part 1: Experiments and FE model validation,” *Journal of Constructional Steel Research,* vol. 147, pp. 408-421, August 2018.

[97] L. Gerard, L. Li, M. Kettler and N. Boissonnade, “Steel I-sections resistance under compression or bending by the Overall Interaction Concept,” *Journal of Constructional Steel Research,* vol. 182, July 2021.

[98] ANSI/AISC, “360-22 Specification for Structural Steel Buildings,” 2022.

[99] G. Langone, U. Ali and B. Rossi, “[Submitted] Tests of hybrif stainless steel I-profile columns under pure compression,” *ASCE Journal of Structural Engineering,* 2025.

[100] G. Shu, S. Yang, X. Jin, S. Dong, Q. Jiang and B. Zheng, “Study on the bearing capacity of S600E high-strength stainless steel welded cross-sections,” *Journal of Constructional Steel Research,* vol. 175, December 2020.

[101] M. Theofanous and L. Gardner, “Testing and numerical modelling of lean duplex stainless steel hollow section columns,” *Engineering Structures,* vol. 31, no. 12, pp. 3047-3058, December 2009.

[102] H. Yuan, Y. Wang, Y. Shi and L. Gardner, “Stub column tests on stainless steel built-up sections,” *Thin-Walled Structures,* vol. 83, pp. 103-114, October 2014.

[103] L. Yang, M. Zhao, D. Xu, F. Shang, H. Yuan, Y. Wang and Y. Zhang, “Flexural buckling behavior of welded stainless steel box-section columns,” *Thin-Walled Structures,* vol. 104, pp. 185-197, 2016.

[104] L. Gardner, A. Talja and N. Baddoo, “Structural design of high-strength austenitic stainless steel,” *Thin-Walled Structures,* vol. 44, no. 5, pp. 517-528, May 2006.

[105] B. Young and Y. Liu, “Experimental Investigation of Cold-Formed Stainless Steel Columns,” *Journal of Structural Engineering,* vol. 129, no. 2, January 2003.

[106] J. Becque and K. Rasmussen, “Experimental investigation of local-overall interaction buckling of stainless steel lipped channel columns,” *Journal of Constructional Steel Research,* vol. 65, no. 8-9, pp. 1677-1684, August-September 2009.

[107] K. Sachidananda and K. D. Singh, “Numerical study of fixed ended lean duplex stainless steel (LDSS) flat oval hollow stub column under pure axial compression,” *Thin-Walled Structures,* vol. 96, pp. 105-119, November 2015.

[108] L. Gardner and M. Theofanous, “Discrete and continuous treatment of local buckling in stainless steel elements,” *Journal of Constructional Steel Research,* vol. 64, no. 11, pp. 1207-1216, November 2008.

[109] I. Arrayago, K. Rasmussen and E. Real, “Full slenderness range DSM approach for stainless steel hollow cross-sections,” *Journal of Constructional Steel Research,* vol. 133, pp. 156-166, June 2017.

[110] B. Schafer, “Progress on the Direct Strength Method,” in *CCFSS Proceedings of International Specialty Conference on Cold-Formed Steel Structures*, 2002.

[111] ASCE, “Specification for the Design of Cold-Formed Stainless Steel Structural Members,” American Society of Civil Engineers , Reston, Virginia, 2021.

[112] M. Ashraf, L. Gardner and D. Nethercot, “Structural Stainless Steel Design: Resistance Based on Deformation Capacity,” *ASCE Journal of Structural Engineering,* vol. 134, no. 3, 2008.

[113] A. Liew and L. Gardner, “Ultimate capacity of structural steel cross-sections under compression, bending and combined loading,” *Structures,* vol. 1, pp. 2-11, 2015.

[114] O. Zhao, S. Afshan and L. Gardner, “Structural response and continuous strength method design of slender stainless steel cross-sections,” *Engineering Structures,* vol. 140, pp. 14-25, June 2017.

[115] C. Miki, K. Homma and T. Tominaga, “High strength and high performance steels and their use in bridge structures,” *Journal of Constructional Steel Research,* vol. 58, no. 1, pp. 3-20, January 2002.

[116] F. Walport, M. Kucukler and L. Gardner, “Stability Design of Stainless Steel Structures,” *ASCE Journal of Structural Engineering,* vol. 148, no. 1, October 2021.

[117] G. Shi, X. Zhu and H. Ban, “Material properties and partial factors for resistance of high-strength steels in China,” *Journal of Constructional Steel Research,* vol. 121, pp. 65-79, June 2016.

[118] H. Ban and G. Shi, “A review of research on high-strength steel structures,” *Proceedings of the Institution of Civil Engineers - Structures and Buildings,* vol. 171, no. 8, pp. 581-658, August 2018.

[119] N. Schillo, A. Taras and M. Feldmann, “Assessing the reliability of local buckling of plates for mild and high strength steels,” *Journal of Constructional Steel Research,* vol. 142, pp. 86-98, March 2018.

[120] B. Kutelu, S. Seidu, G. Eghabor and A. Ibitoye, “Review of GTAW Welding Parameters,” *Journal of Minerals and Materials Characterization and Engineering,* vol. 6, pp. 541-554, 2018.

[121] R. Paventhan, P. Lakshminarayanan and V. Balasubramanian, “Optimization of Friction Welding Process Parameters for Joining Carbon Steel and Stainless Steel,” *Journal of Iron and Steel Research International,* vol. 19, p. 66–71, January 2012.

7. APPPENDIX

Table A.1. Stub Column Test Data from Literature

Fabricated I-section stub column test data collected from literature, including measured geometries, measured material properties, and ultimate loads.

- Section ID indicates the label given to each section in the source publication.
- In the material column, “A” represents austenitic stainless steel, “D” represents duplex stainless steel, and “CS” represents carbon steel (including high strength grades).

Reference	Section ID	Material	L [mm]	h_w [mm]	b [mm]	t_w [mm]	t_f [mm]	$f_{y,\,web}$ [MPa]	$f_{y,\,flange}$ [MPa]	E [MPa]	P_u [kN]
[42]	I-120×60×4×4	A	360	111.7	59.9	3.83	3.82	300	300	192500	274
	I-140×80×3×3	A	420	134.2	79.7	2.75	2.74	291	291	185000	174
	I-90×60×3×3	A	270	84.3	60.3	2.80	2.81	291	291	185000	173
	I-90×60×4×4	A	270	81.6	59.8	3.83	3.83	300	300	192500	266
	I-120×90×3×3	A	360	113.7	90.0	2.78	2.78	297	297	189000	196
	I-100×80×3×3	A	200	93.7	79.5	2.75	2.74	291	291	185000	173
	I-140×140×3×3	A	421	133.8	139.2	2.75	2.74	291	291	185000	211
	I-90×90×3×3	A	270	83.9	89.7	2.77	2.77	297	297	189000	179
	I-60×60×3×3	A	180	54.7	60.2	2.78	2.78	297	297	189000	163
[41]	SC-2H1	A	150	45.0	49.9	2.96	2.96	249	249	203000	153
	SC-2H2	A	300	44.1	98.9	2.94	2.94	249	249	203000	193
	SC-2H3	A	300	95.4	49.7	2.93	2.93	249	249	203000	171
	SC-2H4	A	300	95.4	75.2	2.93	2.93	249	249	203000	200
	SC-2H5	A	300	95.4	99.7	2.92	2.92	249	249	203000	203
	SC-2H6	A	450	145.0	99.6	2.95	2.95	249	249	203000	208
	SC-2H7	A	600	194.8	100.2	2.93	2.93	249	249	203000	206
	SC-2H8	A	600	195.2	150.4	2.95	2.95	249	249	203000	231
	SC-4H1	A	150	45.2	49.3	3.01	3.04	497	497	206000	253
	SC-4H2	A	300	45.6	99.2	3.01	2.99	497	497	206000	290
	SC-4H3	A	300	95.2	50.3	3.01	3.03	497	497	206000	280
	SC-4H4	A	300	96.0	74.8	2.99	3.02	497	497	206000	310
	SC-4H5	A	300	94.3	99.7	3.02	3.02	497	497	206000	323
	SC-4H6	A	450	145.2	99.5	3.02	3.02	497	497	206000	310
	SC-4H7	A	600	195.9	100.1	3.02	3.01	497	497	206000	311
	SC-4H8	A	600	195.4	149.8	3.01	3.02	497	497	206000	360
[44]	I-300×150×7×11	A	840	271.5	150.5	6.92	11.81	237	290	198550	1672
	I-220×110×6×9	A	660	201.8	110.4	6.07	8.91	275	292	195100	1072
	I-150×75×7×10	A	450	130.7	75.8	7.05	9.90	274	267	197250	854
	I-160×82×10×12	A	480	136.5	83.2	9.79	11.72	264	286	198000	1398
	I-203×133×6×8	A	612	189.4	133.9	5.90	7.83	251	281	192500	1090
	I-102×68×5×5	A	305	91.6	68.0	5.01	5.11	222	222	186800	430
	I-152×160×6×9	A	456	134.7	160.6	6.18	8.79	272	227	198050	1163
	I-140×140×10×12	A	420	116.1	140.8	9.71	11.82	260	272	190250	2042
	I-50×50×4×4	A	150	42.5	50.5	3.99	3.91	270	270	190700	281
[40]	I304-492-i	A	2138	482.9	198.0	6.00	6.00	316	316	195250	737
	I304-432-i	A	2037	422.1	173.5	6.00	6.00	316	316	195250	717
	I304-372-i	A	2889	361.1	245.5	6.00	6.00	316	316	195250	894
	I304-312-i	A	3137	301.3	305.0	6.00	6.00	316	316	195250	991
	I304-252-i	A	2938	240.7	245.5	6.00	6.00	316	316	195250	843
	I2205-492-i	D	2141	481.8	196.9	6.00	6.00	651	651	207200	1256
	I2205-432-i	D	2039	422.1	172.9	6.00	6.00	651	651	207200	1015
	I2205-372-i	D	2887	362.0	245.0	6.00	6.00	651	651	207200	1322
	I2205-252-i	D	2935	241.3	245.0	6.00	6.00	651	651	207200	1290
	I2205-312-i	D	3140	301.1	305.0	6.00	6.00	651	651	207200	1445
[43]	I-200x140x6x6	D	600	202.1	138.9	6.01	6.12	516	516	200000	1473
	I-200x140x8x6	D	600	201.1	139.0	5.98	8.04	516	504	200000	1849
	I-200x140x10x8	D	600	199.2	139.0	8.03	10.35	504	501	200000	2540
	I-200x140x12x8	D	600	199.1	139.3	8.14	12.68	504	456	200000	2978
[4]	H440-460W	CS	500	420.3	109.7	6.30	9.70	521	820	215800	2422
	H440-690W	CS	499	420.2	110.1	6.30	9.60	789	820	216100	2887
	H440-355W	CS	499	419.6	110.1	6.70	9.50	402	820	220000	2363
	H350-690W	CS	400	329.2	109.8	6.50	9.50	789	820	216100	2802
	H350-460W	CS	396	330.1	110.4	6.60	9.60	521	820	215800	2445
	H350-355W	CS	296	329.3	110.0	6.80	9.70	402	820	220000	2371
	H230-690W-L1	CS	252	207.8	110.3	6.20	9.80	789	820	216100	2674
	H230-690W-L2	CS	462	208.1	110.8	6.40	9.60	789	820	216100	2641
	H230-460W-L1	CS	251	207.5	109.9	6.60	9.70	521	820	215800	2458

	H230-460W-L2	CS	462	208.7	109.8	6.60	9.60	521	820	215800	2378
	H230-355W-L2	CS	462	209.3	110.0	6.70	9.70	402	820	220000	2302
	H230-355W-L1	CS	251	209.1	109.6	6.80	9.70	402	820	220000	2369
[37]	190-3	CS	895	190.1	190.0	5.00	5.00	411	411	202000	932
	190-1	CS	895	190.1	190.0	5.00	5.00	411	411	202000	933
	240-2	CS	1095	241.1	240.0	5.00	5.00	411	411	202000	1000
	240-1	CS	1095	241.1	240.0	5.00	5.00	411	411	202000	995
	310-2	CS	1395	311.0	310.0	5.00	5.00	411	411	202000	1104
	310-1	CS	1395	311.0	310.0	5.00	5.00	411	411	202000	1087
[39]	I-150×75×6-1	CS	321	137.5	75.9	6.14	6.14	972	972	203341	1621
	I-150×75×6-2	CS	320	136.9	76.0	6.10	6.10	972	972	203341	1671
	I-200×150×6-1	CS	599	187.7	149.7	6.01	6.01	972	972	203341	2223
	I-200×150×6-2	CS	600	188.1	150.0	5.96	5.96	972	972	203341	2080
	I-80×60×6-2	CS	210	67.1	59.3	5.96	5.96	972	972	203341	1217
	I-80×60×6-1	CS	209	66.9	59.2	6.03	6.03	972	972	203341	1251
	I-90×70×6-2	CS	240	78.5	69.5	6.01	6.01	972	972	203341	1405
	I-90×70×6-1	CS	239	77.8	69.2	5.97	5.97	972	972	203341	1394
	I-150×150×6-1	CS	449	137.4	149.2	5.98	5.98	972	972	203341	2104
	I-150×150×6-2	CS	450	137.4	150.0	6.07	6.07	972	972	203341	2180
	I-120×120×6-1	CS	359	107.2	119.3	5.99	5.99	972	972	203341	2136
	I-120×120×6-2	CS	361	106.9	119.6	6.03	6.03	972	972	203341	1930
	I-70×70×6-2	CS	211	58.1	69.3	5.94	5.94	972	972	203341	1264
	I-70×70×6-1	CS	209	57.8	69.3	6.01	6.01	972	972	203341	1300
	I-50×50×6-1	CS	148	37.9	49.2	5.98	5.98	972	972	203341	951
	I-50×50×6-2	CS	149	37.0	49.2	6.06	6.06	972	972	203341	947
[36]	I3SC1	CS	450	180.0	136.0	6.00	6.00	725	725	211000	1706
	I2SC1	CS	400	150.0	116.0	6.00	6.00	725	725	211000	1590
	I1SC1	CS	350	120.0	96.0	6.00	6.00	725	725	211000	1367
[38]	H300×200×12×12	CS	798	300.8	199.8	12.66	12.66	516	516	200000	5309
	H300×200×10×10	CS	800	301.0	199.3	10.23	10.23	550	550	280100	4461
[45]	L1-15-120	CS	1001	601.0	74.0	4.95	4.95	322	322	202963	721
	L2-14-80	CS	2001	401.0	71.0	4.90	4.80	322	322	202963	618
	L1-15-80	CS	999	309.0	77.0	4.80	4.80	322	322	202963	746
	L2-24-120	CS	1999	399.0	119.0	5.10	5.10	322	322	202963	721
	L2-24-80	CS	1999	399.0	121.0	4.93	4.93	322	322	202963	783